

## TECHNICAL REPORT DOCUMENTATION PAGE

1. Report No.  TX -0-1400-1	2. Government Accession No.	3. Recipient's Catalog No.	
4. Title and Subtitle: "Investigation of Wind-Rain-Induced Cable-Stay Vibrations on Cable-Stayed Bridges: Final Report"		5. Report Date: August 2005	
		6. Performing Organization Code: TechMRT	
7. Author(s): R.S. Phelan, K.C. Mehta, P.P. Sarkar & L. Chen		8. Performing Organization Report No.: 0-1400-1	
9. Performing Organization Name and Address Texas Tech University Department of Civil Engineering Box 41023 Lubbock, Texas 79409-1023		10. Work Unit No. (TRAIS)	
		11. Contract or Grant No. Project 0-1400	
12. Sponsoring Agency Name and Address Texas Department of Transportation Research and Technology P. O. Box 5080 Austin, TX 78763-5080		Type of Report and Period Sept 1998-Aug 2001	
		14. Sponsoring Agency Code	
15. Supplementary Notes			
<p>16. Abstract: In recent years, large-amplitude cable-stay vibrations have been observed on a number of bridges in the U.S. and abroad during relatively low wind speeds with the presence of rain. Typically, the wind-rain-induced vibration problem has not received adequate attention from bridge designers - resulting in the current need for mitigation devices. Excessive vibrations accelerate fatigue of the cable-stays and cause distractions to passing motorists.</p> <p>Two bridges in Texas have experienced wind-rain-induced cable-stay vibration problems: The Fred Hartman and Veterans Memorial Bridges located respectively, in Baytown and Port Arthur, Texas. Generally, vibration has been observed in moderate to heavy rain at wind speeds of 15 m/s (34 mph) or less. This Report documents the results of three years of study of the cable stay vibration problem on these two bridges by researchers from Texas Tech University, under contract to TxDOT. The scope of the TTU effort includes background research, wind tunnel tests, and field instrumentation and monitoring. Researchers from TTU have developed an innovative aerodynamic ring as a mitigation for cable-stay vibration. Based on limited data, it appears the circular rings work in mitigating wind-rain-induced cable-stay vibration.</p>			
17. Key Words cable stay vibrations; cable stay aerodynamics; current mitigation devices		18. Distribution Statement No restrictions. This document is available to the public through the National Technical Information Service, Springfield, Virginia 2161	
19. Security Classif. (of this report): Unclassified	20. Security Classif. (of this page): Unclassified	21. No. of Pages 95	22. Price

## **NOTICE**

The United States Government and the State of Texas do not endorse products of manufacturers. Trade or manufacturers' names appear herein solely because they are considered essential to the object of this report.

**INVESTIGATION OF WIND-RAIN-INDUCED  
CABLE-STAY VIBRATIONS ON  
CABLE-STAYED BRIDGES: FINAL REPORT**

by

R. Scott Phelan, Ph.D., P.E., TTU Assistant Professor  
Kishor C. Mehta, Ph.D., P.E., TTU Horn Professor  
Partha P. Sarkar, Ph.D., ISU Associate Professor  
Lizhong Chen, TTU Ph.D. candidate

Project Number 0-1400

Report Number 0-1400-1

conducted for the

Texas Department of Transportation

by the

**CENTER FOR MULTIDISCIPLINARY RESEARCH IN TRANSPORTATION**

**TEXAS TECH UNIVERSITY**

August 2005



## ACKNOWLEDGEMENTS

The authors would like to gratefully acknowledge the financial support of the Texas Department of Transportation (TxDOT). Assistance by Keith Ramsey and Elton Brown of the TxDOT Bridge Inspection Group and Stanley Shafer of the TxDOT Beaumont District was especially helpful. In addition, comments and assistance from Randy Poston and Mike Lynch of Whitlock, Dalrymple, Poston and Associates (WDP), Nick Jones of Johns Hopkins University, Department of Civil Engineering and Karl Frank, Sharon Wood and Michael Kreger of the University of Texas at Austin are appreciated. Special thanks go to Analog Devices for their donation of the initial batch of accelerometers. Also, the authors would like to thank Carlos Morales, a TTU civil engineering architecture graduate student, for rendering many of the figures presented in this report.

A special acknowledgement goes to Thomas Gardner. A major portion of his TTU master's thesis is referenced in this report. Mr. Gardner, under supervision of Drs. Mehta and Sarkar, developed the 2-D force-damper apparatus used in the TTU wind tunnel tests. Also, Mr. Gardner was responsible for most of the field instrumentation setup on the four TTU-instrumented Veterans Memorial Cable-Stays. In addition, recognition goes to Dr. Zhongshan Zhao for his contribution to the wind tunnel tests and preliminary field result analyses.

## **IMPLEMENTATION STATEMENT**

This research evaluates technologies potentially capable of mitigating wind-rain-induced cable-stay vibrations for bridges. Wind tunnel tests are not likely to have commercial implementation prospects. However, the potential for a full-scale cable-stay test site for predicting vibrations is suggested by the researchers.

Based on the positive results from field and wind-tunnel tests, the proposed aerodynamic circular rings, with slight modifications, could be ready as retrofits for implementation on existing bridges that experience wind-rain-induced cable-stay vibrations. Any implementation scheme would have to be custom-designed for a particular bridge and would be subject to approval from the Texas Department of Transportation.

Prepared in cooperation with the Texas Department of Transportation and the U.S. Department of Transportation, Federal Highway Administration.



## **AUTHOR'S DISCLAIMER**

The contents of this report reflect the views of the authors who are responsible for the facts and the accuracy of the data presented herein. The contents do not necessarily reflect the official view of policies of the Texas Department of Transportation or the U.S. Federal Highway Administration. This report does not constitute a standard, specification, or regulation.

## **PATENT DISCLAIMER**

Prior to the official commencement of this TxDOT Research Project 0-1400, TTU researchers applied for two patents on circular ring cable-stay vibration mitigation. However, there was no invention or discovery conceived or first actually reduced to practice including art, method process, machine, manufacture, design, or composition of matter in the course of this project which is or may be patentable under the patent laws of the United States of America or any foreign country.

## **ENGINEERING DISCLAIMER**

Not intended for construction, bidding, or permit purposes. The engineer in charge of the research study was R. Scott Phelan, Texas Tech University, Lubbock, Texas.

## **TRADE NAMES AND MANUFACTURERS' NAMES**

The United States Government and the State of Texas do not endorse products or manufacturers. Trade or manufacturers' names appear herein solely because they are considered essential to the object of this report.

## SI\* (MODERN METRIC) CONVERSION FACTORS

APPROXIMATE CONVERSIONS TO SI UNITS					APPROXIMATE CONVERSIONS FROM SI UNITS				
Symbol	When You Know	Multiply By	To Find	Symbol	Symbol	When You Know	Multiply By	To Find	Symbol
<b>LENGTH</b>					<b>LENGTH</b>				
in	inches	25.4	millimeters	mm	mm	millimeters	0.039	inches	in
ft	feet	0.305	meters	m	m	meters	3.28	feet	ft
yd	yards	0.914	meters	m	m	meters	1.09	yards	yd
mi	miles	1.61	kilometers	km	km	kilometers	0.621	miles	mi
<b>AREA</b>					<b>AREA</b>				
in <sup>2</sup>	square inches	645.2	square millimeters	mm <sup>2</sup>	mm <sup>2</sup>	square millimeters	0.0016	square inches	in <sup>2</sup>
ft <sup>2</sup>	square feet	0.093	square meters	m <sup>2</sup>	m <sup>2</sup>	square meters	10.764	square feet	ft <sup>2</sup>
yd <sup>2</sup>	square yards	0.836	square meters	m <sup>2</sup>	m <sup>2</sup>	square meters	1.195	square yards	yd <sup>2</sup>
ac	acres	0.405	hectares	ha	ha	hectares	2.47	acres	ac
mi <sup>2</sup>	square miles	2.59	square kilometers	km <sup>2</sup>	km <sup>2</sup>	square kilometers	0.386	square miles	mi <sup>2</sup>
<b>VOLUME</b>					<b>VOLUME</b>				
fl oz	fluid ounces	29.57	milliliters	mL	mL	milliliters	0.034	fluid ounces	fl oz
gal	gallons	3.785	liters	L	L	liters	0.264	gallons	gal
ft <sup>3</sup>	cubic feet	0.028	cubic meters	m <sup>3</sup>	m <sup>3</sup>	cubic meters	35.71	cubic feet	ft <sup>3</sup>
yd <sup>3</sup>	cubic yards	0.765	cubic meters	m <sup>3</sup>	m <sup>3</sup>	cubic meters	1.307	cubic yards	yd <sup>3</sup>
NOTE: Volumes greater than 1000 l shall be shown in m <sup>3</sup> .									
<b>MASS</b>					<b>MASS</b>				
oz	ounces	28.35	grams	g	g	grams	0.035	ounces	oz
lb	pounds	0.454	kilograms	kg	kg	kilograms	2.202	pounds	lb
T	short tons (2000 lb)	0.907	megagrams (or "metric ton")	Mg (or "t")	Mg (or "t")	megagrams (or "metric ton")	1.103	short tons (2000 lb)	T
<b>TEMPERATURE (exact)</b>					<b>TEMPERATURE (exact)</b>				
°F	Fahrenheit temperature	5(F-32)/9 or (F-32)/1.8	Celcius temperature	°C	°C	Celcius temperature	1.8C + 32	Fahrenheit temperature	°F
<b>ILLUMINATION</b>					<b>ILLUMINATION</b>				
fc	foot-candles	10.76	lux	lx	lx	lux	0.0929	foot-candles	fc
fl	foot-Lamberts	3.426	candela/m <sup>2</sup>	cd/m <sup>2</sup>	cd/m <sup>2</sup>	candela/m <sup>2</sup>	0.2919	foot-Lamberts	fl
<b>FORCE and PRESSURE or STRESS</b>					<b>FORCE and PRESSURE or STRESS</b>				
lbf	poundforce	4.45	newtons	N	N	newtons	0.225	poundforce	lbf
lbf/in <sup>2</sup>	poundforce per square inch	6.89	kilopascals	kPa	kPa	kilopascals	0.145	poundforce per square inch	lbf/in <sup>2</sup>

\* SI is the symbol for the International System of Units. Appropriate

## TABLE OF CONTENTS

<b>TABLE OF CONTENTS</b> .....	xi
<b>LIST OF FIGURES</b> .....	xii
<b>LIST OF TABLES</b> .....	xiv
<b>CHAPTER 1 - INTRODUCTION</b> .....	1
1.1 Overview.....	1
1.2 Background.....	1
1.3 Fred Hartman Bridge .....	2
1.4 Veterans Memorial Bridge.....	5
1.5 Advisory Panel.....	6
<b>CHAPTER 2 – CABLE-STAY VIBRATION BACKGROUND</b> .....	9
2.1 Chapter Overview .....	9
2.2 Background.....	9
2.3 Earlier TxDOT Field Observations.....	11
2.4 Cable-Stay Aerodynamics .....	12
2.5 Previous Reported Field Observations on Bridges.....	19
2.6 Mitigation Devices.....	20
<b>CHAPTER 3 – TTU WIND TUNNEL TESTS</b> .....	25
3.1 Past Observations on Wind Tunnel Models.....	25
3.2 CSU Wind Tests .....	27
3.3 TTU Wind Tunnel Section Model Tests.....	37
3.4 Wind Tunnel Tests Summary .....	50
<b>CHAPTER 4 – TTU FIELD TESTS AND RESULTS</b> .....	51
4.1 Instrumentation Setup for Fred Hartman Bridge .....	51
4.2 Instrumentation Setup for Veterans Memorial Bridge.....	52
<b>CHAPTER 5 – FIELD RESULTS</b> .....	55
5.1 Overall Results for Veterans Memorial Bridge.....	55
5.2 Major Veterans Memorial Cable-Stay Accelerations Event .....	56
5.3 Aerodynamic Ring Installation .....	58
5.4 Field Events after Ring Installation.....	59
5.5 Summary .....	74
5.6 Conclusions .....	76

<b>CHAPTER 6 –SUMMARY AND CONCLUSIONS</b> .....	77
6.1 Wind Tunnel Results.....	77
6.2 Field Site Results.....	77
6.3 Future Research.....	78
<b>REFERENCES</b> .....	81
<b>APPENDIX A</b> .....	83
<b>APPENDIX B</b> .....	85

## LIST OF FIGURES

Figure 1.1	Fred Hartman Bridge .....	2
Figure 1.2	Veterans Memorial Bridge.....	5
Figure 2.1	Yaw, Inclination, Equivalent Yaw and Wind Attack Angles .....	10
Figure 2.2	Upper Rivulet on Cable-Stay .....	10
Figure 2.3	Velocity-Restricted Behavior of Wind-Rain-Induced Vibration.....	11
Figure 2.4	Various Aerodynamic Countermeasures Investigated by Matsumoto et al.....	23
Figure 3.1	Wind-Tunnel Model Setup in the Meteorological Wind Tunnel At CSU.....	28
Figure 3.2	Model at $\alpha = 0^\circ$ and $\beta^\circ$ Showing an Artificial-Upper-Water Rivulet ...	28
Figure 3.3	Aerodynamic Devices Tested .....	28
Figure 3.4	(a), (b) Vertical Displacement Response (rms) of Section Model (D= 10.2cm).....	30
Figure 3.4	(c), (d), (e) Vertical Displacement Response (rms) of Section Model (D= 10.2cm) .....	31
Figure 3.5	$H_1^*$ for Cable With and Without Mitigation Devices.....	33
Figure 3.6	Total Critical Damping at Different Wind Speeds .....	34
Figure 3.7	Formation of upper water rivulet on a yawed and inclined Cable.....	35
Figure 3.8	Prevention of upper water rivulet with Circular Rings.....	35
Figure 3.9	Directions of the Mean Aerodynamic Forces .....	35
Figure 3.10	2DOF TTU Cable with Rings and Suspension System .....	38
Figure 3.11	2DOF TTU Cable-Stay Setup in Wind Tunnel Section Model .....	39
Figure 3.12	Variation of Lift and Drag with Yaw Angle (bare cylinder) .....	41
Figure 3.13	Comparison of Responses of Bare Cylinder for each Yaw Angle.....	42
Figure 3.14	Response of Cylinder with Rivulet at $\beta^* = 15^\circ$ .....	43
Figure 3.15	Response of Cylinder with Rivulet at $\beta^* = 25^\circ$ .....	44
Figure 3.16	Response of Cylinder with Rivulet at $\beta^* = 35^\circ$ .....	44
Figure 3.17	Response of Cylinder with Rivulet at $\beta^* = 45^\circ$ .....	45
Figure 3.18	Response of Cylinder with Rivulet at $\beta^* = 55^\circ$ .....	45
Figure 3.19	Response with Covering of Sandpaper and No Rivulet at $\beta^* = 35^\circ$ .....	46
Figure 3.20	Response with Covering of Sandpaper with Rivulet at $\beta^* = 35^\circ$ .....	46
Figure 3.21	Comparison of Responses of cylinder with and without Sandpaper (no rivulet) .....	47
Figure 3.22	Response of Cylinder with Circular Rings Spaced at $4D$ , $\beta^* = 35^\circ$ .....	47
Figure 3.23	Response of Cylinder with Circular Rings Spaced at $2D$ , $\beta^* = 35^\circ$ .....	48
Figure 3.24	Variation of Lift and Drag with Yaw Angle.....	48
Figure 3.25	Aerodynamic Ring Effectiveness at Low Wind Speed with Rivulet....	49
Figure 3.26	Aerodynamic Ring Effectiveness at High Wind Speed without Rivulet.....	49
Figure 4.1	Veterans Memorial: Instrumentation Scheme and Wind Angle.....	54

Figure 5.1	Veterans Memorial 5 g Cable-Stay Vibration Event: Simultaneous Wind Speed and Direction, Rainfall, and Stay Acceleration.....	57
Figure 5.2	Full-Scale Aerodynamic Ring Installation.....	58
Figure 5.3	B14HZ One-Minute RMS Acceleration vs. Wind Speed (before rings).....	62
Figure 5.4	B14HZ One-Minute RMS Acceleration vs. Wind Speed (after rings).....	62
Figure 5.5	C14HZ One-Minute RMS Acceleration History vs. Wind Speed (Before January 10, 2001 – No Rings).....	63
Figure 5.6	C14HZ One-Minute RMS Acceleration History vs. Wind Speed (After January 10, 2001 – No Rings).....	63
Figure 5.7	B14HZ One Minute RMS Acceleration Distribution with Wind Speed and Direction (Before January 10, 2001 - Without Rings).....	66
Figure 5.8	B14HZ One Minute RMS Acceleration Distribution with Wind Speed and Direction (After January 10, 2001 – With Rings).....	67
Figure 5.9	C14HZ One Minute RMS Acceleration Distribution with Wind Speed and Direction (Before January 10, 2001 – Without Rings).....	70
Figure 5.10	C14HZ One Minute RMS Acceleration Distribution with Wind Speed and Direction (After January 10, 2001 – Without Rings) .....	71
Figure 5.11	Dominating Mode Distribution of B14HZ (Before Ring Installation, i.e. Before January 10, 2001) .....	72
Figure 5.12	Dominating Mode Distribution of B14HZ (After Ring Installation, i.e. After January 10, 2001) .....	73
Figure 5.13	Dominating Mode Distribution of C14HZ (Before January 10, 2001, No Rings).....	73
Figure 5.14	Dominating Mode Distribution of C14HZ (After January 10, 2001, No Rings).....	74

## LIST OF TABLES

Table 1.1	Fred Hartman Bridge: Cable-Stay Geometry and Frequency (WDP, 1999).....	4
Table 1.2	Veterans Memorial Bridge: Cable-Stay Geometry and Frequency (WDP, 2002).....	6
Table 3.1	Videotaped Vibration Events of the Fred Harman Bridge Stay Cables.....	32
Table 3.2	Force Coefficients.....	36
Table 5.1	“Good Records” vs. Total Number of Records .....	55
Table 5.2	“Good Records”: Accelerations Greater than 0.5g.....	56
Table 5.3	All Events (>2.5g) without Rings from August 1, 1999 to January 10, 2001 .....	59
Table 5.4	All Events (>2.5g) from January 10, 2001 to July 10, 2001 (B14 with Rings, C14 without Rings).....	60
Table 5.5	Number of Good Records (>0.5g) for each Cable-Stay from August 1999 to July 2001.....	61
Table 5.6	Maximum One Minute RMS Acceleration on All Channels Before and After January 10, 2001.....	64
Table 5.7	Acceleration RMS of B14HZ (With Rain, With Wind Direction from 315° to 345° .....	66
Table 5.8	Acceleration RMS of C14HZ (With Rain and Wind Direction Between 15° and 45°).....	69
Table 5.9	Cable-Stay Behavior Summary Table .....	75

# CHAPTER 1

## INTRODUCTION

This report: (1) presents an overview of research conducted prior to this project on the Fred Hartman and Veterans Memorial Bridges located at Baytown and Port Arthur, Texas, respectively, (2) provides a background on current mitigation devices, (3) summarizes wind tunnel tests performed at Colorado State University (CSU) and Texas Tech University (TTU) on “passive” aerodynamic ring system, (4) describes field instrumentation, and (5) summarizes field test results. Parallel complimentary studies of cable-stay vibrations and their implications are continuing at Johns Hopkins University and the University of Texas at Austin (see Section 1.5); their results are not included in this report.

### 1.1 Overview

This final report documents major findings concerning the cable-stay vibration problem for bridges in Texas under investigation. Chapter 1 of the report provides a background to the Fred Hartman and Veterans Memorial Bridges, along with a listing of the Advisory Panel set up by the Texas Department of Transportation, TxDOT, to investigate the problem. Chapter 2 provides a rather thorough background of cable-stay aerodynamics, field observations and potential mitigation strategies. Chapter 3 documents wind tunnel tests performed at Colorado State University and Texas Tech University and serves as a basis for the field-testing of prototype aerodynamic rings. Chapter 4 presents the field instrumentation used at each bridge. Chapter 5 presents field results TTU researchers obtained on the Veterans Memorial Bridge, both before and after ring installation. The report concludes with a summary of results and recommendations for future research in Chapter 6. The report also has Appendices A and B. In Appendix A there is a Glossary of common Wind Engineering terms. Appendix B presents criteria that can be used to evaluate closure of bridges to traffic in case of high winds.

### 1.2 Background

In recent years, large-amplitude cable-stay vibrations have been observed on a number of bridges in the U.S. and abroad during relatively low wind speeds in the range of 5 to 15 m/s (11-34 mph)—with and without the presence of rain. Wind-rain-induced cable-stay vibration is an aerodynamic phenomenon that was relatively unknown until recently. The proposed cause of the vibration problem is the change in cross-sectional shape of the cable-stay that occurs when rain forms one or more beads, or rivulets, along the cable surface. This modified cross section affects the aerodynamics of the cable-stay and, as a result, large vibrations occur at wind speeds above the known vortex shedding wind speeds for cylindrical bodies. Typically the wind-rain-induced vibration problem has not received adequate attention from bridge designers. Excessive vibrations accelerate fatigue of the cable-stays and cause distractions to passing motorists.

Organized efforts have been made by engineers under contract to TxDOT to determine the vibration characteristic of cable-stays under ambient conditions. Generally, vibration has been observed in moderate to heavy rain at wind speeds of 15 m/s (34 mph) or less. When accompanied by rain, this phenomenon has been called “wind-rain-induced

vibration”, and has been observed in recent years on many cable-stayed bridges around the world. Excessive cable-stay vibrations can distress the cable-stays themselves and subject them to stress states for which they were not designed. Long-term fatigue damage to the cable-stays is another concern. In addition, the safety perception to the public is an important issue.

The Fred Hartman Bridge near Baytown, Texas and the Veterans Memorial Bridge near Port Arthur, Texas are long-span cable-stayed bridges. Large amplitude cable-stay vibrations have been observed numerous times at both of these bridges, usually during rain with relatively low winds. As a result of excessive cable-stay vibrations, a number of guide pipes of the cable-stays have been damaged.

In addition to this report, other researchers have documented cable-stay aerodynamic instabilities occurring during rain with wind events (Hikami et al., 1988). Occurrences of extreme vibration also have been observed with wind only (Main et al., 1999; Matsumoto et al., 1995).

### **1.3 Fred Hartman Bridge**

The Fred Hartman Bridge (Figure 1.1), also known as the Baytown Bridge, is a cable-stayed bridge that crosses the Houston Ship Channel and connects Loop 201 in Baytown with State Highway 225 in LaPorte, Texas. The total length of the bridge is 754 m (2475 ft) with five spans including a central span of 381 m (1,250 ft).



**Figure 1.1** Fred Hartman Bridge

Each of the bridge's twin decks is 24 m (78 ft) wide and is supported by two planes of inclined cable-stays arranged in a fanned configuration on each side of two diamond-shaped towers. Thus, there are eight planes of cables for the two decks with a total of 192 cables; each plane of cables consisting of 24 cables of variable lengths and diameters. Each cable-stay has a number of strands with cement grout housed inside a Polyethylene (PE) pipe. PE pipes from 11 to 18 cm (4.3 to 7.1 inches) in diameter are wrapped by weatherproof tape. The two concrete towers, supporting the twin decks side-by-side, are joined at the deck level. The composite deck consists of concrete roadway slabs that are stiffened by steel girders and transverse steel beams. The bridge was opened to traffic in 1995. The longest cable-stays are approximately 198 m (650 feet) in length. Cable-stay vibrations at the Fred Hartman Bridge have been observed to reach amplitudes of five times the cable diameter, or more.

The main parameters of the cable-stays that are of direct relevance to cable vibration and mitigation, such as cable length, cable-stay design tension and the fundamental frequency, are given for the Fred Hartman bridge in Table 1.1. The frequencies of higher modes are theoretically integer multiples of the fundamental frequency (i.e. first mode) and are not listed in this table.

**Table 1.1** Fred Hartman Bridge: Cable-Stay Geometry and Frequency (WDP, 1999)

<b>Cable-stay</b>	<b>Length (ft)</b>	<b>Design Tension (kips)</b>	<b>Fundamental Frequency (Hz)</b>
1	565.5	1147	0.668
2	559.4	1174	0.687
3	548.9	1002	0.655
4	493.6	729	0.720
5	449.4	828	0.810
6	406.1	699	0.864
7	364.1	440	1.032
8	323.9	585	1.104
9	286.3	456	1.255
10	252.5	405	1.355
11	223.0	346	1.794
12	197.1	341	1.700
13	195.3	371	1.944
14	220.9	359	1.545
15	251.1	427	1.523
16	286.5	485	1.263
17	326.0	538	1.096
18	368.4	614	1.000
19	412.7	720	0.944
20	458.3	753	0.838
21	505.1	861	0.770
22	552.5	797	0.700
23	600.6	963	0.654
24	649.1	1018	0.585

#### 1.4 Veterans Memorial Bridge

The Veterans Memorial Bridge (Figure 1.2) is located near Port Arthur, Texas. It provides for crossing over the Neches River on State Highway 87. The main structure of the bridge consists of five spans with a total length of 451 m (1,480 ft) including a central span of 195 m (640 ft). The bridge deck is a precast concrete box girder that is supported by four planes of cable-stays, each of which is arranged in a vertical harped configuration and anchored to the concrete tower. The bridge was opened to traffic in 1991. The design tension and the fundamental frequency for each of the 14 cable-stay lengths are given in Table 1.2



**Figure 1.2** Veterans Memorial Bridge

**Table 1.2** Veterans Memorial Bridge: Cable-Stay  
Geometry and Frequency (WDP, 2002)

<b>Cable-stay</b>	<b>Length (ft)</b>	<b>Design Tension (kips)</b>	<b>Fundamental Frequency (Hz)</b>
01	36.9	545	10.9
02	58.9	548	7.0
03	80.6	543	5.1
04	102.0	531	4.0
05	123.6	515	3.3
06	145.2	495	2.9
07*	166.8	478	2.5
08*	188.4	457	2.2
09	210.0	431	1.9
10	231.6	411	1.7
11	253.2	396	1.6
12	274.8	383	1.4
13	296.4	374	1.3
14*	318.0	369	1.2

*Note: Cable Stays C07, B08, B14 and C14 (B and C planes, see Figure 4.5), as indicated with an \* in this table, were instrumented by TTU with two 2-axis accelerometers each.*

### **1.5 Advisory Panel**

Concerns by TxDOT regarding the observed large amplitude vibration of cable-stays at both the Fred Hartman Bridge and Veterans Memorial Bridge prompted an evaluation of the in-service performance of these bridges. An advisory panel of university experts and consultants was assembled to assist TxDOT in conducting this evaluation in 1998. In addition to TxDOT, the advisory panel consists of:

- Whitlock, Dalrymple, Poston & Associates, Inc. (WDP).
- University of Texas at Austin (UT).
- Texas Tech University (TTU),
- Johns Hopkins University (JHU).

### 1.5.1 WDP & Associates, Inc.

WDP was charged with the responsibility of the field evaluation of damage caused by large amplitude cable-stay vibrations, as well as with overall program management and coordination duties. Prominent contributions by WDP are as follows:

- Vibration testing of stays to assess damage and characterization of cable-stay dynamics.
- Preparation of repair plans and specifications for a temporary restrainer system and repair of fatigue damage to guide pipes to Fred Hartman.
- Design, implementation and evaluation of prototype viscous dampers for cable-stay vibration mitigation at Fred Hartman and Veterans Memorial Bridges.
- Evaluation of a Freyssinet proprietary mechanical damper on selected stays at Fred Hartman.

A final report documenting the major accomplishments of research performed by WDP and JHU was submitted to TxDOT by WDP, April 30, 2001 (WDP 2001). TTU results presented in this 0-1400 final report compliment results presented in the WDP report. Retrofit installation tasks remain for WDP.

### 1.5.2 University of Texas at Austin

The principal contribution of the UT-Austin researchers has been in assessing the implication of large amplitude wind-rain-induced vibrations on the cable-stay grout and potential fretting and fatigue damage of the 7-wire strands that comprise an individual cable-stay. Several salient milestones from the UT work are as follows:

- Analytical study of the bending stresses and potential fatigue stress damage induced by large amplitude vibrations.
- Instrumentation and monitoring of grout and polyethylene pipe of selected stays at the Fred Hartman Bridge to assess potential damage and analytical model calibration.
- Development of a full-scale laboratory test to assess fatigue and fretting resistance of stays to large amplitude vibrations.

### 1.5.3 Texas Tech University

The principal areas of contribution by TTU researchers has been the aerodynamic characterization of the wind-rain-induced cable-stay vibration phenomenon, development of meteorological instrumentation for field studies, and the exploration of aerodynamic damping devices. Prominent milestones achieved from the TTU work are as follows:

- Review of literature to develop background on cable-stay vibration.
- Wind tunnel testing to characterize wind-rain-induced cable-stay vibrations.
- Wind tunnel evaluation and development of aerodynamic damping strategies for cable-stay vibration mitigation.
- Development of a 22-channel field instrumentation system for the Veterans Memorial Bridge and system monitoring.

- Evaluation of multiple “aerodynamic rings” as a prototype damper.
- Monitoring and analysis of the behavior of cable-stays both before and after ring installation.

Results of these tests and analyses of data are presented in this report.

#### 1.5.4 Johns Hopkins University

A principal contribution of JHU has been the development, implementation, and long-term monitoring of vibration instrumentation at both the Fred Hartman and the Veterans Memorial Bridges. Salient milestones from the JHU work are as follows:

- Development, implementation and maintenance of a 64-channel and a 24-channel system for vibration monitoring of Fred Hartman and Veterans Memorial Bridges, respectively.
- Continuous monitoring of field data acquisition systems for a period of over 3 years.
- Database development and management of more than 5,000 five-minute records from the Fred Hartman Bridge and of more than 3,200 five-minute records from the Veterans Memorial Bridge.

## CHAPTER 2

### CABLE-STAY VIBRATION BACKGROUND

#### 2.1 Chapter Overview

This chapter presents a thorough background of cable-stay aerodynamics and parameters relevant to the wind-rain-induced cable stay vibration phenomenon. The chapter includes initial TxDOT field observations of the Fred Hartman and Veterans Memorial Bridges taken in 1996. Cable-stay aerodynamic theory is presented, followed by field observations for a number of international cable-stayed bridges. The chapter concludes with an overview of currently available cable-stay vibration mitigation devices. Aerodynamic theory utilizes its own terms that are not typically common to bridge designers; a glossary of aerodynamic terms is given in Appendix A.

#### 2.2 Background

Cables used as bridge stays are usually made of high strength steel. They function as tensile structural members and are very flexible. Their inherent low structural damping in transverse oscillation, typically 0.1% of critical (Davenport, 1995), is easily overcome by aerodynamic influences. This combination of flexibility and low damping make the ordinarily smooth-surfaced circular cable-stays in cable-stayed bridges prone to excessive cross-wind vibrations. Contrary to what one might initially expect, it is not always the longest stays that have the most vibration problems. For a given plane of stays only two or three stays may vibrate, which are not necessarily adjacent to one another. The most extreme visible vibration occurs in one of the first three modes.

Hikami and Shiraishi (1988) tested a rigid model in simulated wind-rain-induced vibration condition to investigate the role of rain in cable vibrations. A 2.6 m long model with the same surface material (polyethylene pipe) and diameter (140 mm) as the original was used. Without simulated rain, cables with inclination angle,  $\alpha = 45^\circ$  and yaw angle,  $\beta = -45^\circ$  or  $45^\circ$  (see Figure 2.1) were found to be stable.<sup>1</sup> With simulated rain,  $\beta = -45^\circ$  was stable and  $\beta = 45^\circ$  was unstable. Vibrations with a steady amplitude of 11 cm (4.3 in) were observed for the latter in the wind speed range of 9 to 13 m/s (20 to 29 mph). Matsumoto et al. (1995) demonstrated the aerodynamic similarity between an inclined/yawed cable ( $\alpha, \beta$ ) and a yawed cable with  $\beta^*$ . They also argued that the axial flow in the wake of a yawed cable played an important role in cross-wind cable vibration. They concluded that in order for galloping instability to occur, the yaw angle must be greater than  $25^\circ$ .

---

<sup>1</sup> For an explanation of angles, refer both to Figure 2.1 and to Section 2.4.1.

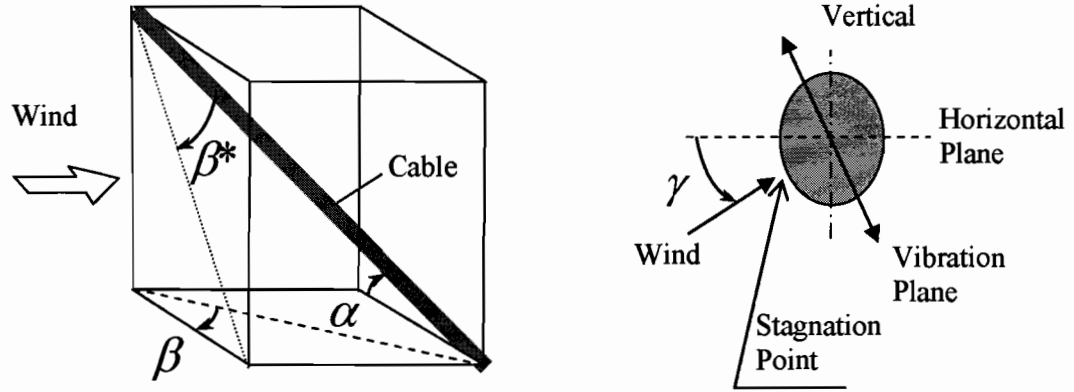


**Figure 2.1.** Yaw ( $\beta$ ), Inclination ( $\alpha$ ), Equivalent Yaw ( $\beta^*$ ) and Wind Attack ( $\gamma$ ) Angles.

The effect of artificial rain was also studied by Matsumoto et al. (1995) employing an artificial rivulet. The location of the artificial rivulet was characterized by an angle  $\theta$  measured from the stagnation point (line). This is illustrated in Figure 2.2.

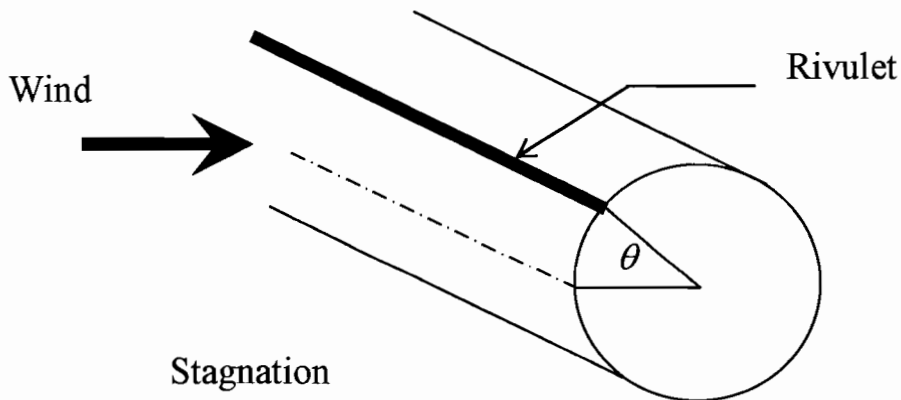


**Figure 2.2** Upper Rivulet on Cable-Stay

Parametric study of an artificial rivulet location indicated that the aerodynamic responses of a yawed cable were very sensitive to the location of the upper rivulet. Comparisons were also made with the responses of a bare cable. Cables, yawed or non-yawed, were found aerodynamically unstable for certain locations of the upper rivulet. The Scruton number and the turbulence level in the incident flow were reported to affect the cable's dynamic responses. Three types of cable responses were identified: a) "divergent", b) "velocity-restricted", and c) a combination of these two as shown in Figure 2.3.

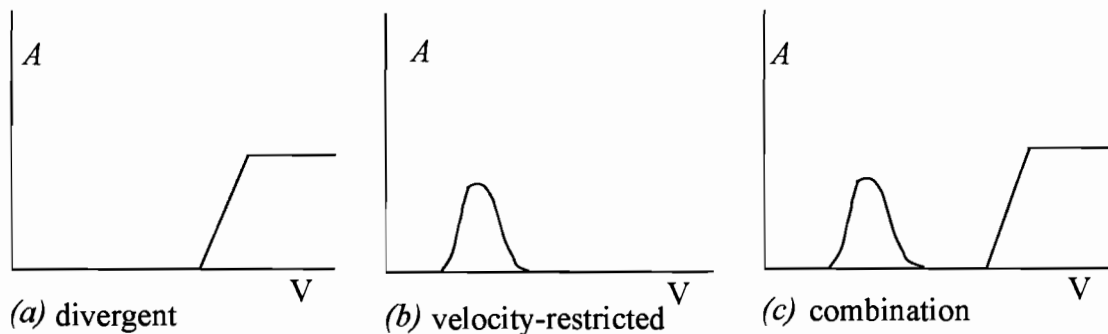


**Figure 2.3** Velocity-Restricted Behavior of Wind-Rain-Induced Vibration (V; velocity, A; amplitude)

### 2.3 Earlier TXDOT Field Observations

Prior to the commencement of this research project, TxDOT began to document the cable-stay vibration problem. Analysis of several vibration events videotaped by TxDOT at the Fred Hartman Bridge from April 1 to April 4, 1996 indicated that the cable-stay vibrations typically occurred in the first three modes. A summary of observations is cited in WDP (1998). The frequencies were estimated by counting the number of cycles during a fixed period of time. The limited information provided from the earlier field observations strongly suggested that large amplitude vibrations were due to the combined action of wind and rain. Information concerning wind speed, wind direction and precipitation was deemed essential to a more precise understanding of the environmental conditions when specific cables experienced large oscillations.

The fact that only a few neighboring cables experienced large amplitude vibration in a wind-rain-induced vibration condition at any one time seems to indicate that the formation of rivulet(s) governed the aerodynamic forcing on the cables within the wind speed range observed. This implication is supported by the following facts: (1) the neighboring cables are similar in terms of diameter, inclination, natural frequency and damping characteristics; (2) the location of the upper rivulet on the windward side is dependent on the balance of wind pressure, gravity, friction and surface tension acting on the rivulet.

Specifically, the wind speed and direction, the curvature/diameter and surface condition of cables are important factors in the formation and location of the upper rivulet. It is known that for a particular inclined cable, a continuous upper rivulet would form under a certain combination of all of these parameters.

Full-scale studies of the actual cause of the vibration are expensive, time consuming, inconvenient, and inevitably involve uncontrolled, randomly varying environmental factors. For these reasons, it is difficult to develop a full understanding of the mechanism of vibration based solely on full-scale studies. TTU researchers have investigated both full-scale studies and wind tunnel tests. The focus of the wind tunnel portion of this study was to observe the behavior of cable-stays in a more controlled wind tunnel environment by using section models.

## 2.4 Cable-Stay Aerodynamics

Theories and explanations on the mechanisms of cable-stay vibration put forward by researchers generally address three issues. They are (1) the aerodynamics of inclined cables, (2) the destabilizing role of axial flow in the wake of an inclined/yawed cable, and (3) the effect of the upper rivulet formation on the windward surface of the cable. In addition, a) high-speed vortex shedding, b) modal frequencies, c) dominant modes of vibration, d) low Scruton numbers, and e) aerodynamic damping and response parameters are considered responsible for some observed vibrations. Each is discussed in the following subsections.

### 2.4.1 Aerodynamics of inclined cables

Yawed and inclined cables generally can be considered (a) to be aerodynamically unstable and (b) to satisfy galloping criteria as a result of the generation of axial flow (along the axis of the cable) in the wake of the cable (Matsumoto et al., 1995). These criteria can occur in wind without accompanying rain.

#### *Inclination and Yaw Angles*

Two basic angular parameters, the cable-stay inclination angle  $\alpha$  and the yaw angle  $\beta$  (see Figure 2.1) are defined. The inclination angle  $\alpha$  is the angle the cable forms with the horizontal plane. The yaw angle  $\beta$  is defined as the angle between the cable's projection on the horizontal plane and the vertical plane normal to the wind direction. Yaw angle  $\beta$  is equal to  $0^\circ$  when the wind is perpendicular to the vertical plane containing the cable;  $\beta$  is greater than  $0^\circ$  when the wind is in the direction of cable descending as shown in Fig. 2.1.

Matsumoto et al. (1995) went further to study section model responses for yaw angles of  $0^\circ$  to  $45^\circ$  and found that the onset critical velocity that causes vibration is almost independent of yaw angle. In addition, the response of the cylinders increased with yaw angles up to  $45^\circ$ . From testing of inclined and yawed cylinders and comparing the results to yawed-only cylinders, Matsumoto et al. (1995) found that each case yielded essentially the same response. The equivalent yaw angle, actual yaw angle, and inclination angle, can be related geometrically as follows in Equation 2-1. Note that for  $\alpha = 0$ ,  $\beta = \beta^*$ .

$$\beta^* = \sin^{-1}(\sin \beta \cos \alpha) \quad [2-1]$$

where  $\beta^*$  = equivalent yaw angle on a horizontal plane,

$\beta$  = actual yaw angle, and

$\alpha$  = inclination angle.

In uniform flow, the aerodynamics of an inclined and yawed cable ( $\alpha$ ,  $\beta$ ) is equivalent to that of a yawed cable ( $0^\circ$ ,  $\beta^*$ ) having an inclination angle of  $0^\circ$  and a yaw angle of  $\beta^*$ .

### *Wind Angle of Attack*

The wind angle of attack  $\gamma$ , as defined in Figure 2.1, can be shown to be:

$$\gamma = \tan^{-1} \left[ -\frac{\sin \alpha}{\tan(90^\circ - \beta)} + \frac{\tan \phi \cos \alpha}{\sin(90^\circ - \beta)} \right] \quad [2-2]$$

where  $\phi$  is the angle that the mean wind vector makes with the horizontal plane.

$\alpha$ ,  $\beta$  are defined in Equation 2-1

Typically,  $\phi$  is approximately equal to zero.

### *Reduced Velocity*

For accurate wind tunnel analysis, the reduced velocity of the cable-stay section must be calculated. Reduced velocity, RV, is defined as follows:

$$RV = \frac{U}{nD} \quad [2-3]$$

where  $n$  = system natural frequency,

$D$  = characteristic dimension (diameter), and

$U$  = velocity of the oncoming flow.

Though it appears that the reduced velocity is simply the inverse of the Strouhal number, precise determination of the vortex shedding frequency is difficult. Therefore, since large responses are associated with vortex shedding during lock-in, where the vortex shedding frequency and system natural frequency match, the system natural frequency is used to define reduced velocity.

### *Summary of Relevant Recent Research*

Matsumoto et al. (1995) determined that an essential aerodynamic component of cable-stay vibration is coupling between vertical and horizontal vibration. This was based on full-scale observations as well as wind tunnel section model studies. A section model was restrained to vibrate along an inclined plane rather than the vertical plane, and an unstable response was observed.

Intuitively, as the yaw angle increases, so does the magnitude of axial flow in the wake of a cylinder. This axial flow interrupts the natural vortex shedding that occurs. Matsumoto et al. (1995) suggested that a possible mechanism of aerodynamic instability in cable-stays is the axial flow in the wake of a yawed cable (yawed with respect to the wind flow direction). It is suggested that the axial flow acts as a splitter plate that, when inserted in the wake of a yawed circular cylinder, causes an unstable response. The splitter plate (axial wind flow in the case of cable-stays) produces unsteady circular flow on the leeward side of the cylinder. This unsteady circular flow occurs above the splitter plate during downward motion of the cylinder and below the splitter plate during upward motion. The decreased pressure associated with the unsteady circular flow produces alternating positive

and negative lift cycles on the cylinder. The inclusion of a water rivulet on the upper windward portion of the cylinder further increases the separation of flow, thus supplementing the already occurring unsteady flow. This type of flow produces an effect similar to that of wake galloping, which has been observed in transmission lines (Hikami, 1988).

#### 2.4.2 Destabilizing role of axial-flow

Galloping instability occurs when the sum total of the inherent system damping and the aerodynamic damping produced by fluid flow about a body is negative, thereby producing a response that grows until the limit state of the nonlinear system is reached. This occurs for cables with or without an upper rivulet. The axial-flow velocity increases with oncoming velocity at a certain rate depending on the yaw angle  $\beta$  (Fig. 2.1). Galloping occurs when the axial flow reaches more than 30% of the approaching velocity. Galloping instability has been observed for  $\beta > 25^\circ$ . The instability appears to take place at  $RV \geq 70$ , irrespective of  $\beta$ . The worst response occurs at  $\alpha = 0^\circ$  and  $\beta = 45^\circ$  and decreases for lesser or higher values of  $\beta$ .

#### 2.4.3 Rivulet effect

The upper rivulet generally is an excitation factor, whereas the lower rivulet is a damping factor. In other words, the upper rivulet causes destabilization or stabilization of response depending on its position whereas the lower rivulet generally is stabilizing.  $\theta > 60^\circ$  is considered critical for  $\beta = 45^\circ$  (Matsumoto et al., 1995). Model tests by Bosdogianni and Olivari (1996) found that the shape of the rivulet did not change the response significantly and the position of the lower rivulet played an insignificant role. Flamand (1993) conducted wind-tunnel tests on a rigid model of diameter 16 cm (6.3 inches) covered with standard polyethylene (PE) casing. In order to simulate the rain formation and wind-rain-induced cable vibration, clean PE casing and PE casing with soot surface conditions were tested. In the wind speed range tested, 6 to 13 m/s (13 to 29 mph), the upper rivulet was observed to form only with PE casing plus soot at the wind speed of about 10 m/s (22 mph), and significant vibration with limited amplitude occurred. The soot was generated from fuel-oil combustion. It was designed to reproduce the deposition of atmospheric pollutants on cable-stays. The sooted cable surface was no longer water-repellent and therefore facilitated rivulet formation. The formation of an upper rivulet was observed only in the wind speed range of 7 to 12 m/s (16 to 27 mph).

In general, the maximum amplitude response of the velocity-restricted type tends to decrease and the onset velocity of galloping instability increases with increasing Scruton number (Matsumoto, 1998). Large amplitude galloping vibration can occur at Scruton numbers as high as 200, which implies that very high structural damping might be required to effectively suppress cable-stay vibrations, with or without rain, of prototype cable-stays at high natural wind speeds.

Hikami et al. (1988) studied a section model in the wind tunnel and simulated rain by using spray nozzles. Hikami et al. (1988) used the same wind speed and Reynolds number as the prototype, but the Scruton number (see Section 2.4.7) for the wind tunnel model was half that of the prototype due to differences in mass and damping.

Yaw and inclination angles in this study were  $\pm 45$  degrees each. The natural frequency of oscillation for this section model and suspension system was 2 Hz. As will be

described in Chapter 3, an unstable response was found for the case with rain where the wind was in the direction of declination, and a stable response was found for the case with rain where the wind was in the direction of inclination. The adverse response occurred in the wind speed range of 9 to 13 m/s (20 to 29 mph).<sup>2</sup> Hikami et al. (1988) also found that a more adverse response occurred for systems with frequencies of approximately 1 Hz. It was observed that at wind speeds below the onset velocity of cylinder vibration, the rain water droplets ran down around the circumference of the cable section forming a rivulet on the lower, leeward side of the cable. Above the onset velocity, a drag force acts upon the individual water droplets that overcome friction and gravity and an upper rain rivulet forms in addition to the lower rivulet. Focusing on the formation of the rain rivulets, Hikami et al. (1988) found that when the stay declines in the direction of the wind within a limited wind speed range, the upper windward rivulet forms in addition to the lower leeward rivulet. The aerodynamic force generated with the upper rivulet acted to excite the cable while the aerodynamic force generated with the lower rivulet acted to dampen the motion of the cable. As the stay vibrates due to upper and lower rivulet formation, the upper and lower rivulets oscillate with the same frequency as the cable motion (Hikami et al., 1988).

#### 2.4.4 High-speed vortex shedding

Matsumoto et al. (1995) considered high speed vortex shedding as a phenomenon that could cause excessive vibration. During high speed vortex shedding, non-coherent von Karman vortex sheets shed at different frequencies ( $n_1, n_2$ ) along the yawed cylinder length. At random intervals, a single von Karman vortex sheet is shed coherently along the entire length of the cylinder whose frequency is lower than that of the smaller, non-coherent vortices ( $n_s = n_1 - n_2$ ). Neither axial flow or formation of a rivulet is a requirement for this to occur. The intermittent 2-D von Karman vortices that are shed at a frequency  $n_s = n_1 - n_2$  correspond to a reduced velocity (RV) of 40, or any integral multiple of 40.

Perhaps contrary to the work of Hikami (1988) and Matsumoto (1995), Verwiebe (1998) emphasized the importance of the rain water rivulet in changing the forces on the cable-stay. Verwiebe (1998) presented evidence that the effective shape of the cross section of the cable-stay depends on the momentary location of the rain water rivulet(s). The rivulet(s) oscillates around the cable-stay surface and changes shape continuously, thus modifying the cross sectional shape in a time dependent manner. As the cross-sectional shape varies with time, so do the pressure distribution on the cylinder surface and the resulting forces on the cable-stay. If the wind force incident upon the cable is varying with the same frequency as the cable oscillation and with the same sign, then positive work is done and vibration of the cable system ensues. Verwiebe (1998) suggests that initial oscillation of the cylinder is required before the positive work done by the rain and wind interaction can cause an increase in the cable-stay oscillations. The range of wind speeds where oscillation occurs is about 5 to 20 m/s (11 to 45 mph) — which includes the speeds reported in previous experiments of Hikami et al. (1988) and Matsumoto et al. (1995). Note that Verwiebe (1998) performed experiments at yaw angles of 0° and 90° with inclination of 30° only and the frequency of vibration was 8.9 Hz, which is well above the frequency of 2 Hz or less used by Hikami et al. (1988) and Matsumoto et al. (1995). Verwiebe (1998)

---

<sup>2</sup> Actual wind speeds, rather than the non-dimensional reduced velocity (RV), are used when precise data of the testing apparatus is not available.

argues that the motion of the rivulets is paramount to the excessive vibration of the cable system and points out that studies on fixed cross sections may only yield instantaneous results and show galloping instability which is not the actual phenomenon.

#### 2.4.5 Modal frequencies

In the field, natural vibration modal frequencies and damping values of the cable-stays generally are determined by manually exciting the cable-stay and analyzing the resulting vibration data taken from accelerometers attached to the cable-stay. Reported natural frequency values vary from 0.6 Hz for the longest Fred Hartman cables and up to 11 Hz for the shortest Veterans Memorial cables (Whitlock, Dalrymple, Poston, and Associates, 1999). Damping values in modes 1 to 3 ranged from 0.15% of critical for the longest stays to 0.6% of critical for the shortest stays. Flexibility and low inherent damping combine to make the cable-stays vulnerable to vibration caused by exterior influences such as wind and rain.

The natural vibration occurring during a pure wind condition appears to differ from the von Karman vortex oscillation phenomenon. The frequency of vibration is well below the critical frequency of von Karman vortex shedding for a cylindrical body (Hikami et al., 1988). It has also been observed that most of the large amplitude stay vibration occurs when the wind is in the direction of declination of the stays (Hikami et al., 1988; Main et al., 1999). Significant vibrations also occur for winds in the direction of stay inclination, but do so during instances of very heavy rainfall (Main et al., 1999). Hikami et al. (1988) observed that at low wind speeds during rainy conditions, the water droplets that contact the stay collect and form a rivulet on the lower surface of the stay. This rivulet oscillates circumferentially with the same frequency as the stay vibration. Within a certain wind speed range, 8-15 m/s (18-34 mph), two rivulets may form on the upper and lower portions of the stay. Large amplitude vibration during rain and wind events occurred in the same wind speed range (Hikami et al., 1988). This “velocity-restricted” response was also evident in the full-scale measurements of Main et al. (1999). Most studies to date have suggested that the predominant vibration occurs transverse to the oncoming flow; however, full-scale data reported by Main et al. (1999) have shown that the stay oscillations under rainfall actually have a degree of two-dimensionality. That is, the stays vibrate in an elliptical pattern rather than a predominately vertical pattern. As will be discussed in the next chapter, TTU researchers developed a 2-D force damper apparatus precisely to capture this elliptical pattern in the wind tunnel model analysis (see Section 3.2).

#### 2.4.6 Dominant modes of vibration

Main and Jones have instrumented the Fred Hartman, where significant wind-rain-induced vibrations have occurred (Main, et al., 1999). “Triggered” events are recorded when a predetermined acceleration and/or wind speed threshold is exceeded. It has been noted that each individual cable seems to vibrate at a particular lower-mode shape. For example, a long Fred Hartman cable-stay, 183 m (601 ft) in length with a fundamental frequency of 0.65 Hz, vibrates predominately in the 3<sup>rd</sup> mode, though not in the first two. Similarly, a mid-length Fred Hartman cable-stay, 87 m (286 ft) in length with a fundamental frequency of 1.2 Hz, has been found to vibrate predominately in the 2<sup>nd</sup> mode, though not in the first.

Higher modes of vibration in the cables also have been found on both the Fred Hartman and the Veterans Memorial. It is generally accepted—though unproven—that cables vibrating in lower modes cause more damage than cables vibrating in higher modes, since lower-mode vibrations generally cause larger displacements. However, it is entirely possible that higher mode vibrations occur often enough and produce greater deflection curvature, to produce significant fatigue loadings, and possibly even greater loadings, on the cable-stays due to cycles of reversed stressing.

Considering the physics of the rivulet formation, it is difficult to conceive that the rivulet is consistently located at the most critical location along the full cable length. It is possible that the rivulet primarily causing the vibration at the lower wind speeds forms at the critical location only over a partial cable length. This could explain why there is a preference for certain lower-modes to vibrate.

#### 2.4.7 Scruton number

The Scruton number is an important parameter in model tests. It is a non-dimensional parameter that reflects the a) relative effects of excitation force, b) mass/stiffness property and c) damping characteristics of the dynamic responses of a cable-stay in wind. Researchers use the Scruton number to relate wind tunnel tests of scale section models to full-scale cable behavior. The Scruton number<sup>3</sup> is defined in this report as follows:

$$Sc = \frac{4\pi m \zeta_m}{\rho D^2} \quad [2-4]$$

where  $m$  = mass per unit length of the cylinder,

$\zeta_m$  = critical damping ratio (mechanical),

$D$  = diameter of the cylinder, and

$\rho$  = air density.

In general, the maximum amplitude response of the velocity-restricted type tends to decrease and the onset velocity of galloping instability tends to increase with an increasing Scruton number (Matsumoto, 1998). Large amplitude galloping vibration can occur at Scruton numbers as high as 200, which implies that very high structural damping might be required to effectively suppress cable vibrations, with or without rain, of prototype cable-stays at high natural wind speeds.

#### 2.4.8 Aerodynamic damping and response parameters

The Glauert-Den Hartog criterion for galloping is based upon static-force coefficients. However, the galloping phenomenon can be also described as an aeroelastic instability that is similar to the single-degree-of-freedom (SDOF) flutter found in the linearized domain; true for incipient motions only. Thus, the critical speed for the onset of galloping can be precisely found by the flutter theory.

---

<sup>3</sup> Sometimes the Scruton number is defined without the  $4\pi$  term shown in Equation 2-4.

The cause of the SDOF flutter can be explained by an overall, or total, damping  $\zeta_T$  of a structural system. It is a summation of the mechanical damping  $\zeta_m$  and the aerodynamic damping  $\zeta_{aero}$  of the system, and can be written as:

$$\zeta_T (RV) = \zeta_m + \zeta_{aero} (RV) \quad [2-5]$$

In Equation 2-5,  $\zeta_m$  is measured at zero wind speed and  $\zeta_{aero}$  is dependent on a reduced velocity, RV. The aerodynamic damping ( $\zeta_{aero}$ ) is a function of the cross-sectional shape of the structure and is often plotted as a non-dimensional number  $H_1^*$  (RV), known as a flutter derivative. A more detailed description of flutter derivatives can be obtained in Simiu and Scanlan (1996). Eight flutter derivatives including the  $H_1^*$  were used in the analysis of bridge-deck flutter (Sarkar, 1992).  $H_1^*$  (RV) can be defined as:

$$H_1^* (RV) = \frac{4m(\zeta_m - \zeta_T (RV))}{\rho B^2} = \frac{-4m\zeta_{aero} (RV)}{\rho B^2} \quad [2-6]$$

where  $\rho$  is the density of air,

$m$  is the mass per unit length of the structure,

$B$  is the representative across-wind or along-wind dimension of the cross section.

Other terms in Equation 2-6 are defined in Equation 2-5. A positive  $H_1^*$  (RV) is an indication of aeroelastic instability or SDOF flutter. The critical reduced velocity,  $RV_{cr}$ , is the value of RV at which  $\zeta_{aero}(RV)$  is negative so as to nullify  $\zeta_m$  (i.e.,  $\zeta_T = 0$ ).  $RV_{cr}$  gives the value of critical wind velocity  $U_{cr}$  at which aeroelastic instability or initiation of large vibration occurs.

While  $H_1^*$  can be obtained from wind-tunnel tests using section models, the aerodynamic damping in any particular mode of vibration of the prototype cable can be predicted by:

$$\zeta_{aero} = -\frac{\rho D^2}{2mL} H_1^* \int_0^L \psi^2(x) dx \quad [2-7]$$

where  $m$  is the mass per unit length of the cable,

$L$  = length of the cable

$D$  = diameter of the cable, and

$\psi(x)$  is the mode shape of the cable.

Since the mode shapes of a cable are sinusoidal, the value of the integral in Equation 2-7 is  $L/2$ . The total damping of the cable can be calculated using Equation 2-5.

## **2.5 Previously Reported Field Observations on Bridges**

Though field observations of the cable-stay vibration problem have become somewhat more common recently, traditionally, documented cases have been relatively rare. The following documents major recorded cable-stay vibrations divided into appropriate subsections.

### 2.5.1 Velocity-restricted vibrations

Cable-stay vibrations on the Brotonne Bridge, with a central span of 320 m (1050 ft), over the Seine River in France have occurred at a wind speed of about 15 m/s (34 mph) at 20° to 30° with respect to the bridge axis (Wianecki 1979). Also on the Meikonishi Bridge, with a main span of 405 m (1330 feet) in Japan, cables that experienced no significant vibration under wind action alone were observed to experience large-amplitude oscillations in wind-rain-induced vibration conditions (Hikami and Shiraishi 1988). Wind-rain-induced vibrations were at much lower frequencies with much higher amplitudes than that of the vortex-induced vibrations. It seems that there was a range of wind speeds, 7 to 15 m/s (15 to 34 mph) and a narrow range of wind angles that induced significant vibration for individual cables. The observed frequency range was 1 to 3 Hz. Typical diameter of the cables was 14 cm (5.5 in). Vibrations occurred when cables were declined in the direction of wind. Only PE (polyethylene) tube lapped cables with 14 to 20 cm (5.5 to 7.9 inch) diameters experienced wind-rain-induced vibrations, Matsumoto et al. (1992). Wind-rain-induced vibrations occurred at a reduced wind velocity, RV, in the range of 20 to 90, i.e. 6 to 18 m/s (13 to 40 mph). At the time of large-amplitude vibrations, wind was blowing skewed to the bridge axis. Also, cables that were located on the leeward side of the bridge pylons vibrated. Vibrations were almost in-plane. Maximum amplitude was up to 2 m (6.6 ft). At the Tenpozan Bridge in Japan, Matsumoto et al. (1995) observed that the longest cable of 186 m (610 ft) experienced wind-rain-induced vibration in the first and second modes in the velocity range of 8 to 12 m/s (18 to 27 mph). The amplitude of the second mode vibration was lower, approximately  $\frac{1}{4}$  that of the first.

### 2.5.2 Single-moded vs. multiple-moded vibration

Cable vibrations up to the third mode were observed on the Brotonne Bridge, Wianecki (1979). Also, eye-witness accounts, observed from approximately 100 m (328 ft) from the bridge, reported vibrations of 30 cm (12 in) in single amplitude in the first mode. On the Meikonishi Bridge, cable-stay vibrations were mostly of a single mode, and there were only a few occasions that two or three modes were involved (Hikami and Shiraishi 1988). Power spectrum density diagrams of the response of the longest cable on the Higashi Kobe Bridge indicated multiple-moded vibration at reduced velocities of approximately 400, 200, 120, 80 and 40 (Matsumoto et al. 1995). Cable-stay vibrations were usually multiple-moded, non-stationary and exhibited wave-propagation type oscillations (Matsumoto et al., 1998).

### 2.5.3 High wind speeds without rivulet formation

At a mean wind speed of 40 m/s (89 mph) on the Higashi-Kobe Bridge, the inclined cables having 12 axial protuberances, were observed to experience vibrations similar to wind-rain cable vibrations. The axial protuberances were designed to suppress wind-rain-induced vibrations. In this particular case, rivulets did not form because of the surface treatment. It was not certain if the response was velocity-restricted or not, Matsumoto (1998).

### 2.5.4 Effect of rivulet

At the Meikonishi Bridge in Japan, cable-stays that were stable in windy conditions vibrated significantly in wind-rain conditions (Hikami and Shiraishi, 1988). Water rivulet formation on the lower surface of the cable-stays was observed in the field. The lower rivulet was shifted to the leeward side and oscillated in the circumferential direction of the cable-stays. Later laboratory tests on a rigid cable model having the same diameter and surface conditions as the prototype revealed the formation of another rivulet along the upper windward surface of the cable when the cable was descending in the direction of wind. According to Matsumoto et al. (1995), inclined cables in the leeward side of a bridge pylon can have both an upper and a lower rivulet. The balance of the gravity force, wind pressure and water-surface tensile force acting on the rivulet determined the location of the upper rivulet. Upper rivulets at certain locations were aerodynamically destabilizing.

### 2.5.5 Effects of turbulence

Matsumoto et al. (1992) noted that all the five bridges on which cable vibrations of large amplitude occurred were located near or facing the sea, i.e., the turbulence level in the approaching wind was quite low. The turbulence could play different roles in either reducing the amplitudes (stabilizing effect) or reducing the critical-onset velocity (destabilizing effect) depending on the yaw angle, presence of rivulet, etc.

### 2.5.6 Low-damping in lateral oscillation of cable-stays

Hikami and Shiraishi (1988) reported that a critical damping ratio of 0.1% to 0.4% was measured for the cable-stays of the Meikonishi Bridge. A damping ratio of 0.5% or above might be needed to effectively suppress cable vibration of the velocity-restricted type (Geurts et al., 1998). Much higher damping might be needed to reduce cable vibrations at high wind speeds (Matsumoto, 1998).

### 2.5.7 Reynolds number effect

Many cable vibrations have been observed in the range of Reynolds number of 60,000 to 200,000, i.e. the sub-critical range. The combination of the wind speed range of 7 to 15 m/s (15 to 33 mph) and the cable diameter range of 8 to 20 cm (3 to 8 in) might be associated with the importance of the Reynolds number to velocity-restricted vibrations at relatively low wind speeds (Matsumoto, 1998).

## **2.6 Mitigation Devices**

Currently, cable-stay oscillations caused by wind-rain-induced aerodynamic forces are controlled by one, or a combination of the following methods: (1) single-point

mechanical dampers, typically at the base of each cable, (2) restraining cable devices connecting adjacent cables at various locations along the length of the cable, resulting in a reduced effective length for each cable and/or (3) aerodynamic damping approaches such as grooves, protuberances or circular rings. The former method is considered a “concentrated” damping mechanism, while the latter two are considered “distributive.”

### 2.6.1 Single-point mechanical dampers

The traditional method—and the currently selected Fred Hartman retrofit solution—is a combination of passive single-point mechanical dampers and restraining devices. Mechanical dampers generally are linear viscous mechanisms, somewhat similar to an automobile shock absorber. However, they also can be non-linear, computer-controlled mechanisms. Mechanical dampers are a proven technology. However, they generally: (1) can be expensive to install, (2) may need periodic maintenance, and (3) typically require substantial cable-stay displacements to occur before the damping mechanism becomes functional.

### 2.6.2 Restrainers

Restrainers are employed to tie adjacent cable-stays together at discrete points along the cable. Restrainers are effective solutions because one cable adjacent to another oscillating cable generally will not be oscillating. (However, this may not hold true for parallel cable systems like the Veterans Memorial.) When adjacent cables do oscillate together, many times they will vibrate out of phase or in different modes from each other. In these typical cases, restrainers are able to utilize the stiffness of adjacent cables to prevent a particular cable from oscillating. If the restrainer is unable to prevent oscillations, it continues to be considered beneficial in that it causes the cable-stay to vibrate at higher modes, with less deflection amplitude, as it “fixes” intermediate nodal points. Again, though a higher mode vibration is visually less dramatic, significant fatigue loadings can occur. Restrainers also are a proven technology. However, they are fairly difficult to install—particularly at cable-stay heights generally required. Also, restrainers have had problems due to failure through loosening of the attachments to the cable-stays.

### 2.6.3 Aerodynamic devices

While mechanical dampers and/or restrainers are effective, they require routine maintenance and can be costly to implement. Also, they can decrease the aesthetic appeal of a cable-stayed bridge. Further, mechanical dampers typically can be optimized for a few modes of vibration only. Therefore, it may be desirable to determine a solution to the cable-stay vibration problem through aerodynamic means.

Aerodynamic devices potentially have certain advantages. They a) can be effective over a wide range of wind speeds, and may perform even better at higher wind speeds, if properly designed; b) are generally cost-effective and demand little maintenance efforts, thus they can function reliably; c) can function over a wide range of vibration modes, d) can be designed to be aesthetically pleasing; and e) can reduce the effect of the aerodynamic forces before the cable-stay begins to vibrate substantially, where mechanical devices must dissipate energy of the cables that are already vibrating.

Various forms of aerodynamic solutions to the vibration of smooth-surfaced, circular cables have been sought. While some can be adopted only at the design stage, others are feasible for retrofitting as well. Aerodynamic countermeasures usually modify the surface of the cable-stay cross section to improve its aerodynamic performance in terms of reducing the excitation from the moving air or increasing the aerodynamic damping. Matsumoto et al. (1995) listed three types of cable-stay surface/cross section modifications: 1) surface dimpling, 2) parallel axial protuberances, and 3) elliptical plates. A variation of the elliptical plate is helical strake which has been used successfully on chimneys to reduce vortex-induced vibrations. Figure 2.4 shows some aerodynamic countermeasures investigated by Matsumoto et al. (1997).

In practical applications of aerodynamic countermeasures, helical wires have been used at the Normandy Bridge; axial protuberances were successfully designed to reduce the cable vibrations at low wind speeds on Higashi Kobe Bridge; dimpled surface treatment has been made on the Tataru Bridge according to Matsumoto (1998). On the other hand, rigid model tests conducted by Matsumoto et al. (1997) found that elliptical plates could be very effective in reducing the dynamic response of a cable. In a model test by Flamand (1993), wires of diameter 1.5mm were introduced to a model cable of 100 mm at intervals of  $30^\circ$  to disrupt the circumferential motion of the rivulet. Spiral (helical) wires were also tested. Combinations of different wire diameters and pitches were studied. The wire of 1.3 mm wound at 0.3 m pitch was found to be the most effective. Double helix was also tested.

These aerodynamic devices are designed to prevent the formation of a continuous upper water rivulet, which was considered to make the cross section aerodynamically unstable, or to interrupt the axial flow in the wake of an inclined cable. The axial flow was considered responsible for instability of cables at high wind speeds without the rain.

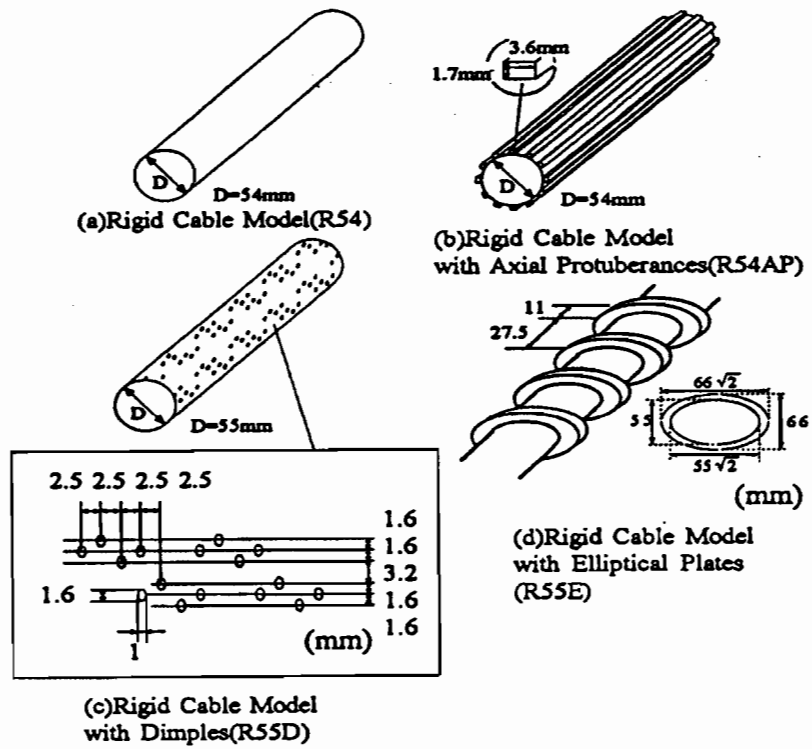


Fig. 2.4 Various aerodynamic countermeasures investigated by Matsumoto et al.



## CHAPTER 3

### TTU WIND TUNNEL TESTS

The TTU wind tunnel studies conducted in Colorado State University and Texas Tech University wind tunnels investigated helical strakes, elliptical rings and circular rings. Wind tunnel tests were conducted on elastically supported section models of the cable-stays. The section models were allowed either one-degree (vertical oscillation), as reported in Sarkar et.al. (1998), or two-degrees of freedom (vertical and torsional oscillation), as reported in Sarkar and Gardner (2000). The focus of this portion of the research project has been to observe the characteristics of cylinder oscillation under the influences of rain and wind and to determine the mechanism of flow about the cylinder that causes adverse vibration. In addition, based on these wind tunnel studies, methods to control the vibrations of the cable-stays have been proposed. To simulate varying wind directions incident upon the cable-stays, the section models were tested with various yaw angles.

The primary goal of the wind-tunnel tests has been to study the effectiveness of cable-stay mitigation devices, i.e., helical strake, elliptical ring and circular ring, in reducing the amplitude of vibration to an acceptable level. A parametric study of these devices was performed (diameter, pitch, etc.) to find optimum configurations. A secondary goal has been to identify the aerodynamic damping with and without mitigation devices in order to quantify the amplitude of vibration and the critical speed for the onset of vibration in the prototype.

Experimental designs, wind tunnel tests conducted in CSU and TTU wind tunnels, and results are reported in this chapter.

#### 3.1 Past Observations on Wind Tunnel Models

A great deal of information was known prior to this study—some of which was verified during the current TTU wind-tunnel tests. It is a well known fact that yawed or yawed and inclined (i.e. yawed-inclined) cables (without rain) have a tendency to exhibit galloping beyond a critical wind speed because of the axial flow that is generated in the wake of the cable. These cables exhibit only divergent-type response at higher wind speeds. In addition, an upper rivulet can form at relatively low wind speeds to make the cable-stay prone to large-amplitude vibration.

Both elastically supported rigid models (or section models) and flexible models of cable-stays have been used in wind-tunnel tests to assist in understanding the fundamental features of cable vibration. Most researchers have employed rigid models. In the case of rigid model tests, yawed models and yawed-inclined models have been utilized. These two types of models are aerodynamically similar. The advantage of rigid models is that they are easier to build and set up. They have been useful to reveal the most essential features of wind-rain-induced cable vibration. The main disadvantage is their incapability of realistically reproducing coupled vibrations of more than one mode. This is a limitation in the modeling as slender cables contain multiple lateral modes of vibration and can be excited to vibrate in combinations of different modes.

### 3.1.1 Response of elastically supported rigid models

A rivulet at an angle  $\theta$  from the stagnation point from the given wind direction was shown previously in Figure 2.2. At an upper rivulet angle of approximately  $\theta = 70^\circ$ , the cable can vibrate severely. Though lower rivulets also form, these do not appear to produce instability. Considering the elliptical cable cross-section along the wind direction, combined with the “bulge” of the upper rivulet, one can see that an “airfoil shape” becomes the leading edge into the wind. Thus, for a declining cable-stay, lift is produced.

Sketches shown in Figure 2.3 suggest that cable responses can be divergent and/or velocity-restricted. For bare cables, divergent responses were observed only for yawed angles greater than  $25^\circ$ . Depending on the location of the artificial rivulet, models might exhibit both types of response or no significant response at all. While the introduction of an artificial rivulet is convenient and instrumental in the understanding of the role of the rivulet in prototype cable vibrations, it must be understood that rivulets form on real cables only under certain combinations of wind direction, wind speed, cable inclination, cable surface condition, etc. Further, rivulets on prototype cables were observed to be oscillating in the circumferential direction, and thereby interacting with the cable motion, whereas the artificial rivulet is stationary. Therefore, caution must be exercised when interpreting the wind-tunnel results from model tests using an artificial rivulet.<sup>4</sup>

A possible explanation of the velocity-restricted response as observed in the full-scale monitoring of the vibrations at low wind speeds follows. The scenario is wind accompanied by rain. For commonly encountered inclined cables with diameters varying between 8 to 20 cm (3 to 8 inches), as wind speed increases beyond 7 m/s (15 mph), an upper rivulet can form on cables that are descending in the wind direction. The mean location of the rivulet shifts away from a stationary point with increasing wind speed. When the rivulet is formed at certain locations, the cable shows a tendency to have a divergent response and exhibits galloping with large amplitude motion. The large-amplitude motion remains limited because the cable has a non-linear stiffness. Not all cable-stays in a cable-stayed bridge will exhibit this behavior at the same time as they have different attitudes toward the wind. As the wind speed increases further, the upper rivulet shifts further away from the stagnation point and is eventually blown off the cable at a wind speed greater than 15 m/s (33 mph). Thus, the mechanism that caused the aeroelastic instability disappears. The result is a velocity-restricted response within 7-15 m/s wind speed. Beyond 15 m/s of wind speed, the rivulet is out of the scenario and some inclined and yawed cables will still have a tendency to exhibit large amplitude vibration, but only beyond a critical speed. The large amplitude motions will not reduce with increasing wind speed as occurred in the lower-wind speed range. The actual motion of the cable is along an inclined plane depending on the angle of attack and is more complex than SDOF galloping-type response because of either the interaction of the oscillation of the rivulet with the cable motion or the cable’s richness in vibration modes.

### 3.1.2 Response of flexible models

Results from wind-tunnel tests on a flexible cable model are reported by Matsumoto (1998). Depending on: a) the wind speed, b) different modes, or c) combinations of the two,

---

<sup>4</sup> Nonetheless, when one compares field results presented in Chapter 5 of this report with the wind-tunnel results presented in this chapter, strong similarities in cable-stay behavior are observed.

the cable model can be excited. The general tendency is that higher modes are excited at higher wind speeds. Wave-propagation type cable vibrations also have been observed.

### 3.2 CSU Wind Tunnel Tests

The primary goal of the wind-tunnel tests was to study the effectiveness of the mitigation devices, i.e., helical strake, elliptical ring and circular ring, in reducing the amplitude of vibration to an acceptable level. A parametric study of these devices was performed (diameter, pitch, etc.) to find optimal configurations. The secondary goal was to identify the aerodynamic damping with and without the mitigation devices in consideration in order to quantify the amplitude of vibration and the critical speed for the onset of vibration in the prototype.

#### 3.2.1 Experimental Design and Wind-Tunnel Tests

The test setup (Fig. 3.1) consisted of a yawed (in horizontal plane) section model of a cable (10.2 cm or 4" diameter and 0.97 m or 3'-2" length) that could vibrate in a vertical plane along a single degree of freedom.

To simulate three-dimensional effects of the wind-model interaction, the model was tested without any end plates. The model was suspended elastically (with springs) from a pair of force balances fixed to two separate small frames. This force balance-spring-model combination was fixed to an outside frame 1.73m x 1.73m (5'8" x 5'8") in cross section and 1.37m or 4'6" in depth (along-wind dimension). The dimensions of the outside frame were chosen to fit inside the 1.83 m x 1.83 m (6' x 6') Meteorological Wind Tunnel (MWT) at Colorado State University (CSU).

All dynamic tests were performed with the model fixed at  $\alpha = 0^\circ$  and  $\beta = 37^\circ$  in smooth flow without any rain (Fig. 3.1). This was the maximum value of  $\beta$  obtained with the experimental setup which was close to the worst case as reported in earlier studies ( $\alpha = 0^\circ$  and  $\beta = 45^\circ$ ). The effect of the upper rivulet on the stability of vibration was studied by fixing an artificial rivulet (semi-elliptical cross section, 10 mm in width and 5 mm in height) on the upper side of the model (Fig. 3.2) Two locations with angles of  $\theta = 65^\circ$  and  $70^\circ$  (Fig. 2.1) were tested to verify the effect of the location on the stability. The model was tested with and without any mitigation devices. The effect of the Scruton number on the amplitude was tested as well. The first set of experiments were done with a low Scruton number,  $Sc = 7.6$  ( $m = 3.02 \text{ kg/m}$ ,  $\zeta_m = 0.25\%$ ,  $D = 0.102 \text{ m}$ ,  $n = 1.0 \text{ Hz}$ ), and the second set of experiments were performed with a high Scruton number,  $Sc = 54.6$  ( $m = 7.85 \text{ kg/m}$ ,  $\zeta_m = 0.69\%$ ,  $D = 0.102 \text{ m}$ ,  $n = 1.0 \text{ Hz}$ ). The Scruton number for cable A23 of the Fred Harman bridge (next in length to the longest cable A24) is estimated as  $Sc = 44.7$  ( $m = 74.7 \text{ kg/m}$ , assuming the first-mode damping  $\zeta = 0.15\%$ ,  $D = 0.16 \text{ m}$ ).

The experimental setup was chosen as a single-degree-of-freedom (vertical) model, similar to the majority of past researchers. Although this simple setup does not capture all the features of the motion of the prototype cables under wind and rain, it does capture the aerodynamic phenomena causing instability and the effectiveness of the devices in damping out the motions.

#### 3.2.2 Aerodynamic Devices Tested

The aerodynamic devices tested are (i) Aerodynamic Plate-Damper (Fig. 3.3a), (ii) Helical Strake (Fig. 3.3b), (iii) Elliptical Ring (Fig 3.3c), and (iv) Circular Ring (Fig. 3.3d).

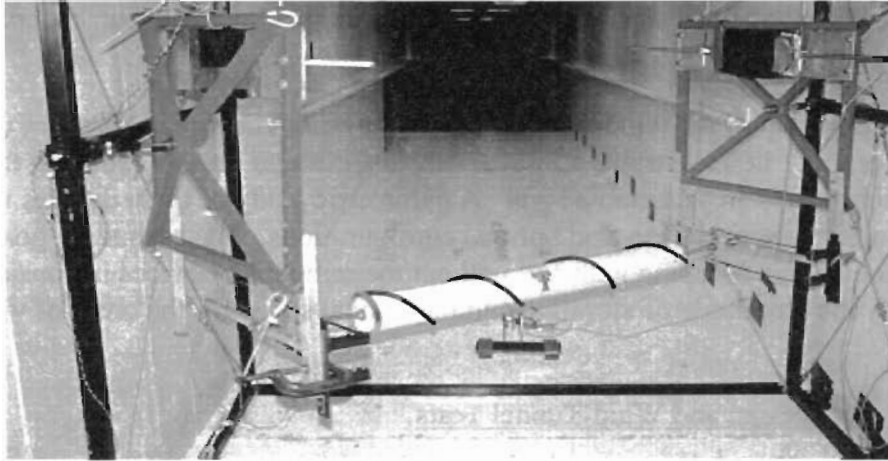


**Fig. 3.1** Wind-Tunnel Model Setup in the Meteorological Wind Tunnel at CSU (viewing downstream)

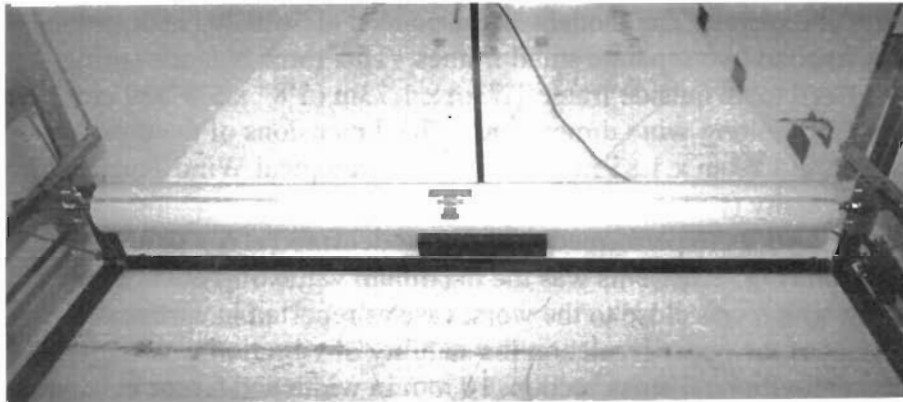
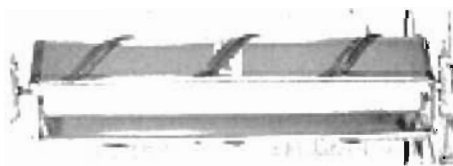
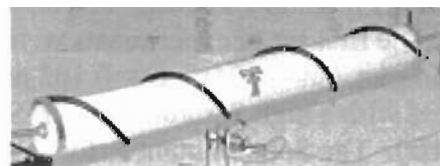


**Fig. 3.2** Model at  $\alpha=0^\circ$  and  $\beta=0^\circ$  showing an artificial-upper-water rivulet



a. Aerodynamic Plate Damper



b. Helical Strake ( $\setminus$  orientation)



c. Elliptical Ring ( $\setminus$  orientation)



d. Circular Ring

**Fig. 3.3** Aerodynamic devices tested

The width of the plate damper was  $3D$  with  $0.5D$  spacing between the center of the plates and the model. Wires of  $D/20$  diameter were fixed on the plates as shown in Fig. 3.3a to prevent the formation of water rivulets. The elliptical rings were made out of wires of  $D/20$  diameter placed at  $45^\circ$  angle to the axis of the model at  $1.5D$  spacing (Fig. 3.3c). These were inclined counterclockwise if viewed in the along-wind direction ( $\backslash$ ). The reverse inclination ( $/$ ) was also tested. Helical strakes were made of wires that were helically wound around the model (Fig. 3.3b). Two different wires of diameters  $D/20$  and  $D/8$  placed at a pitch of  $1.5D$ ,  $3D$ , and  $5D$  were tested. The helical strakes were also tested in both orientations ( $\backslash$  and  $/$  as viewed in the along-wind direction). The inclination angle ( $\phi$ ) of the helical strake with respect to the axis of the model can be calculated as  $\phi = [\tan^{-1} (\text{Circumference of the model/Pitch of helical strake})]$ . Fig. 3.3c shows a  $D/8$  helical strake at a pitch of  $3D$  ( $\backslash$  orientation). The angle  $\phi$  for this case can be calculated as  $\tan^{-1}(\pi/3) = 46.3^\circ$ .

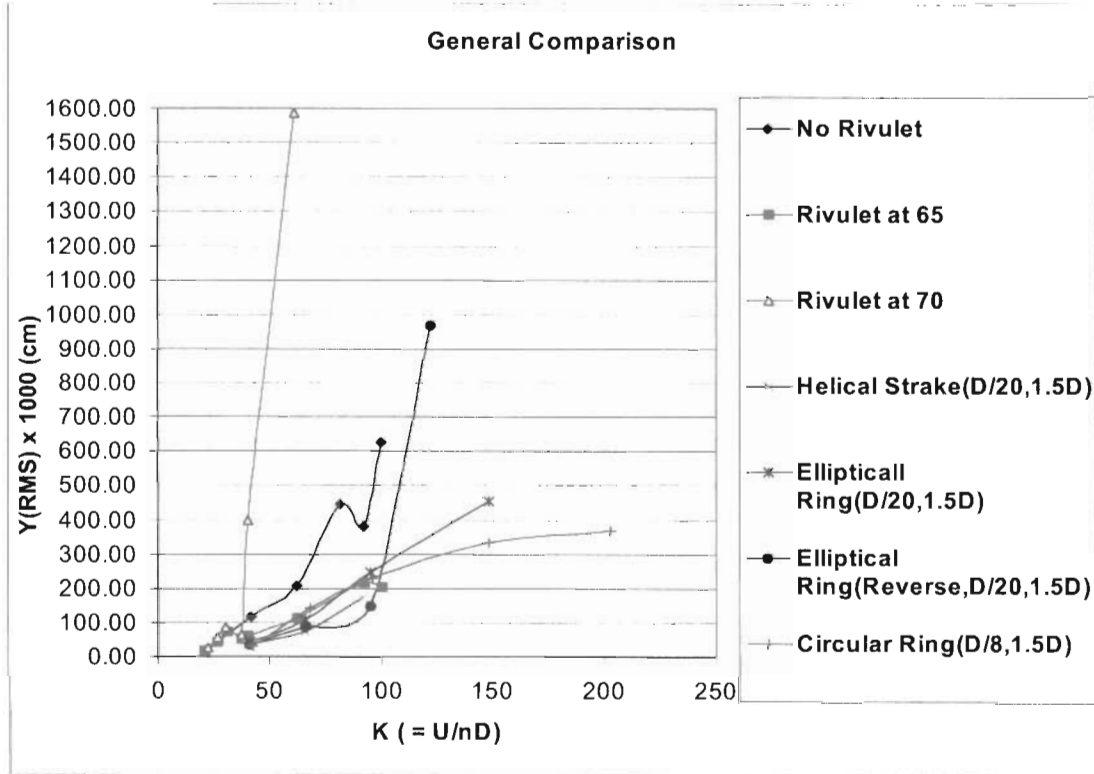
### 3.2.3 RMS Response

The root mean square (RMS) values of the response of the section model at different wind speeds were calculated from the time histories of the displacement along the vertical degree of freedom (60-sec record sampled at 50Hz). These are shown in Fig. 3.4 for all cases considered.

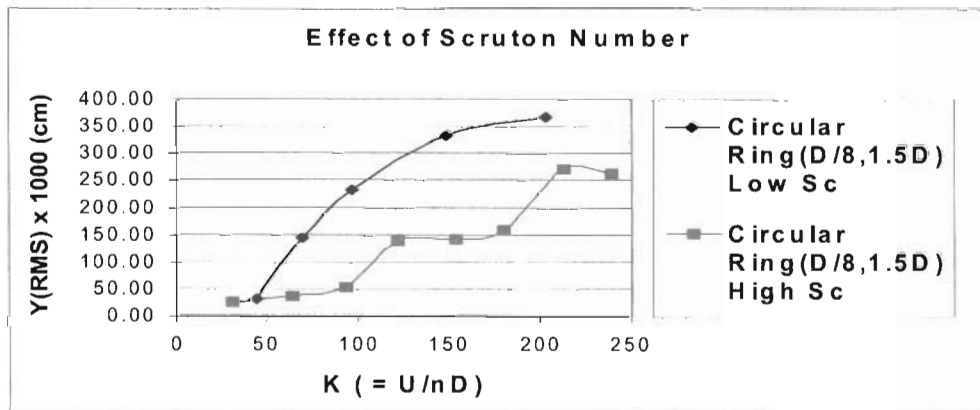
The interpretation of the wind-tunnel RMS response tests with conclusions follow:

- The model ( $\alpha = 0^\circ$ ,  $\beta = 37^\circ$ ) without any rivulet showed galloping instability at  $U/nD \geq 80$  (Fig. 3.4a).
- The model with artificial rivulet (upper) at  $\theta = 70^\circ$  showed galloping instability at  $U/nD \geq 60$  and velocity-restricted response (a crest in the response curve) at a reduced velocity,  $U/nD$ , slightly below 40, similar to the one observed by Matsumoto et al. (1995) (Fig. 3.4a). The artificial rivulet (upper) at  $\theta = 65^\circ$  stabilized the response compared to that of the model without any rivulet (Fig. 3.4a). Thus, the location of the upper rivulet is important. This was also observed by Matsumoto et al. (1995).
- The aerodynamic plate-damper produced the anticipated aerodynamic damping (positive) like an airfoil along the vertical degree of freedom. However, its effectiveness reduced with increasing angle of attack ( $\gamma$ ). Further, it showed instability along torsional degree of freedom beyond a certain  $U/nD$  for a range of angles of attack not including  $\gamma = 0$ . The implication is that the aerodynamic plate-damper cannot be used in the case of a cable that is relatively flexible in torsion and where there can be large variations in the angle of attack.
- The Scruton number affected the response of the model as depicted in Fig. 3.4b. The model with a lower Scruton number produced a higher response than the one with higher Scruton number. This behavior is typical of velocity-restricted response such as Karman-vortex-shedding type, although the aerodynamic phenomenon producing the large amplitudes in this case is different.
- The diameter of the wires constituting the helical strake did not seem to have any significant influence on the response (Fig. 3.4c). Hence, a smaller diameter wire

such as  $D/20$  can be used. The pitch influenced the response but only beyond a certain critical value. The  $D/20$  helical strake with pitch of values  $1.5D$  and  $3D$  performed differently (Fig. 3.4c). The combination of the diameter and the pitch of the helical strake is important.

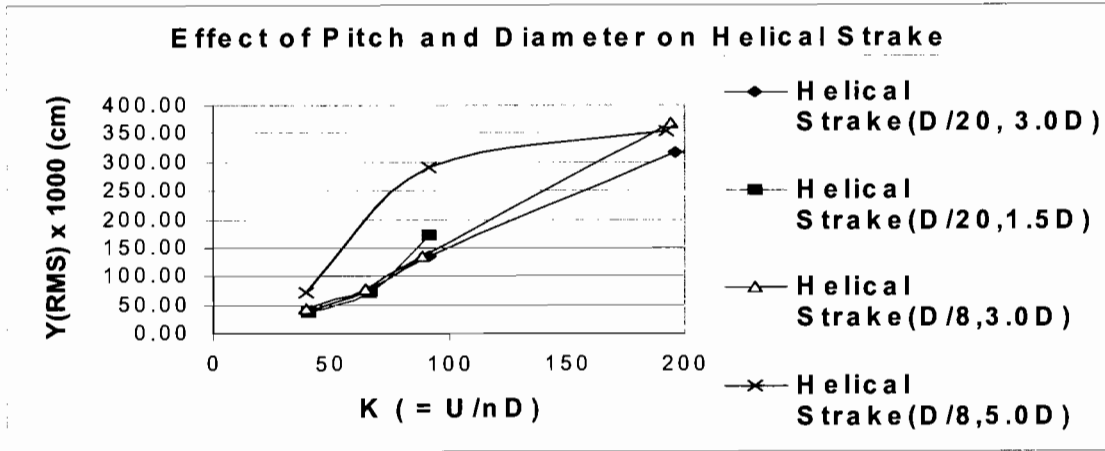


(a)  $Sc = 7.6$

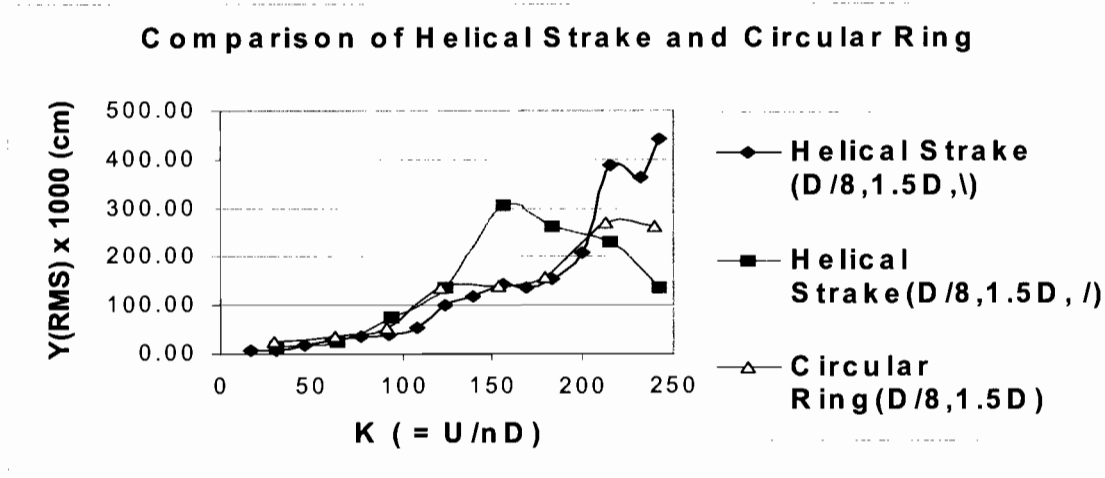


(b) Low  $Sc = 7.6$ , High  $Sc = 54.6$

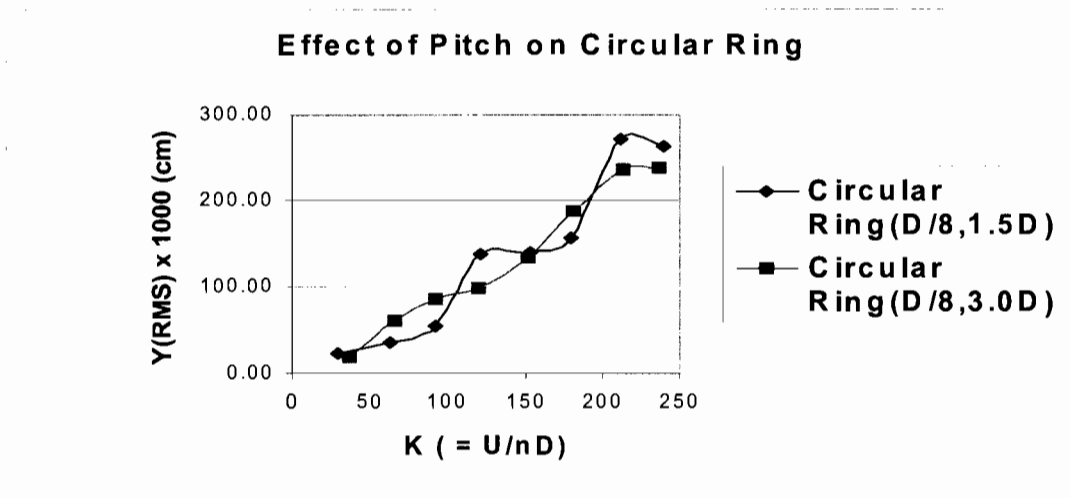
**Fig. 3.4** (a), (b) Vertical displacement response (rms) of section model ( $D = 10.2$  cm)



(c)  $Sc=7.6$



(d)  $Sc=54.6$



(e)  $Sc=54.6$

Fig. 3.4 (c), (d), (e) Vertical displacement response (rms) of section model ( $D=10.2$  cm)

- The orientation of the helical strake influenced the response. Both orientations (/ or \) produced acceptable or visibly low responses (Fig. 3.4d) up to  $U/nD=250$  which correspond to 61 mph for the first mode of vibration and 122 mph for the second mode of vibration of cable A23 of the Fred Hartman bridge.
- The circular ring performed better than the helical strake (in both orientations) if the entire range of  $U/nD$  from 0 to 250 is considered (Fig. 3.4d). A pitch of 1.5D and 3D for the circular ring did not produce any significant difference in response (Fig. 3.4e).
- The elliptical ring performed well in one orientation (\) but produced instability at  $U/nD \geq 120$  in the reverse orientation (/) (Fig. 3.4a). Since the wind angle of attack can vary significantly, this aerodynamic device is not feasible.

### 3.2.4 Measurement and Prediction of Aerodynamic Damping

The damping of a section model can be estimated from its decayed response in free vibration along a single degree of freedom. The damping of the model includes contribution from aerodynamic effect that varies with the wind speed. To measure the damping, the section model in this experiment was displaced in the vertical plane and suddenly released to vibrate freely. This procedure was repeated at different wind velocities. The free vibration response (in the direction of lift) was recorded at each wind speed for 20 seconds at 50 Hz sampling rate.

The non-dimensional number  $H_1^*$  (Eq. 2-6) which gives a measure of the aerodynamic damping, is plotted against the reduced velocity ( $U/nD$ ) in Fig. 3.5. For the model without any mitigation devices,  $H_1^*$  starts increasing beyond a reduced velocity of 40. At a critical reduced velocity of 80,  $H_1^*$  becomes a positive number, which suggests that the yawed cable has negative aerodynamic damping and is susceptible to galloping vibrations. The corresponding critical reduced velocity for the cable with the rivulet for the onset of SDOF flutter or galloping is 60. With the circular rings or helical strake attached,  $H_1^*$  decreases (becomes a larger negative number) in the same region of the reduced velocity, i.e., the circular rings or helical strake has stabilized the yawed cable.

To show how much aerodynamic damping the circular ring and the helical streak will add to one of the prototype cables, the following computation is performed. Cable A23 of the Fred Hartman Bridge, which was reported to vibrate in the second mode at relatively low wind, was chosen as an example (Table 3.1). The total critical damping ratio ( $\zeta_T$ ) of cable A23 of the Fred Hartman Bridge in the second fundamental mode of vibration was calculated assuming a mechanical damping ratio ( $\zeta_m$ ) of 0.1% (using Eqs. 2-5 and 2-7). In this computation, it is assumed that the equivalent yaw angle (i.e.  $\beta^*$ ) of this yawed and inclined cable is  $37^\circ$  for a particular wind direction (can occur with wind at  $33^\circ$  with respect to the bridge axis). The value of  $H_1^*$  measured in the wind tunnel for  $\beta = 37^\circ$  and  $\alpha = 0^\circ$  (Fig. 3.5) was used in this calculation. In this calculation, one value of wind speed was used throughout the length of the cable. In reality, the wind speed is expected to vary along the length of the cables at the prototype site. The mean wind speed at the top of Cable A23 is expected to be almost 10% higher than the mean wind speed at its base<sup>5</sup>.

---

<sup>5</sup> A more refined calculation to account for this variation is desirable.

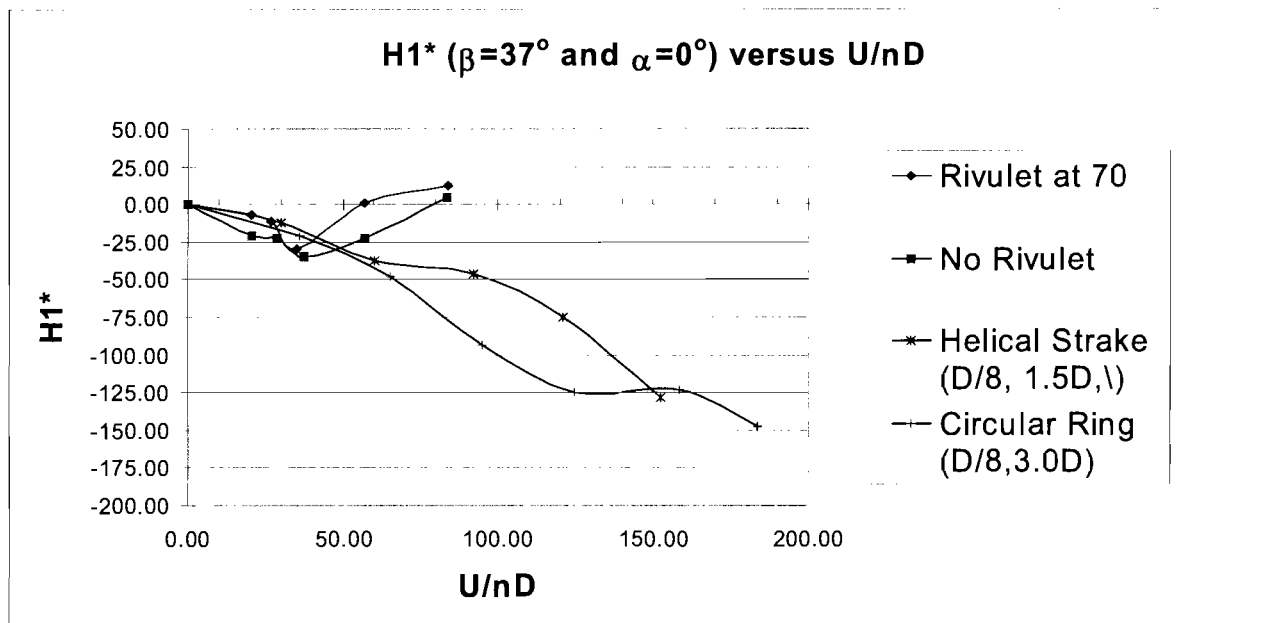


Fig. 3.5  $H_1^*$  for cable with and without mitigation devices

The plot of the total critical damping ratio as a function of wind speed is shown in Fig. 3.6. The total critical damping becomes zero or negative indicating instability in the second vibration mode for this cable without rivulet at 40 mph wind speed or greater. The corresponding value for this cable with rivulet is 35 mph. The same cable with circular ring or helical strake shows a trend of increasing damping up to 70 mph. Also note that these devices increase the damping of the cable to 0.5% and greater for wind speeds of 25 mph or greater, when the problem of vibration was observed to occur. Earlier in this report, it was mentioned that a minimum of 0.5% damping is required to damp out large amplitudes at low wind speeds.

Table 3.1 Videotaped vibration events of the Fred Hartman Bridge stay-cables

Event	Date	Time	Cable	Mode	Frequency (Hz)	Estimated Amplitude peak-peak cm (in)	Location of Amplitude	Remarks
1	4/1	9:00 pm	9	<u>2</u>	2.1	38.1 (15)	middle	rain, wind
2	4/1	4:00 pm	24	<u>2</u>	high	7.6 (3)	?	wind
3	4/3	11:15 am	1,2,3	<u>1</u>	0.8	88.9 (35)	middle	rain, wind
4	4/3	11:20 am	10,11	<u>2</u>	>1.5	10.2 (4)	1/3 from top	rain, wind
5	4/4	6:28 am	15,16	<u>1</u>	1.0	30.5 (12)	middle	rain, wind
6	4/4	6:41 am	23,24	<u>2</u>	1.2	91.4 (36)	middle	rain, wind
7	4/4	6:55 am	24	<u>3</u>	1.8	106.7 (42)	1/3 from top	Gusts up to 50 mph

### Total Critical Damping vs Wind Speed

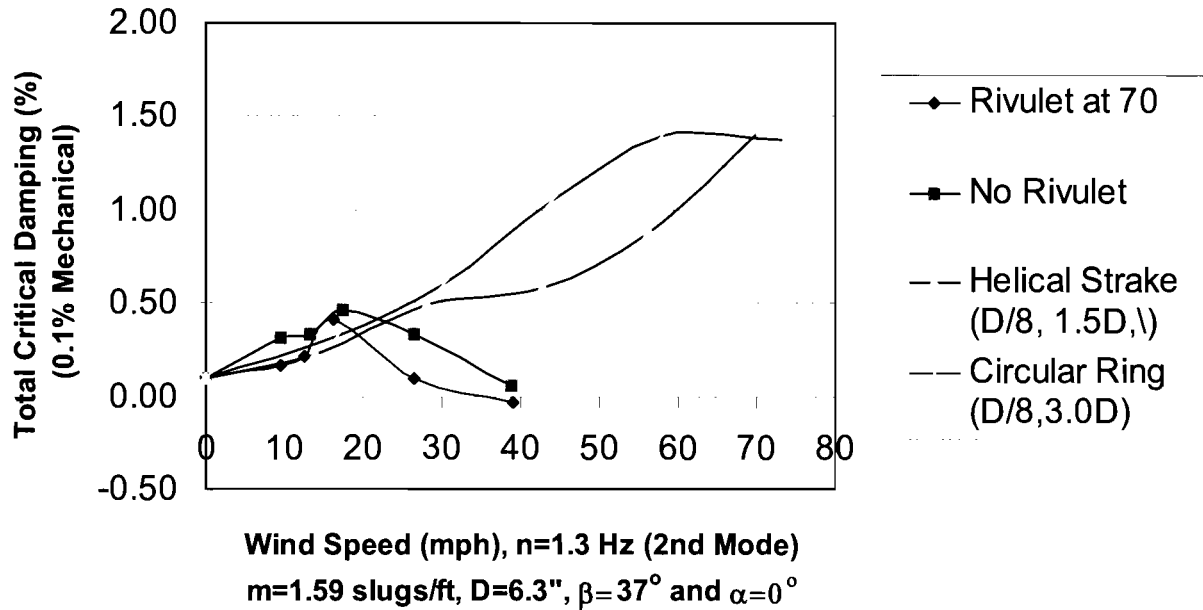


**Fig. 3.6** Total critical damping at different wind speeds

#### 3.2.5 Effectiveness in Prevention of Water Rivulets

The effectiveness of the circular rings to prevent the formation of a continuous upper rivulet was tested on the same section model in simulated rain. The inclined/yawed section model was fixed at  $\alpha = 37^\circ$  and  $\beta = 37^\circ$  and rain was simulated inside the wind tunnel over the entire length of the model. In Fig. 3.7 the formation of an upper rivulet on the bare model is observed at a wind speed of 20 mph. Once the circular rings were mounted as in Fig. 3.8, the rivulet disappeared. Rain-drops that precipitated between two rings on the model were intercepted by the lower ring and fell off from underneath the model. The circular rings reduce the cable length below a critical value that is needed for the raindrops to form a continuous upper rivulet. To explain this further, consider a very short cable that has the same yaw and inclination angles as the section model and a length that is equivalent to the pitch (3D) at which the circular rings were placed. This short cable, if subjected to rain, will not have any rivulet formation because there is not enough length for the raindrops to organize into a rivulet. A single helical strake is expected to behave similar to the circular rings.

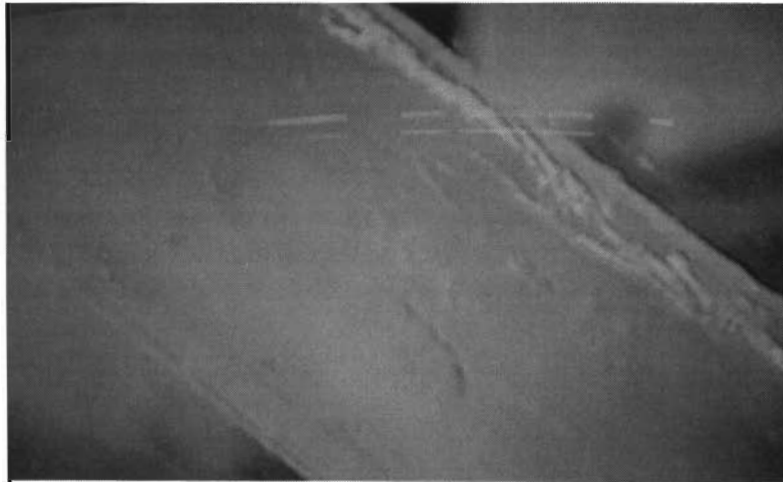


**Fig. 3.7** Formation of upper water rivulet on a yawed and inclined cable

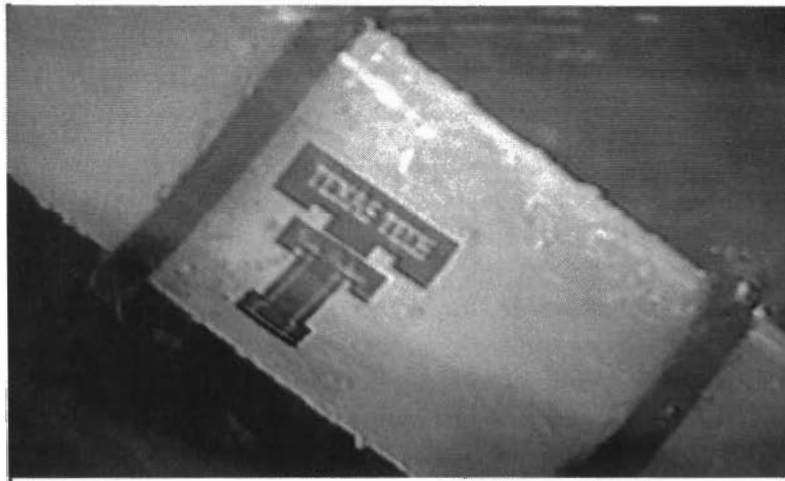


**Fig. 3.8** Prevention of upper water rivulet with circular rings

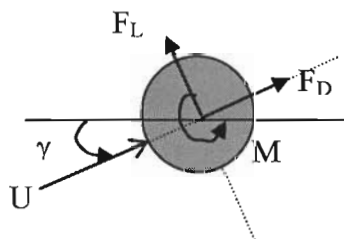


**Fig. 3.9** Directions of the mean aerodynamic forces

### 3.2.6 Force Coefficients

For force measurement, the section model was rigidly fixed at  $\alpha = 0^\circ$  and  $\beta = 0^\circ$  (model axis is normal to the wind direction and on a horizontal plane) and three force coefficients,  $C_D$  (drag),  $C_L$  (lift), and  $C_M$  (moment) were measured.

The mean values of  $C_D$ ,  $C_L$ , and  $C_M$ , as measured in the wind tunnel at separate wind speeds ( $U_{\max} = 80\text{ft/s}$  or  $24.4\text{ m/s}$ , maximum Reynolds number =  $1.67 \times 10^5$ ) and normalized with the model diameter  $D$  for forces and  $D^2$  for moment, are listed in Table 3.2.

**Table 3.2** Force coefficients

Case	Orientation	Parameter	$\alpha$	$\beta$	$C_D$	$C_L$	$C_M$
Helical Strake	\ at $64.5^\circ$ with model axis	D/20 Wire at 1.5D Pitch	$0^\circ$	$0^\circ$	1.33	-0.16	0.37
Helical Strake	\ at $46.3^\circ$ with model axis	D/20 Wire at 3D Pitch	$0^\circ$	$0^\circ$	1.34	-0.14	0.34
Elliptical Ring	\ at $60^\circ$ with model axis	D/20 Wire at 1.5D Pitch	$0^\circ$	$0^\circ$	1.28	-0.03	0.49 median

The  $C_D$  and  $C_L$  of a cable (smooth surface) without any aerodynamic devices are 1.2 and 0, respectively<sup>6</sup>, for sub-critical Reynolds number (equivalent to about  $U=42\text{ mph}$  for A23 cable of Fred Hartman Bridge), beyond which  $C_D$  drops to a lower value (see Simiu and Scanlan, 1996). The coefficients  $C_D$  and  $C_M$  of a cable with circular rings are expected to be marginally different from those of the bare cable. Based on the model tests with elliptical rings,  $C_D$  with circular rings is expected to be slightly lower than 1.28 (5% increase beyond the  $C_D$  of a bare cable) and  $C_M$  much lower than 0.49. The  $C_L$  with circular rings is close to zero. The force coefficients of a cable with circular rings is reported later<sup>7</sup>. The mean aerodynamic forces per unit length ( $F_L$ : Lift Force,  $F_D$ : Drag Force,  $M$ : Moment) on the prototype cable can be calculated as

$$F_L = \frac{1}{2} \rho U^2 D C_L, \quad F_d = \frac{1}{2} \rho U^2 D C_d, \quad M = \frac{1}{2} \rho U^2 D^2 C_m,$$

where  $\rho$  is the density of air ( $1.21\text{ kg/m}^3$  or  $0.0024\text{ slugs/ft}^3$  at standard temperature and pressure),  $U$  is the components of the mean-hourly wind speed normal to the axis of the cable and  $D$  is the diameter of the cable. The directions of these forces are given in Fig. 3.9, where  $\gamma$  is the angle of attack as defined earlier.

### 3.2.7. Explanation of Possible Vibration Mechanisms

A great deal of information was known prior to commencement of this study and some of which was verified during the current wind-tunnel tests. For example, it is a well known fact

<sup>6</sup> See Figure 3.12

<sup>7</sup> See Figure 3.24

that yawed or yawed and inclined cables (without rain) have a tendency to exhibit galloping beyond a critical wind speed because of the axial flow that is generated in the wake of the cable. These cables exhibit only divergent-type response at higher wind speeds. The upper rivulet forms at relatively lower wind speeds to make the cable prone to large-amplitude vibration. A possible explanation of the velocity-restricted response as observed in the full-scale monitoring of the vibrations at low wind speeds follows. The scenario is wind accompanied by rain. The flowing hypothesis is supported by full-scale measurements and observations. For commonly encountered inclined cables with diameters varying between 80 mm to 200 mm, when wind speed increases beyond 5m/s, an upper rivulet forms on cables descending in the wind direction. The mean location of the rivulet continues to shift away from the stationary point with increasing wind speed. When the rivulet is formed at certain locations, the cable shows a tendency to have divergent response and exhibits galloping with large amplitude motion. The large-amplitude motion remains limited as the cable has a non-linear stiffness. Not all stay-cables in a cable-stayed bridge would exhibit this behavior at the same time as they have different attitudes. As the wind speed increases further, the upper rivulet shifts further away from the stagnation point and is eventually blown off the cable at a wind speed greater than 15 m/s. Thus, the mechanism that caused the aeroelastic instability disappears. The result is a velocity-restricted response within 5-15 m/s wind speed. Beyond 15 m/s of wind speed, the rivulet is out of the scenario and some inclined and yawed cables continue to have a tendency to exhibit large amplitude vibration beyond a critical speed. In the range of high wind speeds, the vibrations are limited and non-divergent due to the non-linear characteristic of the cable. The large-amplitude motions do not reduce with increasing wind speed as occurred in the lower-wind speed range. The actual motion of the cable is along an inclined plane depending on the angle of attack (Fig. 2.1) and is more complex than SDOF galloping-type response due to either the interaction of the oscillation of the rivulet with the cable motion or the cable's richness in vibration modes.

### 3.3 TTU Wind Tunnel Section Model Tests

#### *Overview*

Based on the positive results of the single-degree of freedom wind tunnel tests performed at CSU, TTU researchers, under consultation and agreement with TxDOT, began additional wind-tunnel tests using a two-degree of freedom model (Sarkar and Gardner, 2000).

#### 2DOF Suspension System

For this portion of the research project, TTU researchers designed and assembled a two-degree-of-freedom (2DOF) elastic suspension system (vertical and horizontal motions) that enabled the section model to behave similarly to actual cable-stays. The suspension system used is designed to test yawed and inclined section models and is shown in Figure 3.10. Also shown in Figure 3.10 are the circular rings placed on the cable-stay.

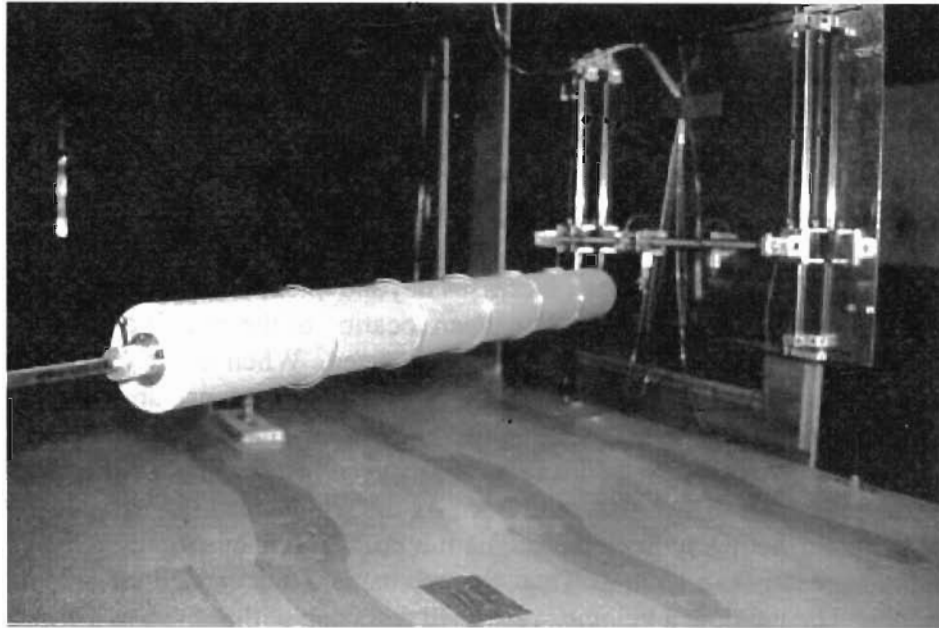


**Figure 3.10** 2DOF TTU Cable with Rings and Suspension System

Section model suspension systems commonly use leaf springs as a means of restraining the translational motion of the model in a given direction. Leaf springs have very low inherent damping but are difficult to use for yawed and/or inclined cases of vibration, as was necessary for this research. In addition, the range of motion of a model attached to a leaf spring forms a circular arc that is acceptable for small displacements (ignoring the small circular motions) but may excessively restrict system response when displacements become large, thus potentially producing errant results near the system limit.

Because of the inclined and yawed nature of bridge cable-stays, it was necessary to construct an elastic suspension system capable of supporting a section model in any configuration of yaw and/or inclination. In addition, as observed in full-scale measurements by several researchers, the nature of vibration of the cable-stays is two-dimensional, i.e., the vibration tends to be elliptic rather than constrained along a particular axis. To allow elliptic motions of the model in varying yaw and inclination configurations, the elastic suspension system developed for this study is able to vibrate along two perpendicular axes—the horizontal, or “streamwise”, and the vertical. In addition, the system has low inherent damping to properly duplicate field conditions.

### *TTU wind tunnel characteristics*

The closed circuit, vertically oriented wind tunnel used in this research has sufficient power to produce wind speeds in excess of 45 m/s (100 mph). The TTU wind tunnel has separate aerodynamic and atmospheric boundary layer test sections. The aerodynamic test section extends for a length of 2.4 m (8 feet) beyond the contraction exit where the flow is least turbulent. The atmospheric boundary layer test section is 122 m (50 feet) downstream of the aerodynamic test section. Each section has a glass viewing window and a large access door. Presented experiments were conducted in the aerodynamic test section that is 1.1m high x 1.8m wide (3'9"H x 5'9"W) following an inlet contraction of 4.5:1. The velocity profile was measured at this location and was found to vary only  $\pm 0.2$  m/s ( $\pm 0.5$  mph) across the wind tunnel cross-section. Turbulence intensity was calculated to be 1.15% with two turbulence reducing screens. Experiments were conducted in the range of 2-36 m/s (5-80 mph). The 2DOF section model with suspension system is shown inside the TTU wind tunnel in Figure 3.11.

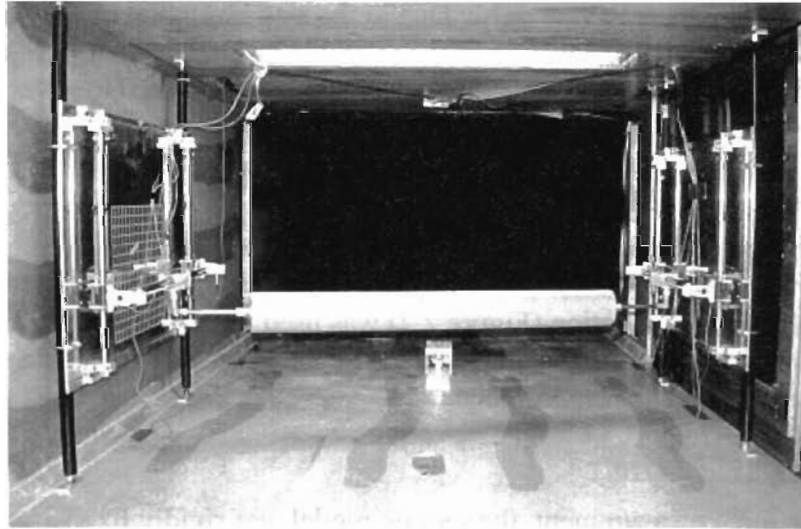


**Figure 3.11** 2DOF TTU Cable-Stay Setup in Wind Tunnel Section Model

The cylinder model used in the 2DOF portion of the study was made of 7.6 cm (3.0 inches) I.D. schedule 40 polyvinyl chloride (PVC) pipe. This pipe has an outside diameter of 8.9 cm (3.5 inches) and a length of 112 cm (44 inches). The same cylinder model was used in all 2DOF test cases. The cylinder model is hollow with a 1.3 cm (0.5 inch) diameter, two piece rod that can slide in and out of the ends of the section model to allow re-positioning of the section model without changing the model length and/or mass.

To allow the section model to be positioned in inclination, the entire system ends (vertical and horizontal supports) were mounted to aluminum plates that were in turn mounted to two 3.2 cm (1.25 inch) diameter steel pipes, each via U-bolts. For yaw positioning, each end mount assembly can be moved relative to one another along the wind tunnel walls by relocating the aluminum plates.

Damping values were 0.25 % of critical for the vertical motion and 0.33% of critical for the horizontal motion. Taking into account the mass and damping of this system, the test section model Scruton number was 31.7 based on vertical damping. This value compares with the full-scale value of  $Sc = 44.7$  (as discussed in Section 2.4.7 of this report).

## *Results*

### *RMS of Response*

The RMS (root-mean-square) values of the displacement response of the section model at several wind velocities were calculated from the acquired time histories along the vertical, horizontal, and combined degrees of freedom. The combined response is the square root of the sum of the squares of vertical and horizontal responses (Equation 3.1). Generally, the RMS value referred to in this report is the RMS of the displacement time histories.

$$\text{Combined RMS} = \sqrt{(\text{Vertical RMS})^2 + (\text{Horizontal RMS})^2} \quad [3.1]$$

Considering Matsumoto et al.'s (1995) equivalent yaw angle definition and suggestion that a yawed-inclined cylinder behaves similarly to a yawed-only cylinder, it was decided to test the section models in yaw only. Due to the size limitation of the Texas Tech wind tunnel, the current model suspension system was capable of inclination angles only up to  $18^\circ$ , which was not sufficient to properly study the effects of inclination. However, yawed angle variations were not limited by the testing apparatus.

### *Response due to Various Yaw Angles (without rings)*

The rivulet location that produced the most extreme response changed with yaw angle. An unstable response was not found beyond the yaw angle of  $40^\circ$  for any rivulet location, therefore the  $\theta = 73^\circ$  location (Figure 2.2) was used for these yaw angles. When the rivulet was located at different angles above or below the point that generated the most extreme response, a more stable response occurred.

### *Drag and Lift Coefficients*

For force measurement, the section model was rigidly fixed at  $\alpha = 0^\circ$  and  $\beta = 0^\circ$  (model axis is normal to the wind direction and on a horizontal plane) and force coefficients, including  $C_D$  (drag), and  $C_L$  (lift) were measured. Lift and drag coefficients are defined, respectively, as:

$$C_L = \frac{F_L}{\frac{1}{2}\rho U^2 A} \quad [3.2]$$

$$C_D = \frac{F_D}{\frac{1}{2}\rho U^2 A} \quad [3.3]$$

where  $F_L$  = lift force,

$F_D$  = drag force,

$\rho$  = air density,

$U$  = wind speed, and

$$A = D \times L \cos \beta^*$$

$D$  = cylinder diameter

$L$  = length of the yawed cylinder

$\beta^*$  = yawed cable angle (see Figure 2.1)

The  $C_D$  and  $C_L$  of a cable (smooth surface) without aerodynamic devices are 1.2 and 0, respectively, for sub-critical Reynolds number (equivalent to about  $U = 42$  mph for the A23 cable of the Fred Hartman Bridge), beyond which  $C_D$  drops to a lower value (see Simiu and Scanlan, 1996). The drag coefficient decreased with increasing yaw angle with and without a rivulet (Figure 3.12). This is due to the change from cross-flow to axial flow and the decrease in projected area with increasing yaw angle.

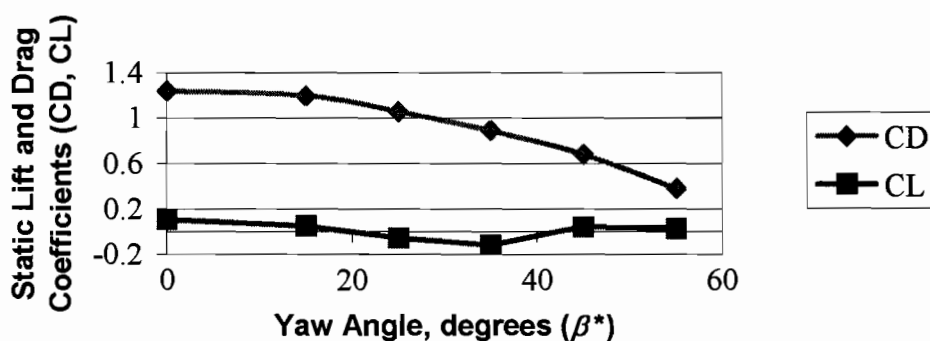


**Figure 3.12.** Variation of Lift and Drag with Yaw Angle (bare cylinder).

Notice the negative lift for  $\beta^* = 20^\circ$  to  $40^\circ$ . Some of this negative lift is attributed to the effect of wind flow over the cylinder ends and interaction of the wind with other components of the elastic suspension system. Error in the lift coefficient calculations was  $\pm 0.11$  and error in the drag coefficients was  $\pm 0.24$ . However, the same trend exists for all cases studied and further study is required before this apparent lift can be accounted for as simply due to the effects of interaction of the wind flow with the suspension system components. For each case of cylinder configuration with and without the upper rivulet, the most negative lift occurred at  $\beta^* = 35^\circ$ . This is important because the most extreme dynamic response also occurred at  $\beta^* = 35^\circ$ . Also note the increase in lift with rivulet at  $\beta^* = 0^\circ$  and the trend thereafter that is similar to the case without rivulet. The lift is expected to increase at  $\beta^* = 0^\circ$  with rivulet due to the increased flow separation region above the cylinder created by the upper rivulet.

If the lift shown in Figure 3.12 is due to end effects, one would expect a continuously decreasing trend. This is because as the cylinder model is yawed more, a larger surface area is available for the wind flow to interact with, resulting in greater applied forces. In contrast to the findings of Matsumoto et al. (1995) where the most extreme vibration case in single degree

of freedom for a smooth cylinder occurred at  $45^\circ$ , the current TTU research finds the most extreme response to occur at  $\beta^* = 35^\circ$  in two degrees of freedom.

An important distinction between the current work and the work of other researchers is TTU's use of a two-degree-of-freedom system rather than a single-degree-of-freedom system. The ability of the two-degree-of-freedom system to move along two axes appears to produce results different from those produced by a vertical motion only suspension system. In addition, the difference in results can be attributed to different Scruton numbers ( $Sc = 1.0$  in Matsumoto et al., 1995, experiments versus  $Sc = 31.7$  for the present 2DOF experiment). However, for the yaw angles where an extreme response was observed, the response was consistent with galloping instability where the displacement continued to grow to the limit of the suspension system. Figure 3.13 shows the responses of the smooth cylinder for the different yaw angles.

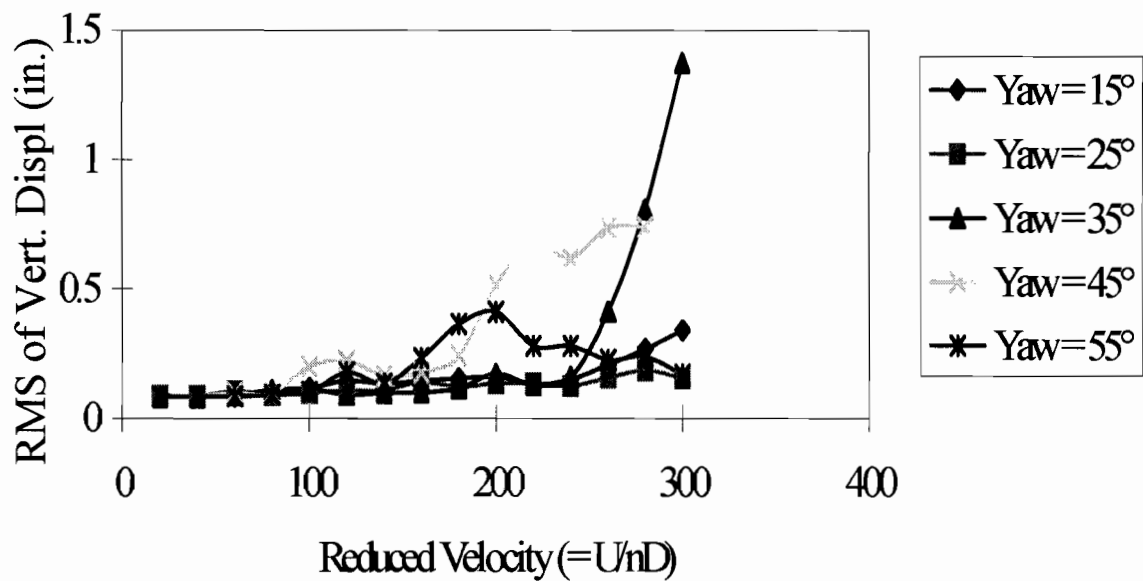


**Figure 3.13** Comparison of Responses of Bare Cylinder for Each Yaw Angle.

To determine the maximum yaw angle where an unstable response may occur with bare cylinders, i.e. when the RMS displacement is greater than 7.6 cm (3 inches), single-degree-of-freedom (vertical vibration only) studies were performed in an attempt to match the results produced by Matsumoto et al. (1995) in which an unstable response was found for  $\beta^* = 45^\circ$ .<sup>8</sup> In the present research, the case of  $\beta^* = 35^\circ$  and  $\beta^* = 40^\circ$ , yielded an unstable response, but a stable response was found for  $\beta^* = 45^\circ$ . Similar results were observed for the same values of  $\beta^*$  in the two-degree-of-freedom tests. Since no unstable response was found for  $\beta^* > 40^\circ$ , it is concluded that the unstable response can be expected for smooth cylinders with yaw angles from  $15^\circ$  to  $40^\circ$  in two-degrees-of-freedom. Unstable responses were found for all cases of yaw angle with an upper rivulet in the most sensitive location and, again, the most extreme response occurred at  $\beta^* = 35^\circ$ .

Interestingly, in all cases of dynamic response with rivulet, the reduced velocity for the onset of vibration occurred in the range of  $RV = 100$  to  $200$ . As the wind speed increased

<sup>8</sup> Beyond an RMS displacement = 7.6 cm (3 in.), the response of the cylinder section model grew seemingly without limit until reaching the end stops of the elastic suspension system.

beyond  $RV = 300$ , the predominant response was in the vertical direction. To compare with reported results at reduced velocities above 300, the system was restrained to vibrate only in the vertical direction. This was required because the drag in the horizontal direction became large enough to push the section model to the suspension system limits. However, up to the  $RV = 300$  limit, the horizontal response was smaller compared to the vertical response. Figure 3.14 shows the response at  $\beta^* = 15^\circ$ .

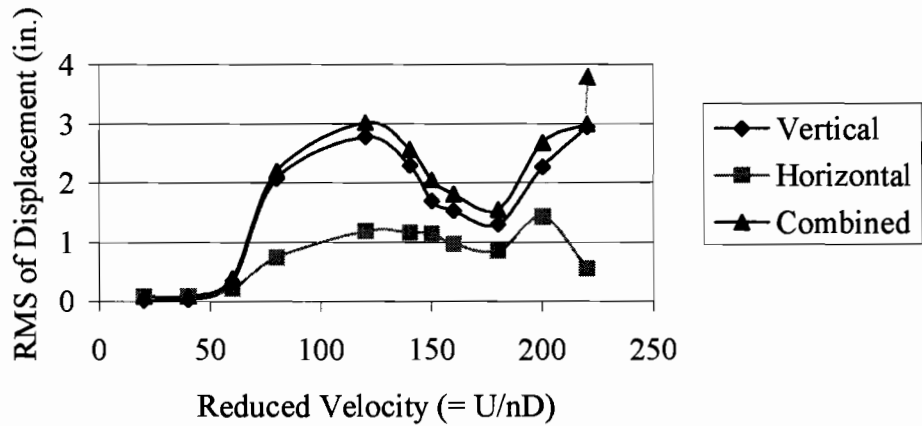


**Figure 3.14** Response of Cylinder with Rivulet at  $\beta^* = 15^\circ$ .

At  $\beta^* = 15^\circ$ , although not evident in Figure 3.14, an unstable response was actually reached for wind speeds beyond  $RV = 220$ . Because the response grew to the system limits beginning at  $RV = 220$ , it was decided not to record runs for one minute at higher wind speeds to prevent damage to the suspension system. A peculiar observation is that the case of  $\beta^* = 15^\circ$  yielded a response similar to that of the smooth cylinders where a divergent response is evident at high reduced velocities ( $RV > 200$ ). In fact, a similar response (not shown) occurred at  $\text{yaw} = 0^\circ$  at even lower wind speeds. Figure 3.15 shows a similar response at  $\beta^* = 25^\circ$ .

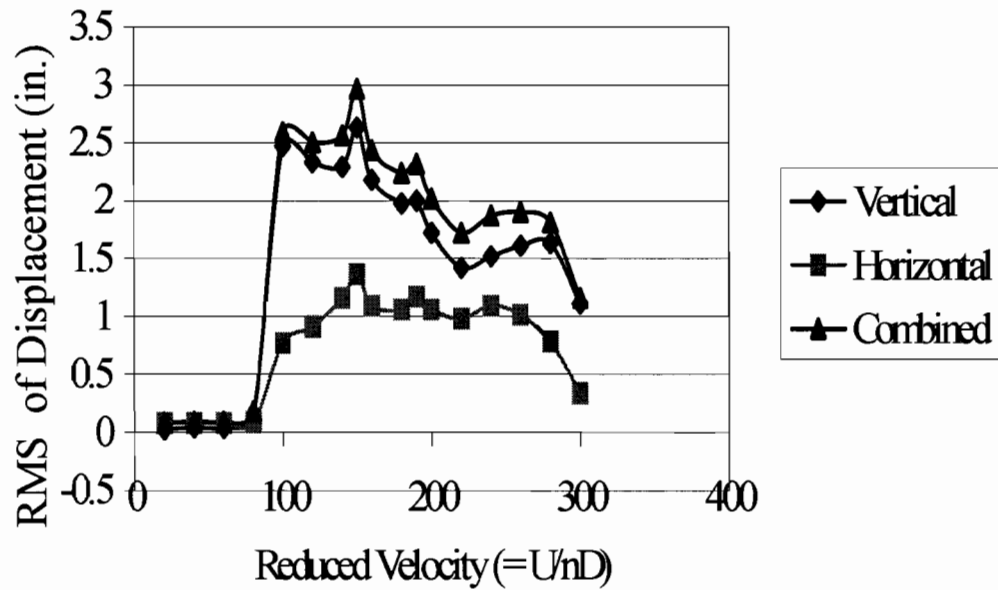


**Figure 3.15** Response of Cylinder with Rivulet at  $\beta^* = 25^\circ$

Notice in Figures 3.14 and 3.15 that the response tapers off gradually above the critical wind speed of  $RV = 150$ . This result is in sharp contrast to the response at  $\beta^* = 35^\circ$ , shown in Figure 3.16.

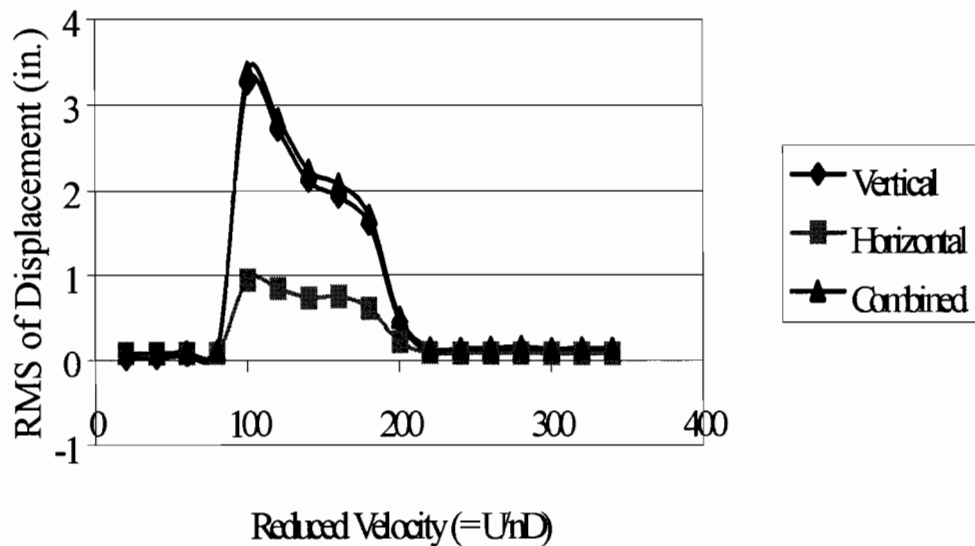


**Figure 3.16** Response of Cylinder with Rivulet at  $\beta^* = 35^\circ$ .

Notice the sharp drop in amplitude after  $RV = 200$  at  $\beta^* = 35^\circ$ . This demonstrates the velocity-restricted response reported by Matsumoto et al. (1995). In Figures 3.17 and 3.18, it is seen that the magnitude of the oscillation is significantly less at  $\beta^* = 45^\circ$  and  $\beta^* = 55^\circ$ , though the range over which the oscillations build is the same as in other yaw angles.

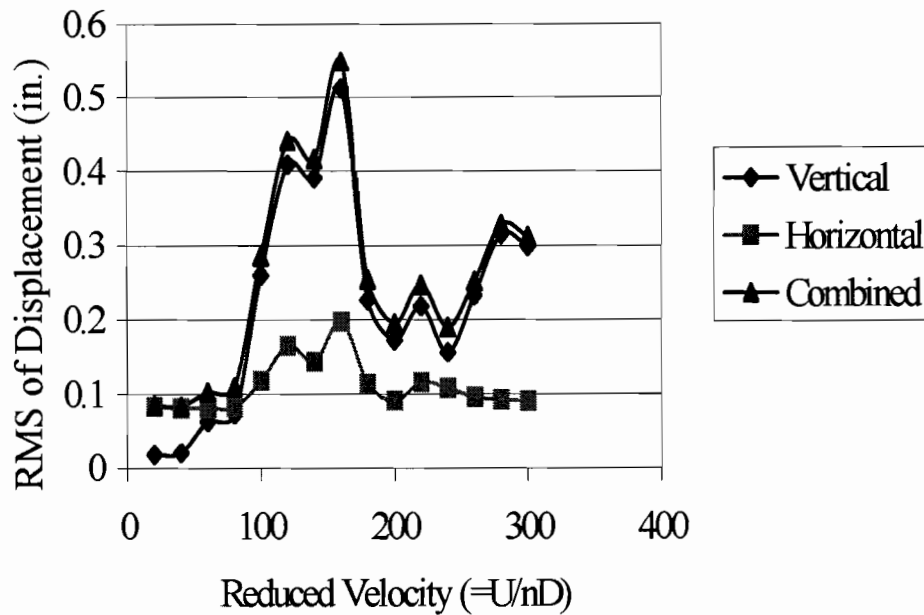


Figure 3.17 Response of Cylinder with Rivulet at  $\beta^* = 45^\circ$ .

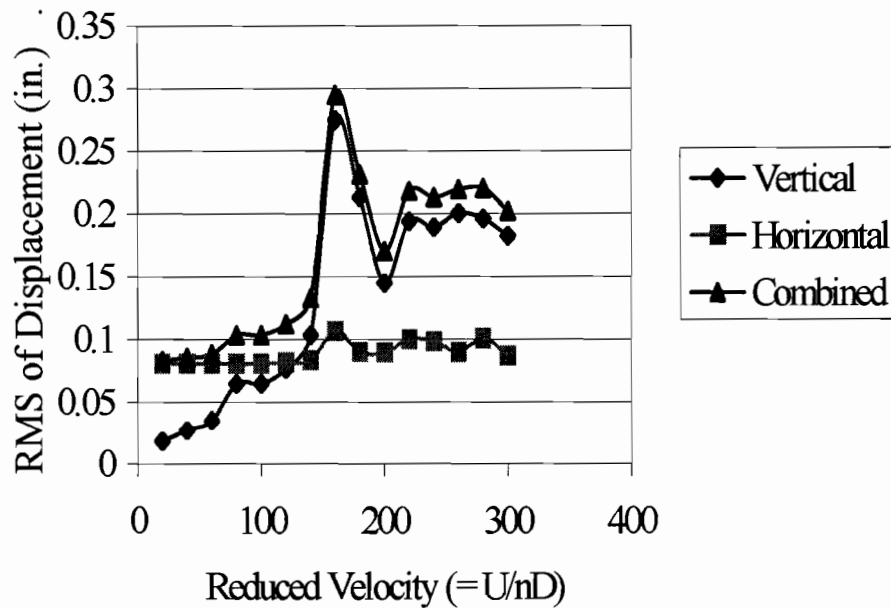
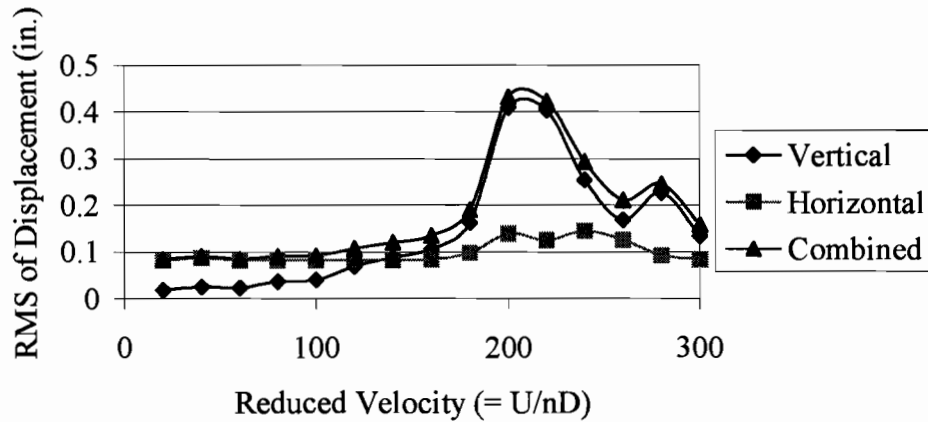


Figure 3.18 Response of Cylinder with Rivulet at  $\beta^* = 55^\circ$ .

Maintaining the  $\beta^* = 35^\circ$  case as the yaw angle with the most extreme response, modification of the surface roughness was made to study the effect on the dynamic response. To facilitate this, 150-grit sandpaper was applied to the cylinder surface. As can be seen in comparing the “Yaw =  $35^\circ$ ” case in Figure 3.13 with the “Combined” case in Figure 3.19, the response without rivulet changed from a divergent type response (smooth cylinder) to a

velocity-restricted type response. There was little effect when a rivulet was added except that the onset velocity for vibration was reduced compared to the other cases (Figure 3.20).



**Figure 3.19** Response with Covering of Sandpaper and No Rivulet at  $\beta^* = 35^\circ$

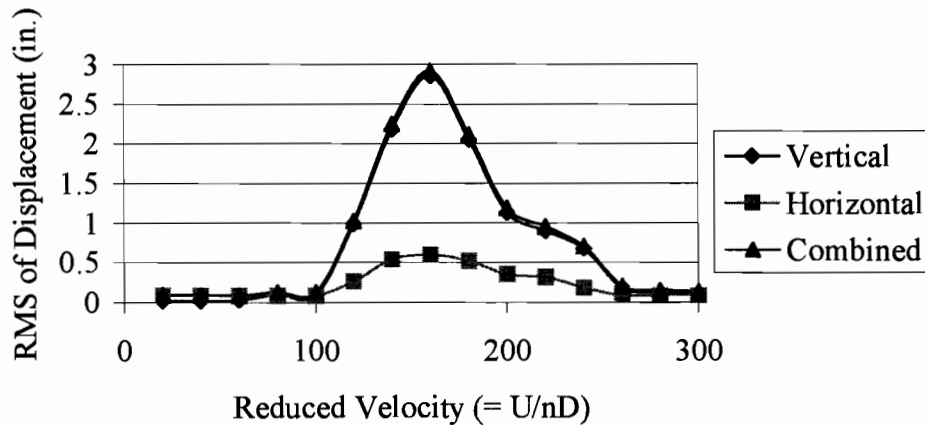


**Figure 3.20** Response with Covering of Sandpaper with Rivulet at  $\beta^* = 35^\circ$

Figure 3.21 shows a comparison of the responses of the cylinder at  $\beta^* = 35^\circ$  for the cases with and without the sandpaper covering. These results suggest that the size of the roughness is important. If the formation of a rainwater rivulet is actually the cause of the cable-stay vibration, then the protuberance of the roughness from the cylinder surface should be sufficient to trap the rain water incident upon the cylinder. If this is achieved, the net effect, with or without rain, is an increase in the cylinder surface roughness, which increases local turbulence and stabilizes the response of the cylinder (Matsumoto et al., 1995).

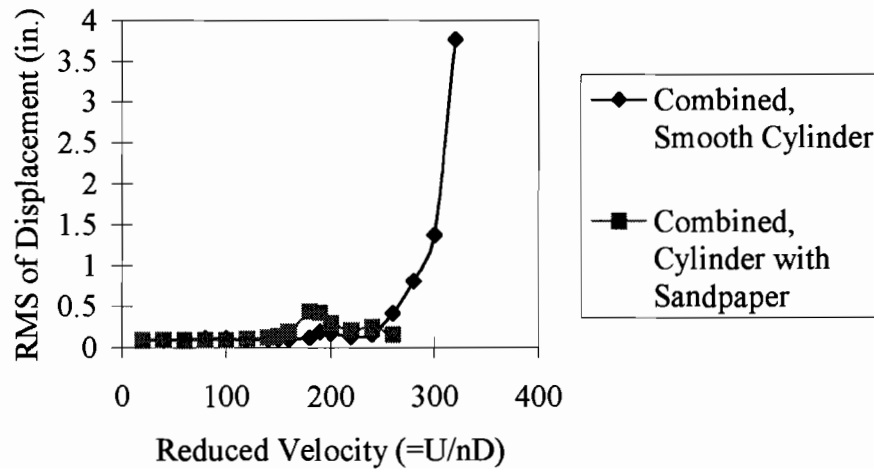


**Figure 3.21** Comparison of Responses of Cylinder with and without Sandpaper (no rivulet)

*Response due to various yaw angles with rings*

In an effort to mitigate the unstable response of a cylinder with rivulet, circular rings were placed on the cylinder at a spacing of two and four times the cylinder diameter, beginning at the cylinder centerline (see Figure 3.10). It was not necessary to use an artificial rivulet in conjunction with the rings as the circular rings would interrupt the continuity of the cylinder surface which is necessary for a uniform rivulet to form (Sarkar et al., 1998).<sup>9</sup> The circular rings were very effective in limiting the response of the yawed cylinder. The spacing of the rings had an effect on the degree to which the response was limited (Figures 3.22 and 3.23).

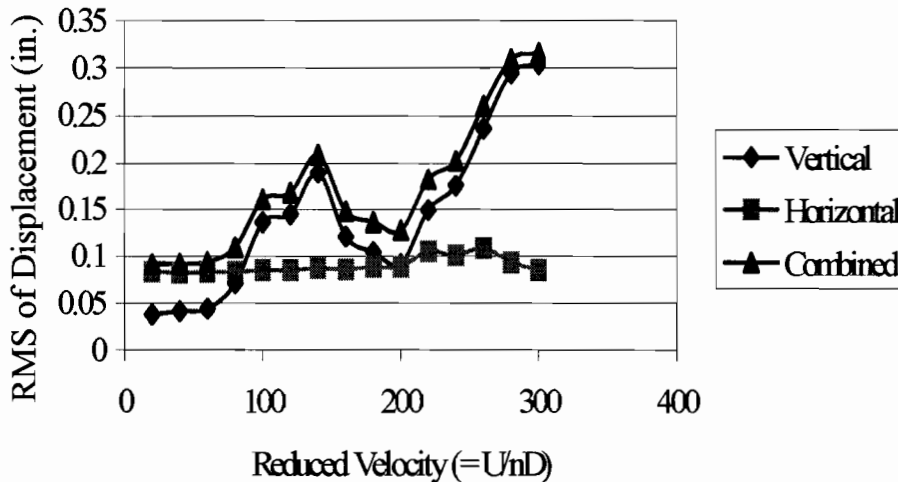


**Figure 3.22** Response of Cylinder with Circular Rings Spaced at  $4D$ ,  $\beta^* = 35^\circ$

<sup>9</sup> However, at times, the artificial rivulet was left on with the circular rings. The rings continued to mitigate the cable-stay vibrations!

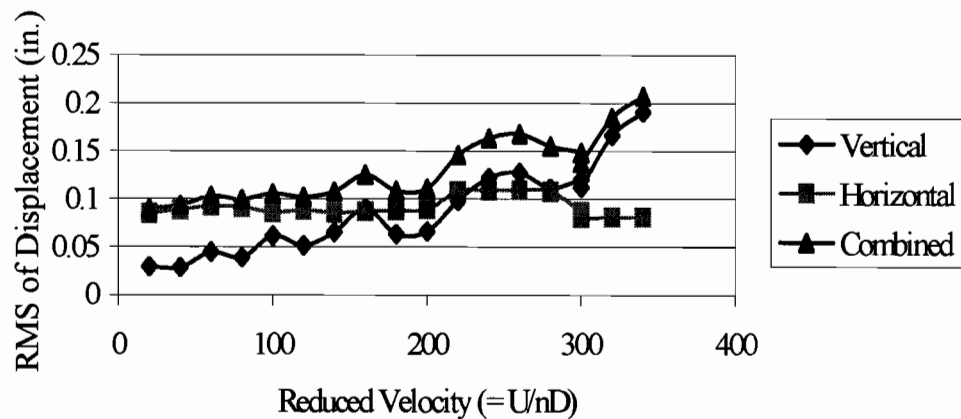


**Figure 3.23** Response of Cylinder with Circular Rings Spaced at  $2D$ ,  $\beta^* = 35^\circ$

Figure 3.24 shows the variation of lift and drag to yaw angles with rings attached. The trend of the lift and drag coefficients compares with the case of the bare cylinder shown in Figure 3.12. Notice again in this case the dip in the lift coefficient at  $\beta^* = 35^\circ$ .

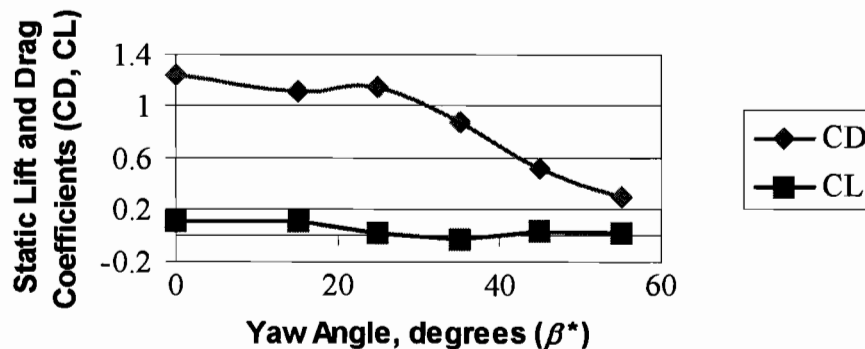


**Figure 3.24** Variation of Lift and Drag with Yaw Angle (cylinder with circular rings at  $2D$  spacing)

*Low wind speed with rivulet (in the wind tunnel)*

Figure 3.25 dramatically shows the potential of the rings in that the cable displacement with a rivulet (artificial) is reduced from an RMS displacement from over 5.5 cm (2.2 in) to 0.8 cm (0.3 in) for a  $4D$  ring spacing, and to 0.5 cm (0.2 in) for a  $2D$  ring spacing.

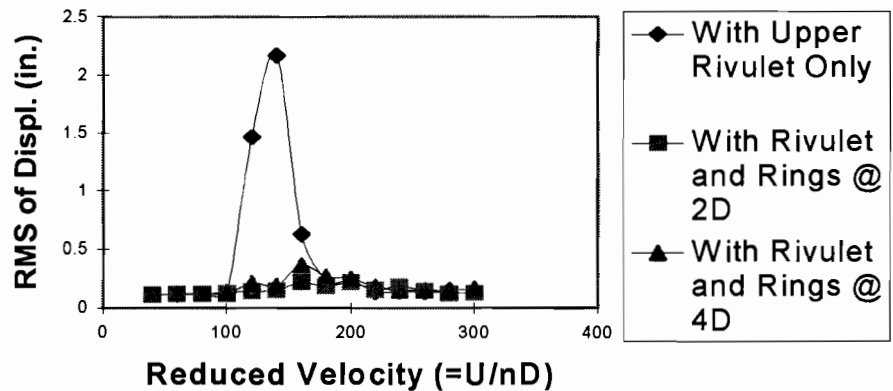


**Figure 3.25** Aerodynamic Ring Effectiveness at Low Wind Speed with Rivulet

The reduced velocity shown in the figure is dimensionless. For the longest cable-stays on both the Fred Hartman and Veterans Memorial bridges, a reduced velocity of 125 that gives the maximum oscillation, corresponds to a wind speed  $U$  of 13.8 m/s (31 mph) and 15.2 m/s (34 mph), respectively, for fundamental frequency  $n$ , and cable-stay diameter  $D$  of these cables. As shown in the figure, the vibration is velocity-restricted. At a reduced velocity of either below 100 or above 175 there is very little vibration.

*High wind speed without rivulet (in the wind tunnel)*

Though not the primary focus of the research to date, several high-speed wind tunnel tests without a rivulet (i.e. without rain) have been performed on the cable-stay section. As shown in Figure 3.26, the vibration of a bare cylinder begins to increase—apparently without bound—at a reduced velocity above 250. With the addition of aerodynamic rings, however, these large RMS displacements at high wind speeds are essentially cancelled—at least in the wind tunnel.

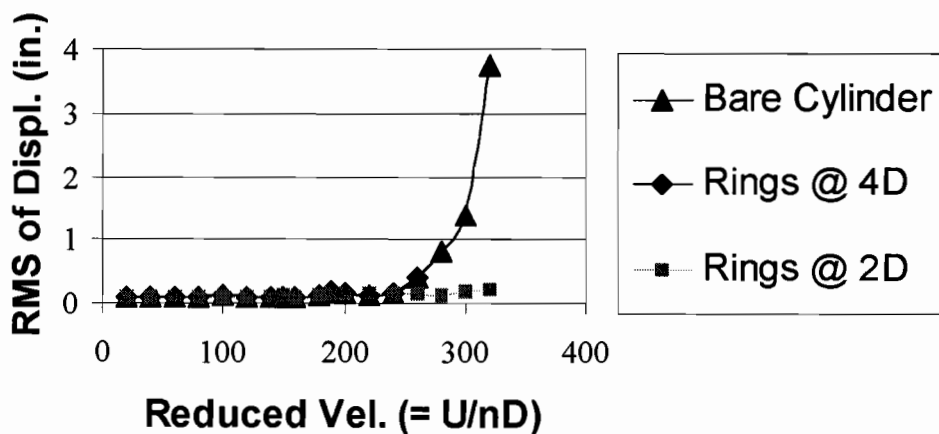


**Figure 3.26** Aerodynamic Ring Effectiveness at High Wind Speed without Rivulet

### 3.4 Wind Tunnel Tests Summary

Yawed circular cylinders exhibit divergent oscillatory behavior when subjected to wind speeds above the known vortex shedding wind speeds in the sub-critical Reynolds number range ( $< 2 \times 10^5$ ) at high reduced velocities ( $RV > 300$ ). This may be due to axial flow in the wake of the cylinder that produces a fluctuating pressure system above and below the cylinder, thereby increasing the vertical and horizontal response.

When the cross-sectional shape of a cylinder is modified by an artificial rain rivulet located  $65^\circ$  to  $75^\circ$  from the stagnation point, an unstable velocity-restricted type response occurs in the critical reduced velocity range of 100-200 for any yaw angle up to  $45^\circ$ . An upper rainwater rivulet presets the separation of flow, resulting in a greater flow separation region (lower pressure) above the cylinder. Within the critical reduced velocity range, an increased response of the cylinder occurs in both the horizontal and vertical directions.

Also, it was demonstrated that increased surface roughness of the cable-stay, limits the velocity-restricted response that typically occurs for a bare cylinder. The divergent response that occurs for a bare, yawed cylinder at high-reduced velocity ( $RV > 300$ ) is not evident in the increased surface roughness case. However, due to the overall similarity of responses for a cable-stay, with and without surface roughness, it is expected that a divergent response will occur for the roughened cylinder—though at higher wind speed than for the bare cylinder case. When a rivulet is added, a velocity-restricted response occurs, but over a more narrow range than occurs with a smooth cylinder with rivulet. Thus, the size of the surface roughness is important. It should be sufficiently large to trap the rainwater and prevent continuous rivulet formation.

A number of different aerodynamic damping devices were tested in the wind tunnel by TTU researchers. The installation of a helical strake, elliptical rings or circular rings resulted in: (a) interruption of the axial wind flow and (b) modification of the cable-stay cross section; and (c) disruption of the formation of a continuous water stream along the cable-stay. Both single-degree of freedom (SDOF) and two-degree of freedom (2DOF) wind tunnel experiments proved the effectiveness of circular aerodynamic rings.

A two-dimensional force-damper apparatus was developed for additional tests in the wind tunnel. The addition of the horizontal degree of freedom had the effect of delaying the onset velocity of large response of the cylinder section model. The response of the system, however, was similar in magnitude to that of a single-degree-of-freedom system. The response in the horizontal direction is important up to  $RV = 280$  for the cylinder section model. Above that value, very little vibration occurs in the horizontal direction.

The velocity-restricted nature of wind-rain-induced cable-stay vibration was demonstrated as both low-wind speed and high-wind speed mitigation behavior of the circular rings were tested. Circular rings attached to the cylinder reduced the system response by up to 90% compared to the bare cylinder case at high reduced velocities. Circular rings with an outside cross-section diameter of  $D/14$ , where  $D$  is the diameter of the cylinder, were attached at regular intervals along the cylinder. The vibration of the cylinder decreases more as the spacing between the circular rings decreases. Currently, a circular ring thickness,  $t$ , between  $D/20$  and  $D/10$  has been found most effective. The damping effect increases with a larger value of  $t$ . As will be discussed in the next chapter, full-scale prototype installation on three cable-stays occurred in January 2001 by the Texas Department of Transportation (TxDOT).

## CHAPTER 4

### FIELD INSTRUMENTATION

Notwithstanding the wind tunnel tests, both bridges, Fred Hartman Bridge and Veterans Memorial Bridge, were instrumented with meteorological and response measuring instruments. Meteorological instruments measured wind speed, wind direction, barometric pressure, temperature and rainfall. Response measuring instruments were slightly different in the two bridges. In the Hartman Bridge accelerometers and displacement sensors measured cable-stay response, accelerometers measured deck vibration and load cells measured mechanical damper force. In the Veterans Memorial Bridge only accelerometers were used to measure cable-stay response. Details of the instrumentation on the two bridges are provided below.

#### ***4.1 Instrumentation Setup for Fred Hartman Bridge***

The full scale measurement system installed on the Fred Harman Bridge monitors the meteorological condition at the bridge site and the dynamic response of the bridge to ambient excitations. Measurements taken at the bridge include: stay cable vibration, deck vibration, damper force, and meteorological conditions.

##### *Measurement of Stay Cable Vibration*

###### Acceleration

In-plane and lateral accelerations of stay cables are measured in g's by tri-axial accelerometers (Crossbow Technologies, [www.xbow.com/Products/Accelerometers.htm](http://www.xbow.com/Products/Accelerometers.htm), Model CXL04LP3) with a  $\pm 4g$  range. The sensitivity of the accelerometers is 500 mV/g and the noise level is 10 mg. The accelerometers are located on the cables at about 20 feet above the deck level.

Instrumented stay cables are: AS1, AS3, AS5, AS9, AS16, AS18, AS20, AS22, AS23, AS24, AN24, BS1, BS8, BS16, BS18, BS24, CS16, CS24, DS1, and DS24.

###### Displacement

Displacement of stay cables is measured in inches by string pot displacement transducers installed at the deck rail level, near the anchorages of the cables.

Four stays were originally instrumented and displacement was measured in the in-plane direction only. Instrumented stays at this stage were: AS9, AS20, AN24 and BS24.

The system was expanded to 4 other cables when dampers were installed on these cables in March, 1999. Since then, both in-plane and lateral displacements are measured at the location of the damper-cable connection. Instrumented stays at this stage are: AS16, AS23, AS24, and BS16.

##### *Measurement of Deck Vibration*

###### Acceleration

Accelerations of the bridge deck are measured at the windward edge of the east deck at mid-span and at location near the anchorage of stays AS9, AS16, AS19 and CS19.

Originally, both vertical and lateral accelerations of the deck were measured in g's by the same tri-axial accelerometers as those used for the stay cables. After November 3, 1999, the tri-axial accelerometer at mid-span and those near the anchorage of stays AS9, AS16, and AS19 were replaced by uniaxial accelerometers with higher resolution and only vertical acceleration has been measured since.

#### *Measurement of Damper Force*

The force exerted in the dampers is measured in pounds by load cells installed in line with the dampers at stays AS16 and AS23.

#### *Measurement of Meteorological Conditions*

##### Wind Speed and Direction

Wind speed and direction are measured at three locations: the top of the south tower, the deck level at mid-span and the deck level at stay AS18. Anemometers used at the deck level are Gill UVWs which is capable of measuring wind speed up to 35 m/s and has a threshold of 0.3 m/s. The one used at the tower top is a propeller-vane anemometer which can measure wind speed up to 60 m/s and has a threshold of 1m/s and a resolution of 0/3 m/s.

##### Rainfall

The amount of rainfall is measured in inches by two rain gauges installed at two locations: the deck level at stay AS18 and the top of the south tower. The resolution of the rain gauges is 0.01 inches.

##### Atmospheric Pressure

The atmospheric pressure at the bridge is measured by a barometer installed at the deck level at stay AS18.

##### Temperature

The temperature is measured in Fahrenheit by a temperature probes installed at he deck level at stay AS18.

All of the transducers used for the measurements were connected to a PC-based data acquisition system located inside the southeast tower. The data received from the transducers are amplified and low-pass filtered using 4 pole Bessel Filters set at 10 Hz before being digitized and continuously monitored by the system. Data files are recorded automatically when threshold wind speed or acceleration levels are exceeded, ensuring that events with large oscillations of the bridge, or those associated with significant meteorological conditions are appropriately captured.

#### **4.2 Instrumentation Setup for Veterans Memorial Bridge**

The Veterans Memorial bridge deck is a precast concrete box girder supported by eight single planes of 14 cable-stays. Labeled "A" through "H" in Figure 4.1, each plane of cable-stays is arranged in a vertical, harped configuration and anchored to a central concrete tower. Researchers from Texas Tech University instrumented 4 of the 112 Veterans Memorial Bridge cable-stays. This instrumentation is complementary to the instruments

previously installed by researchers of Johns Hopkins University. Texas Tech University research personnel in Lubbock, Texas retrieve this data via telephone connections<sup>10</sup>. When a certain acceleration threshold is exceeded, that particular data segment is retained for analysis at a later time.

Two 2-axis accelerometers were attached to each of the four cables—one at the lower approximately  $L/3$  and one at the lower approximately  $L/4$  locations to ensure capture of at least the first 11 modes of vibration. In addition, one 3-axis anemometer, one temperature gauge and two precipitation gauges were installed at the deck level with the desire to capture simultaneous wind speed, wind direction and rain. A total of 22 channels of data were collected at 40 MHz.

The remote processing station continuously records 20-minute data files. In addition to weather data, each data file contains 16 acceleration data sets. A “trigger” occurs within a 20-minute timeframe when: a) the instantaneous acceleration of any of the four cable-stays exceeds a given threshold or b) the total 3-D wind speed is greater than a pre-determined value. If either of these two thresholds is exceeded during one of the 20 minute time periods, the previous and subsequent 20-minute data files are saved to disk. Otherwise the previous data file is deleted automatically. Four large capacity hard drives are installed at the remote station. In addition, two modem lines are installed for remote data monitoring and collection.

Data files recorded to disk (i.e. those not deleted by the DAQ software), are referred to as “records”. Many data files, i.e. records, saved to disk were later determined to not have meaningful data due to a variety of reasons. For example, lightning strikes, power surges, power outages, and accelerometer failures were common at the site. When at least one of the acceleration data channels for a cable-stay could be determined to be good, the 20-minute data file, or record, is categorized as a “good record”. When either a “good record” or continuous series of “good records” occurred for a given cable stay, the single good record or the series of records is categorized as an “event”.

---

<sup>10</sup> High speed internet connections were unavailable on the bridge at the beginning of this project.  
Project 0-1400

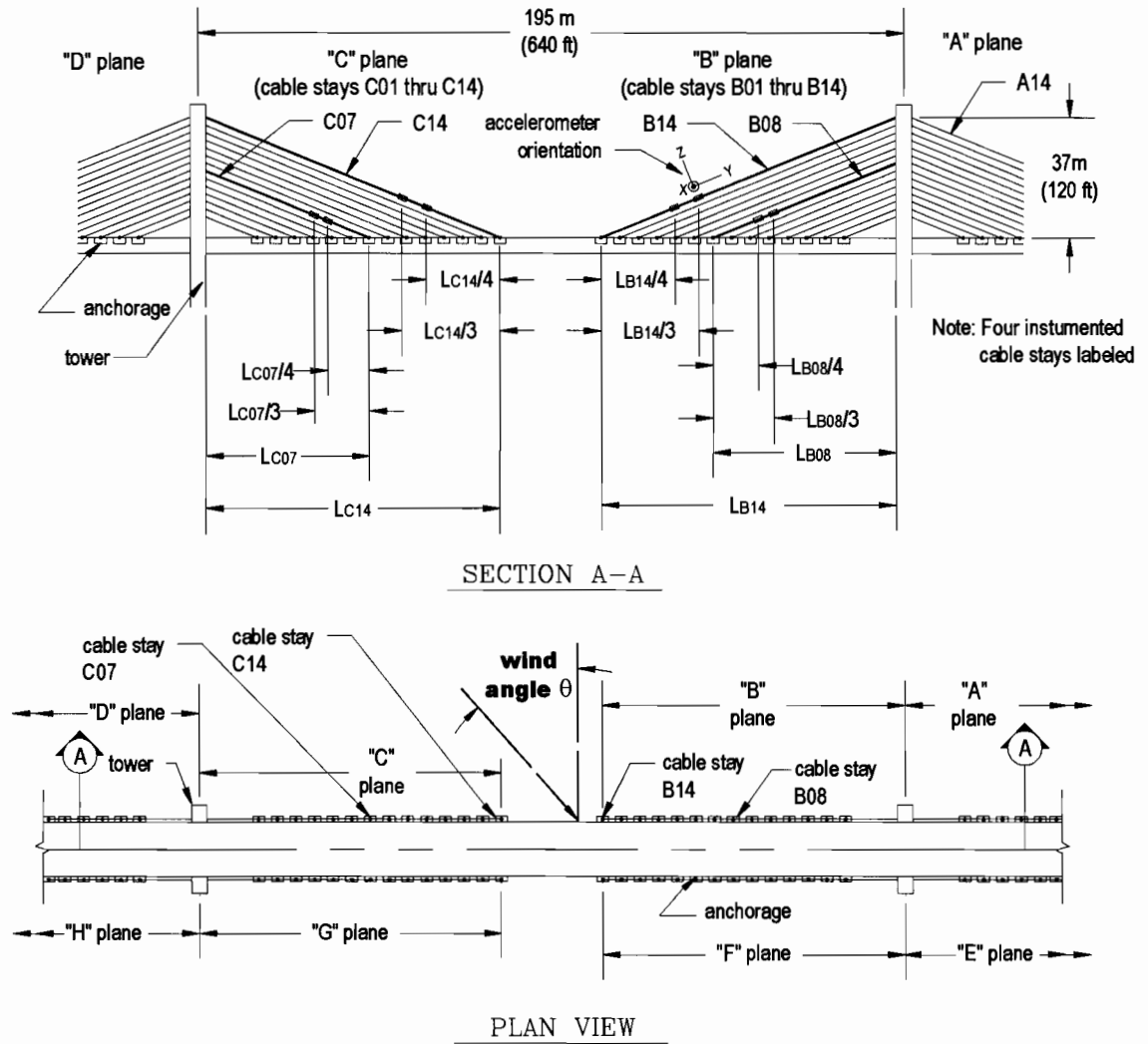


Figure 4.1 Veterans Memorial: Instrumentation Scheme and Wind Angle

## CHAPTER 5

### FIELD RESULTS

Instrumentation described in the previous chapter was connected to three data acquisition systems, (1) Fred Hartman Bridge data acquisition system monitored by John Hopkins University, (2) Veterans Memorial Bridge data acquisition system monitored by Johns Hopkins University and (3) Veterans Memorial Bridge data acquisition system monitored by Texas Tech University.

Johns Hopkins University implemented and maintained a 64-channel data acquisition system of Fred Hartman Bride and a 24-channel system on the Veterans Memorial Bridge. Analysis and results of these data were provided to TxDOT through a WDP Progress Report (WDP, 2001). Johns Hopkins University is continuing to monitor these data acquisition systems in association with the Center for Transportation Research, University of Texas-Austin. Analysis and interpretation of these data are not finalized; they will be available in a CTR, UT-Austin final report.

Analysis and interpretation of data monitored and analyzed by Texas Tech University are presented here. Specifically of interest are the results of cable-stay vibrations prior to and following installations of aerodynamic ‘ring’ dampers.

#### 5.1 Overall Results for Veterans Memorial Bridge

Several site visits were required over the two-year field test time period. Frequently, accelerometers had to be replaced due to the harsh operating environment. However, over 8500 records were obtained on (at least one of) the four TTU-instrumented cable-stays at the Veterans Memorial Bridge from August 1999 to July 2001 as shown in Table 5.1. These files were evaluated to determine if the “trigger” had actually recorded a “good record”. As discussed, an event is defined as either (1) a single good record, or (2) a series of continuous good records, where a cable-stay is continuously vibrating. Due to typical potential field measuring errors (e.g. random periodic instrumentation failure, etc.), a majority of the “recorded” data files did not constitute being categorized as a “good record”.

**Table 5.1** “Good Records” vs. Total Number of Records

	<b>Before 1/10/01</b>	<b>After 1/10/01*</b>
Number of Records	6706	1885
Number of Good Records	274	224

*\*Note, Jan 10, 2001 was the installation date of the aerodynamic rings on Cable-Stays A14, B08 and B14..*

In total, approximately 500 “good records” were obtained. Of these, 252 events were identified with accelerations greater than 0.5 g on at least one of the sixteen acceleration data channels. Table 5.2 summarizes the events found for particular cable-stay acceleration thresholds, both before and after the ring installation. This table shows that more total weather events were recorded on all four cable-stays in the 6 months after January, 2001 than were recorded during the previous 1½ years of monitoring. However, for Cable-Stay B14, after the rings were installed, the number of occurrences with maximum instantaneous accelerations greater than 1.0 g decreased, in general. One of the instantaneous 5 g events listed in Table 5.2 is highlighted in Figure 5.1.

It is important to emphasize that “good events” included in Table 5.2 are actual, recorded data files. As only four cable-stays out of the total 112 were instrumented, it is possible that other cable-stays may have vibrated more than the instrumented cable-stay results presented in this table. In addition, as discussed previously, a portion of the instrumentation was “out” for certain periods during the two-year monitoring period. Thus, values presented in the table can be considered to indicate a reasonable minimum number of occurrences that can be expected for the four cables. Nevertheless, the number of records indicated in the table signifies that a potential fatigue situation is present in these cable-stays.

**Table 5.2. “Good Records”:**—Accelerations Greater than 0.5 g

Maximum Instantaneous Accelerations	Total		B14 only		B14 with Rain	
	Before	After	Before	After	Before	After
>=0.5 and <1.0	31	123	28	53	4	34
>=1.0 and <1.5	26	21	26	14	5	3
>=1.5 and <2.0	5	9	2	5	0	0
>=2.0 and <2.5	1	0	0	0	0	0
>=2.5 and <5.0	3	17	1	1	1	0
>=5.0	3	13	3	0	3	0

*Note: Only for a short period of time, e.g. 3 months, was the acceleration threshold set to 0.5 g before January 10, 2001. The threshold was set to 1.0 g during the other 15 months of this initial time period (i.e. before ring installation). After January 10, 2001 (i.e. after the rings were installed), the acceleration threshold was reset to 0.5 g.*

## 5.2 Major Veterans Memorial Cable-Stay Acceleration Event

Figure 5.1 represents a major accomplishment of this research effort. The parameter plots shown in the figure were obtained from particular instrumentation selected and installed on the bridge by TTU researchers—based on results obtained from the background research discussed in Chapter 2 of this report and on TTU wind tunnel test results presented and discussed in Chapter 3 of this report.

Figure 5.1 shows plots of four parameters—all occurring simultaneously on the Veterans Memorial Bridge on October 8, 1999. The total time for each of the four plots (i.e. Plots A, B, C and D) is 2400 seconds, or 40 minutes. The time of interest is from about 200 to 1700 seconds. Plot A shows the wind speed at the bridge site to be a fairly constant 7 to 9 m/s (15-20 mph) during the time of interest.

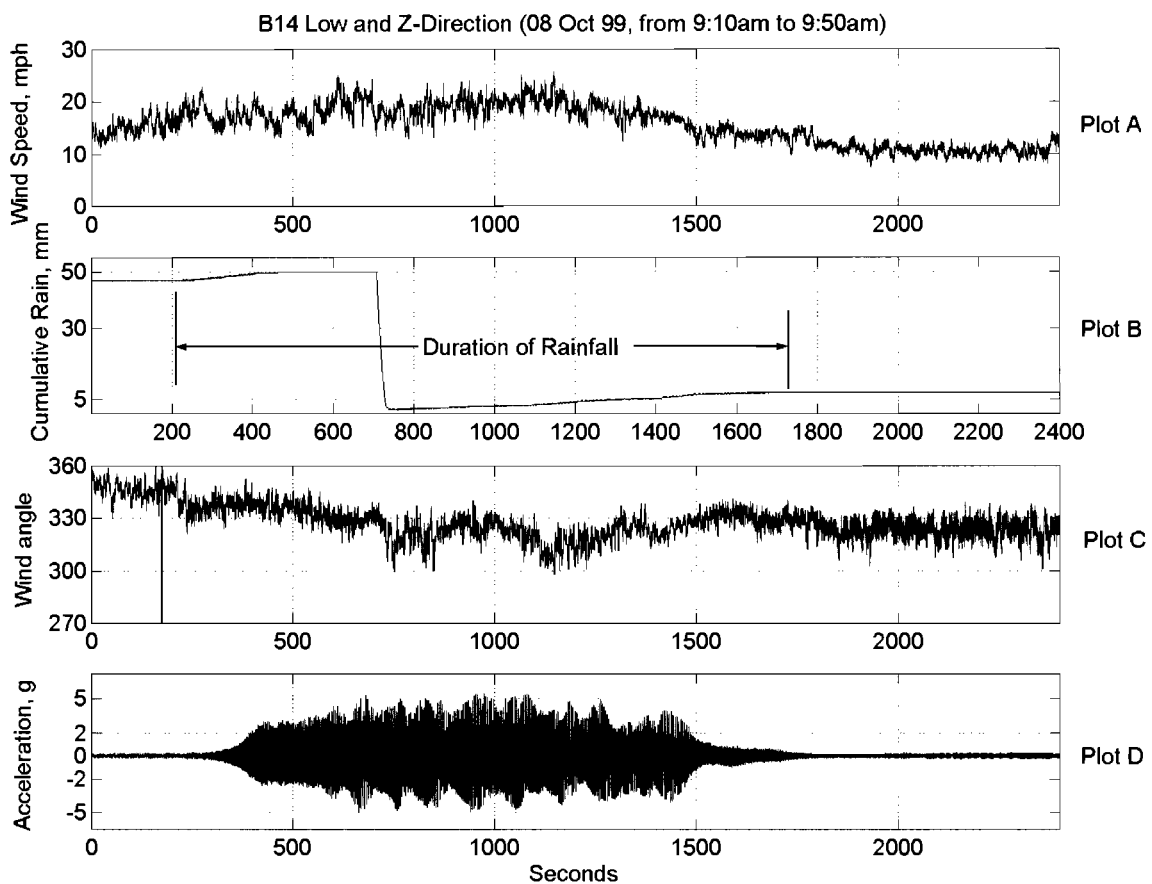


**Figure 5.1** Veterans Memorial 5 g Cable-Stay Vibration Event: Simultaneous Wind Speed and Direction, Rainfall, and Stay Acceleration

Plot B shows the cumulative rainfall to be increasing during the time of interest—indicating that rain is occurring. (When the line in the plot has a slope, it is raining. When the line is horizontal, it is not raining.) The rainfall rate is 0.45 mm/minute, indicating a heavy, steady rainfall. The precipitation gauge is rated at 50 mm capacity. As shown in the

plot, at approximately 750 seconds into the recorded time period, the gage dumped the accumulated water and reset itself. Rainfall was continual for 1500 seconds, or approximately 25 minutes.

Plot C of Figure 5.1 shows the angle of the wind direction to remain in a range of  $300^\circ$  to  $340^\circ$  during the time of interest.<sup>11</sup> As referenced in Figure 4.1, such a wind direction comes in the “declining” direction of Cable-Stay B14, where B14 is the longest cable in the “B” plane of 14 cables on the Veterans Memorial. A “declining” direction refers to when the cable declines, from the tower to the anchorage, in the same direction as the wind. Plot D of Figure 5.1 shows the non-oscillating Cable-Stay B14—when time is less than 300 seconds—to begin instantaneous accelerations of 5 g, almost immediately after the rain begins. The cable-stay continues to oscillate during the time of interest. When the rain ceases, the cable-stay soon returns to its non-oscillating state. In summary, Plots A through D in Figure 5.1 show an actual field event: 1) developing as predicted, 2) oscillating under prescribed conditions, and 3) ceasing to oscillate when contributing conditions vary outside certain ranges. These four plots, combined with wind tunnel results presented in Chapter 3 of this report, suggest the factors causing the wind/rain induced vibration phenomenon now are reasonably well understood.

### 5.3 Aerodynamic Ring Installation

Aerodynamic rings were installed on two of the four TTU-instrumented cables, B14 and B08, and on one JHU-instrumented cable, A14, in mid-January, 2001. Installation of the rings on one of the cable-stays is shown in Figure 5.2. Data was collected and analyzed for one and a half years prior to the ring installation, and for 6 months after. After the rings were installed, there was a total of 14 days having moderate to heavy rains. To assist in the capture of events after ring installation, the trigger acceleration threshold was reduced to 0.5 g.

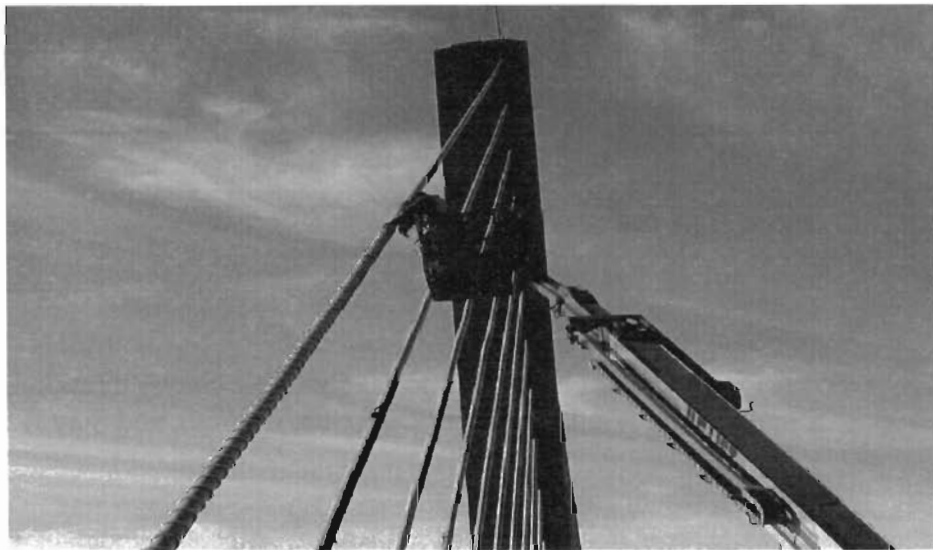


**Figure 5.2** Full-Scale Aerodynamic Ring Installation

<sup>11</sup> Refer to the Plan view in Figure 4.1 for the defined wind angle direction orientation.  
0-1400

## 5.4 Field Events after Ring Installation

Two sets of acceleration events greater than 2.5 g on the four TTU-instrumented cable-stays (i.e. B14, B08, C14, C07) are presented in this report. The first set consists of events recorded before rings were installed on B08 and B14, from August 01, 1999 to January 10, 2001 (approximately 1.5 years). The second set consists of events recorded after rings were installed on B08 and B14, from January 10, 2001 to July 10, 2001 (approximately 0.5 years). Each set is presented using the following three comparisons: (1) one-minute RMS acceleration histories vs. one-minute wind speed (Figures 5.3-5.6), (2) one-minute RMS acceleration history distributions vs. a one-minute wind speed and direction (Figures 5.7-5.10), and (3) dominating vibration modes (Figures 5.11-5.14). As will be discussed subsequently, these comparisons appear to indicate that aerodynamic rings effectively suppress wind-rain-induced vibration of cable-stays in the field.

Tables 5.2 through 5.5 summarize the recorded “good records” and “events” in tabular form. Using the same recorded data and dividing each event into 1 minute RMS data points, Figures 5.3 through 5.10 present the cable-stay behavior in graphical form.

### 5.4.1. Field events with maximum instantaneous acceleration >2.5 g

Before ring installation, four events with instantaneous accelerations >2.5 g occurred on four separate days. These events are listed in Table 5.3. as shown in the table:

- A maximum instantaneous acceleration of 5.8 g, with a maximum wind speed of 12 m/s (26 mph), occurred on Cable B14 with rain (as shown in Fig. 5.1).
- Two of the four recorded events having an instantaneous acceleration > 2.5 g occurred on Cable B14. The other two events presented occurred on Cable C14. Neither cable had rings installed at this time.
- All four recorded events occurred with rain.
- Almost all of the events occurred when the wind speed was between 10 and 12 m/s (23 and 26 mph), with one recorded event reaching 25 m/s (57 mph).

**Table 5.3** All Events (>2.5 g) without Rings from August 1, 1999 to January 10, 2001

NO.	DATE	CABLE	MAXIMUM INSTANTANEOUS ACCELERATION (g)	MAXIMUM WIND SPEED (mph)	RAIN?
1	09-21-2000	B14	5.6	23	YES**
2	01-27-2000	C14	4.9	25	YES
3*	10-08-1999	B14	5.8	26	YES
4	08-03-1999	C14	3.0	57	YES

*Note: The third entry, marked \*, is based on the event presented previously in this report (Figure 5.1). The rain event, marked \*\*, was determined to have rain present based on NOAA data.*

The number of “events” shown in Table 5.3 is small. Again, it is important to note that due to the occurrence of several equipment shutdowns during the monitoring period, additional events were likely missed by the DAQ system. After the ring installation on Cable-Stay B14, a total of three system-wide events triggered (i.e. any event triggers from Cable-Stays B08, B14, C07 or C14), each having an instantaneous acceleration >2.5 g. As shown in Table 5.4, two of these events occurred on Cable-Stay C14 (without rings), while one occurred on Cable-Stay B14 (with rings). The event for B14 was not wind-rain-induced vibration. The only event recorded with rain during this six-month period was a two-day-long event that occurred on (non-ringed) Cable-Stay C14.

**Table 5.4** All Events (>2.5 g) from January 10, 2001 to July 10, 2001  
(B14 with Rings, C14 without Rings)

NO.	DATE	CABLE	MAXIMUM INSTANTANEOUS ACCELERATION (g)	MAXIMUM WIND SPEED (mph)	RAIN?
1	05-26-2001	C14	2.9	20	NO
2	03-27-2001	C14	6.5	28	YES
3	03-11-2001	B14	2.7	19	NO

*Note: All entries were determined to have rain or not have rain based on NOAA data.*

Both precipitation gauges functioned flawlessly during the first 1½ year monitoring period, i.e. “before 1/10/01”. Unfortunately, after analysis of the “after 1/10/01” data, it became apparent that neither precipitation gauge installed at the bridge performed properly during the final six-month monitoring period. Neither gauge recorded significant rainfall during several major rain events, though, based on additional data obtained from the National Oceanic and Atmospheric Administration, NOAA, collected at the nearby Port Arthur, Texas Airport, it appears that rain did occur in the area on March 27, 2001 (NOAA 2001). From Table 5.4, the following can be concluded:

- All three events had a maximum wind speed somewhere between 19~28 mph.
- A maximum instantaneous acceleration of 6.5 g occurred on Cable-Stay C14 with rain during a maximum wind speed of 28 mph.
- Two of the three recorded events occurred on Cable-Stay C14, on which rings were not installed. One of these events occurred without rain.
- Only one event occurred on Cable-Stay B14, on which rings were installed. This event was not wind-rain-induced.
- For a 20 mph wind without rain, Cable-Stay C14 experienced a maximum instantaneous acceleration of 2.9 g. For a similar 19 mph wind without rain, Cable-Stay B14 experienced a maximum instantaneous acceleration of 2.7 g.
- For a 28 mph wind with rain, Cable-Stay C14 experienced a maximum instantaneous acceleration of 6.5 g. Unfortunately, a similar wind speed with rain was not recorded

for Cable-Stay B14. This could indicate that such an event did not occur in the monitoring period—or it could indicate that the rings were effective in preventing the wind-rain-induced vibrations from occurring. Conservatively, with such a limited data set, one can conclude only that the rings may prevent vibrations from occurring.

Table 5.5 shows the number of all “good records” with accelerations greater than 0.5 g for each cable. For example, before January 10, 2001 (i.e. before installation of rings on Cable-Stay B14), there are 4 separate 20-minute “good records” in which at least one channel of Cable-Stay B14 has an instantaneous acceleration greater than 2.5 g.

**Table 5.5** Number of “Good Records” (>0.5 g) for each Cable-Stay from 8/99 to 7/01

MAXIMUM INSTANTANEOUS ACCELERATION	BEFORE JAN. 10, 2001				AFTER JAN. 10, 2001			
	B14	C14	B08	C07	B14	C14	B08	C07
≥0.5 g and <1.0 g	28	7	18	17	53	29	37	78
≥1.0 g and <1.5 g	18	1	2	0	14	4	2	4
≥1.5 g and <2.0 g	2	3	1	2	5	1	0	5
≥2.0 g and <2.5 g	0	0	2	1	0	0	0	4
≥2.5 g	4	2	1	0	1	29	0	21

*Note: The numbers in this table differ slightly from those shown in Table 5.2, as Table 5.2 lists every separate “good record” while this table counts a continuous series of simultaneous “good records” as one “good record”. Also, the four (before) B14 “good records” shown above correspond to the two (before) B14 “events” shown in Table 5.3.*

On Cable-Stay B14, only one event with an acceleration greater than 2.5 g occurs after January 10, 2001. Before January 10, 2001, all four “good records” for Cable-Stay B14 with accelerations greater than 2.5 g are with rain. After January 10, 2001, the greater than 2.5 g “good record” for Cable-Stay B14 is without rain.

#### 5.4.2. One-minute RMS acceleration history vs. one-minute wind mean speed

In order to evaluate the effectiveness of rings, the relationships between one-minute RMS acceleration history and one-minute mean wind speed, before and after ring installation, are plotted for every channel in Figures 5.3, 5.4, 5.5, and 5.6 for Cable-Stays B14 and C14. One-minute RMS accelerations for every identified “good record” and every channel have been calculated. The data of one record is 20 minutes long, so it contains 20 one-minute RMS data points of acceleration. Figure 5.3 shows the one-minute RMS acceleration history of B14HZ<sup>12</sup> vs. wind speed before ring installation, i.e. from August 01, 1999 to January 10, 2001. The maximum RMS acceleration is approximately 1.7 g. Figure 5.3 contains 5400 one-minute RMS points. After ring installation, the one-minute RMS acceleration history of B14HZ is shown in Figure 5.4. From this figure we can see the maximum RMS acceleration decreases to 1.3 g. More importantly, no wind-rain-induced

<sup>12</sup> The “B14” refers to Cable-Stay B14. The “H” refers to the “high” or L/3 position. The “Z” refers to vertical direction of the cable-stay (with respect to acceleration). See Figure 4.1, “Section A-A”.

vibration events were found after the rings were installed. Figure 5.4 contains 4400 one-minute RMS points.

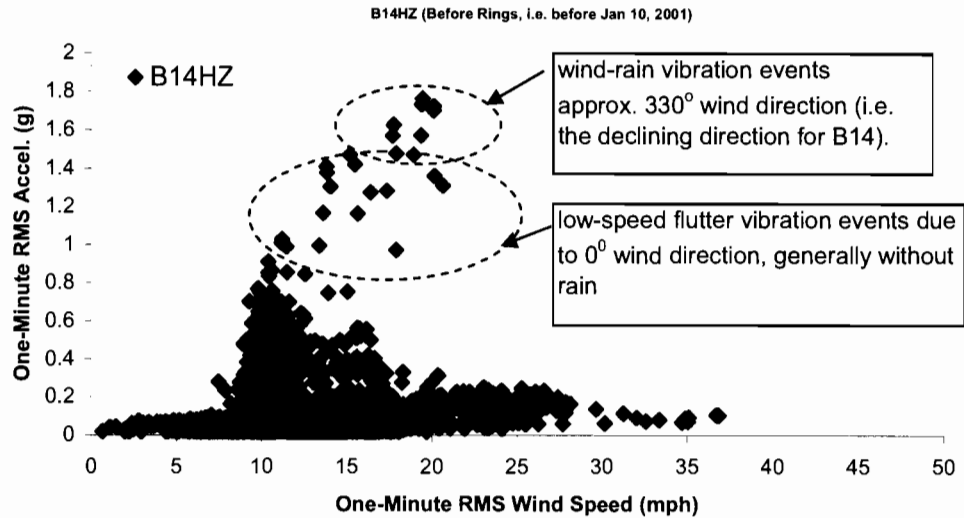


**Figure 5.3** B14HZ One-Minute RMS Acceleration vs. Wind Speed (Before Rings)

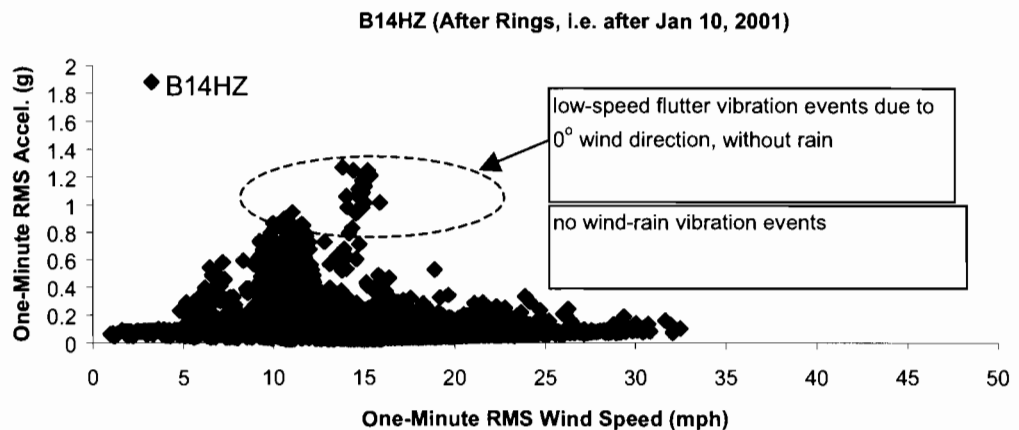


**Figure 5.4** B14HZ One-Minute RMS Acceleration vs. Wind Speed (After Rings)

Figures 5.5 and 5.6 show the one-minute RMS acceleration histories before and after January 10, 2001 respectively for C14HZ. In contrast to B14, no rings were installed on Cable-Stay C14 after January 10, 2001. As indicated in the figures, a significant increase in recorded vibration events occurred on C14 after Jan 10, 2001. The maximum RMS acceleration of C14HZ increased dramatically from 0.8 g to 1.4 g after January 10, 2001.

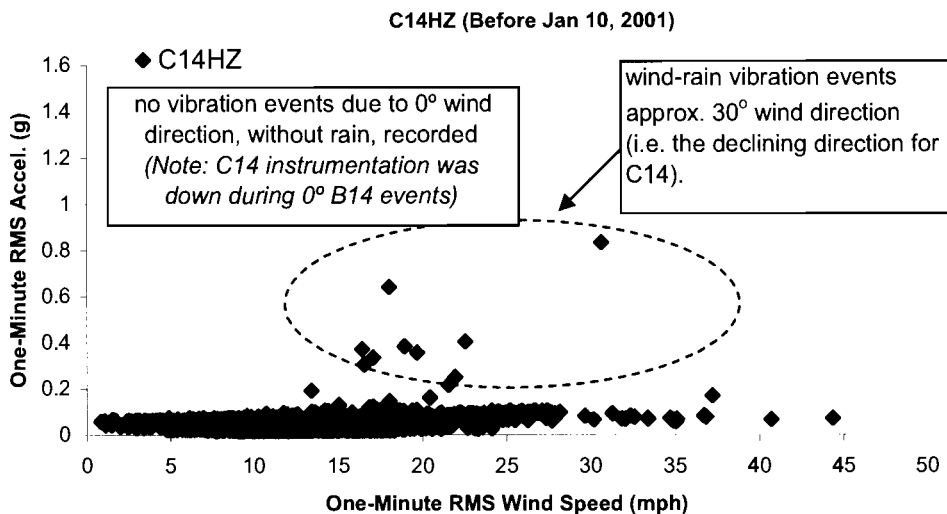


**Figure 5.5** C14HZ One-Minute RMS Acceleration History vs. Wind Speed (Before January 10, 2001—No Rings)

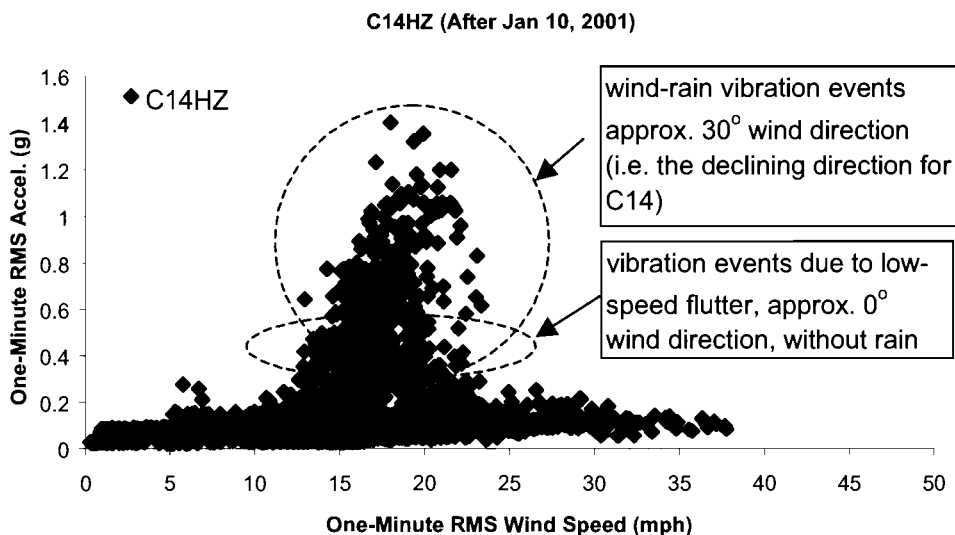


**Figure 5.6** C14HZ One-Minute RMS Acceleration History vs. Wind Speed (After January 10, 2001—No Rings)

Rings were placed on Cables A14, B14 and B08. Though Cable Stay A14 was instrumented, the instruments did not provide useful data. Data for B08 and B14 are similar to each other, with B14 results always more extreme than B08. Therefore, only analyzed data from Cable-Stay B14 is presented in this report. Though the results appear promising, with the limited data collected to date, firm conclusions cannot be made.

Table 5.6 lists the changes of maximum one-minute RMS accelerations for all 16 channels before and after January 10, 2001. As indicated in the table, the “After/Before Ratios” of all channels on cables installed with rings (i.e. B14 & B08) after January 10 are less than 1, with an overall average of 0.5. In contrast, for the channels on cables without rings installed (i.e. Cable Stays C14 & C07), the “After/Before Ratios” are greater than 1, with an overall average of 2.2.

**Table 5.6.** Maximum One-Minute RMS Acceleration on All Channels Before and After January 10, 2001

CHANNEL NO.	MAX RMS ACC BEFORE	MAX RMS ACC AFTER	AFTER/ BEFORE RATIO	AVERAGE OF “A/B” RATIO	WITH RINGS AFTER 1/10/2001?
B14HX	0.8	0.3	0.4	0.6	YES
B14HZ	1.8	1.3	0.7		
B14LX	0.7	0.4	0.5		
B14LZ	2.0	1.6	0.8		
C14HX	0.5	1.2	2.3	2.6	NO
C14HZ	0.8	1.4	1.7		
C14LX	0.5	1.5	3.1		
C14LZ	0.9	2.7	3.1		
B08HX	0.3	0.2	0.5	0.4	YES
B08HZ	1.2	0.2	0.2		
B08LX	0.4	0.2	0.4		
B08LZ	1.3	0.3	0.3		
C07HX	0.4	0.6	1.8	1.9	NO
C07HZ	0.8	1.8	2.3		
C07LX	0.3	0.5	1.5		
C07LZ	0.9	1.8	1.9		

It is noted that very few wind-rain-induced or low-speed flutter<sup>13</sup> events were recorded from Cable-Stay C14 before January 10, 2001. There are several possible explanations for this. Though a wind-rain-induced event may have occurred, it may have happened when at least one component of the DAQ instrumentation system had malfunctioned. Another possibility is that only a few wind-rain-induced events actually occurred from a direction capable of “energizing” Cable-Stay C14 prior to January 10, 2001.

Similarly, the absence of wind-rain-induced events for Cable-Stay B14 after January 10, 2001 is most likely to be due to either: 1) no favorable weather conditions occurred after January 10, 2001, or 2) the rings worked - based on the data collected for wind-rain conditions.

<sup>13</sup> “Low-speed flutter” is used to refer to galloping in this document and it is a velocity-restricted response. It generally occurs without rain.

Again, though the available field data is limited, it appears somewhat reasonable to conclude that the aerodynamic rings have suppressed the vibration of cable-stays during wind-rain-induced vibration events. For “without rain” cases, the rings may not be effective at low-wind speeds, as indicated in both wind tunnel and field tests. The effective aeroelastic damping from the circular rings becomes functional at higher wind speeds. At these higher wind speeds, the divergent cable-stay response is likely to occur without the rings. (Note these higher wind speed cases were not recorded during the field monitoring period, so the expected effectiveness of the rings at the higher field-site wind speeds could not be confirmed.)

#### 5.4.3. One-minute RMS acceleration distributions vs. wind direction and speed

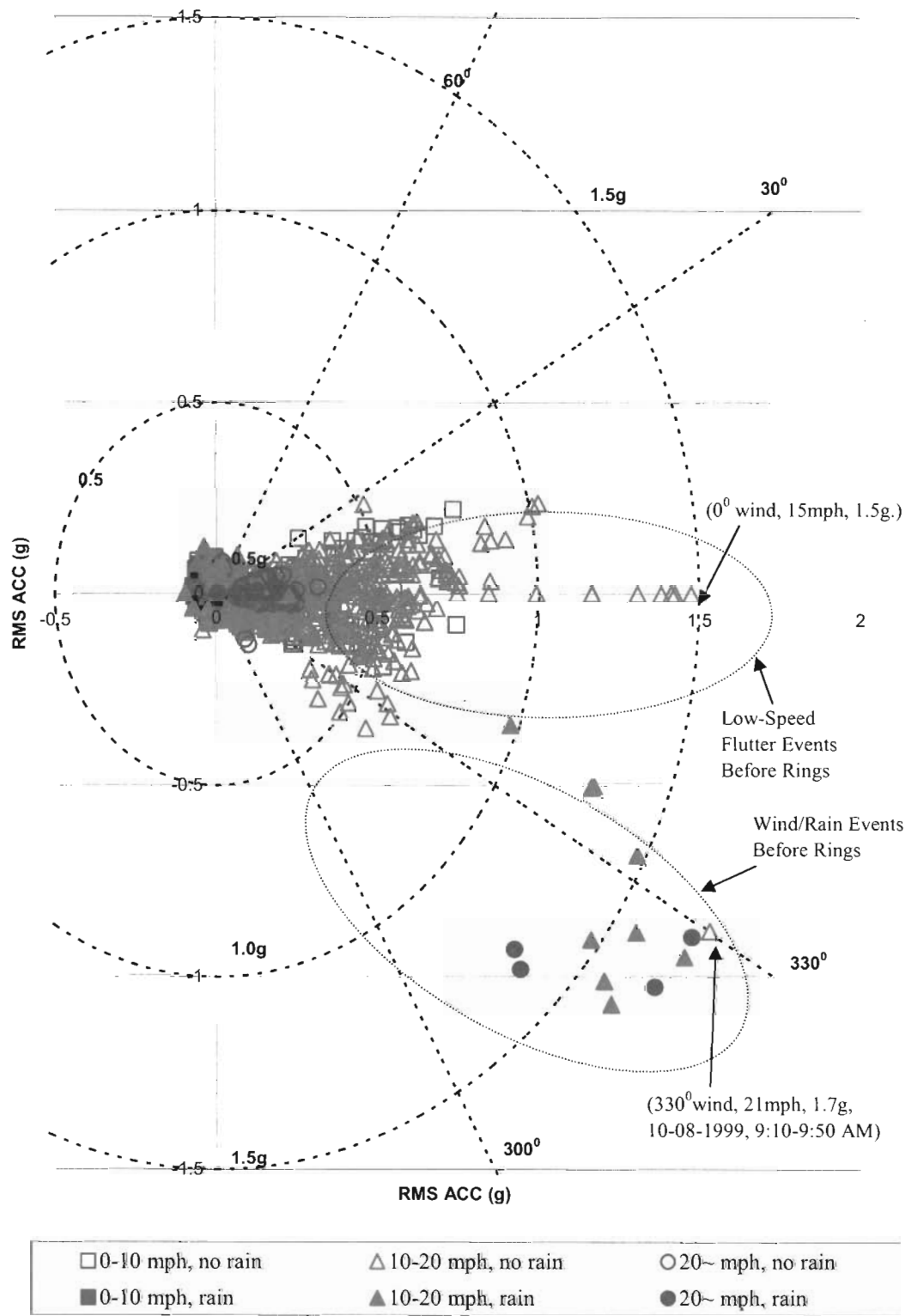
As noted earlier, wind direction has a major effect on the vibration response of cable-stays. When the wind direction angle is  $0^\circ$  (i.e. perpendicular to the cable surface as indicated in Figure 4.1) and without rain generally, the wind-induced vibration is low-speed flutter, i.e. a divergent type. In contrast, when the wind direction angle is approximately  $\pm 30^\circ$  ( $30^\circ$  for C14,  $330^\circ$  for B14), combined with rain, the cable vibration is usually categorized as wind-rain-induced vibration, i.e. a velocity-restricted type, which is shown in Figures 5.7 through 5.10. In order to take wind direction into consideration, all one-minute RMS accelerations, both before and after ring installation, have been plotted about their corresponding directions. Figure 5.7 shows the one-minute RMS acceleration distribution of B14HZ vs. wind direction before ring installation. These 5400 points correspond to points shown in Figure 5.3. The maximum recorded RMS acceleration is approximately 1.5 g with zero degree wind direction (i.e. low-speed flutter) and 6.7 m/s (15 mph) wind speed. With rain, a  $330^\circ$  wind direction, and a 9.4 m/s (21 mph) wind speed, an RMS acceleration of 1.7 g is recorded as indicated in the figure. The former vibration is categorized as low-speed flutter, and the latter is categorized as wind-rain-induced vibration. For this cable-stay, the wind-rain-induced vibration and low-speed flutter typically cause a larger acceleration response than those vibrations caused by vortex shedding.

Figure 5.8 shows the one-minute RMS acceleration distribution of B14HZ after ring installation. These points correspond to points shown in Figure 5.4. In Figure 5.8, low-speed flutter continues to occur. However, the wind-rain-induced vibration appears to have disappeared. Again, as discussed previously, though the amount of data is limited, the preliminary indication is that the aerodynamic rings may be suppressing the wind-rain-induced cable-stay vibration. As expected, the circular rings cannot suppress the low-speed flutter of the cable-stays. However, this low-speed flutter typically does not cause extremely large vibrations.

Table 5.7 lists B14HZ RMS acceleration results with rain and with wind directions between  $315^\circ$  and  $345^\circ$ , both before and after the aerodynamic rings were installed. Based on results shown in the table, when the wind speed is between 9-10 m/s (20-22 mph), before the rings were attached, a maximum RMS acceleration of 1.7 g occurred. In contrast, after rings were installed, a maximum RMS acceleration of only 0.08 g occurred. As this appears to be an order of magnitude reduction, the aerodynamic rings appear to mitigate the wind-rain-induced vibration. Again, this conclusion is subject to previously discussed reservations concerning the limited amount of recorded data.

**Table 5.7. Acceleration RMS of B14HZ**  
 (With Rain, With Wind Direction from 315° to 345°)

NO.	WIND SPEED (mph)	Before Rings (Before January 10, 2001)			After Rings (After January 10, 2001)		
		TOTAL	RMS ACC		TOTAL	RMS ACC	
			FROM	TO		FROM	TO
1	5~10	1		0.03			
2	10~15	1		0.05			
3	15~20	13	0.05	1.7			
4	20~22	2	1.7	1.7			
5	23~25				6	0.07	0.08
6	25~29				16	0.06	0.09



**Figure 5.7.** B14HZ one minute RMS acceleration distribution with wind speed and direction (Before January 10, 2001–Without Rings)

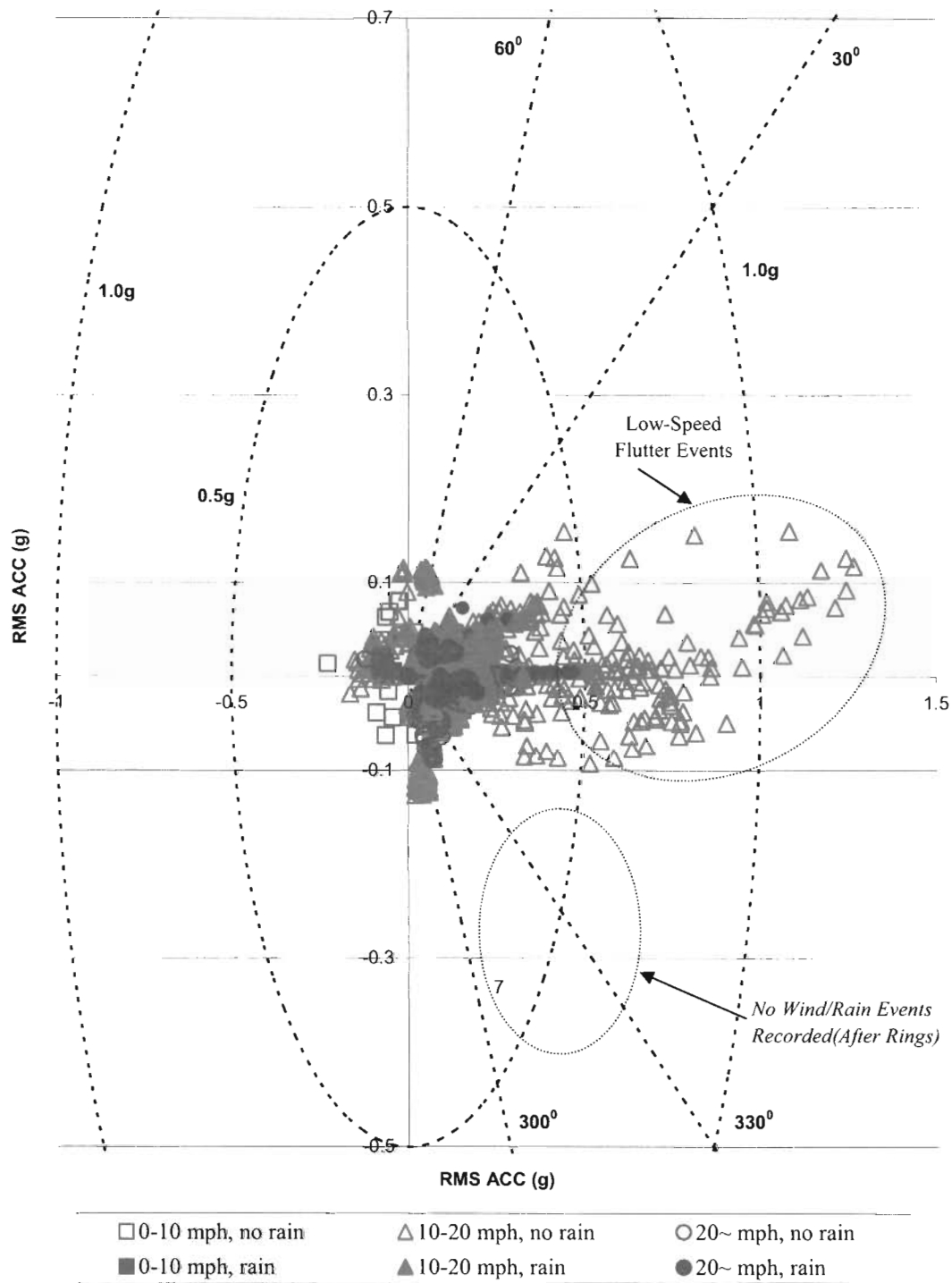


**Figure 5.8.** B14HZ one minute RMS acceleration distribution with wind speed and direction (After January 10, 2001–With Rings)

The RMS acceleration distribution vs. the wind direction for C14HZ, where no rings were installed, is shown in Figures 5.9 and 5.10, before and after January 10, 2001, respectively. Figures 5.9 and 5.10 correspond to Figures 5.5 and 5.6, respectively. Figure 5.9 shows no low-speed flutter events before January 10, 2001, and relatively few wind-rain-induced events for Cable-Stay C14. In contrast, Figure 5.10 shows an extremely high number of wind-rain-induced events after January 10, 2001. C14HZ was expected to experience the same low-speed flutter as B14HZ did before and after January 10, 2001, since they have the same geometric and material properties. However, low-speed flutter events on C14HZ did not occur as often, nor were they as large as the low-speed flutter events on B14HZ (shown in Figure 5.8) that occurred during the same time period. Further investigation has revealed that the absence of recorded C14 low-speed flutter events during the initial monitoring period was likely due to equipment malfunctions during these time periods.

**Table 5.8** Acceleration RMS of C14HZ  
(With Rain and Wind Direction Between 15° and 45°)

NO.	WIND SPEED (mph)	Before Jan 10, 2001 (No Rings)			After Jan 10, 2001 (No Rings)		
		TOTAL	RMS ACC		TOTAL	RMS ACC	
			FROM	TO		FROM	TO
1	5~10	3	0.03	0.04	1		0.07
2	10~15	1		0.06	125	0.02	0.7
3	15~20				395	0.04	1.3
4	20~25	1		0.41	50	0.06	1.2

Similar to Table 5.7, Table 5.8 lists C14HZ RMS acceleration results, with rain and with wind directions between 15° and 45°. Again, though the amount of data is limited, it appears that without the rings installed, Cable-Stay C14 remains prone to wind-rain-induced vibrations.

In Tables 5.7 and 5.8, it is evident that only a few events recorded before and after ring installation had similar wind conditions. Though preliminary results appear favorable, further data collection is necessary to prove the effectiveness (or non-effectiveness) of the rings. However, it appears the rings have no measurable beneficial effect on mitigating the low-speed flutter induced from a 0° wind direction. Nevertheless, again based on limited (perhaps incomplete) field data, it appears probable that the passive rings are effective against wind-rain-induced cable-stay vibrations.

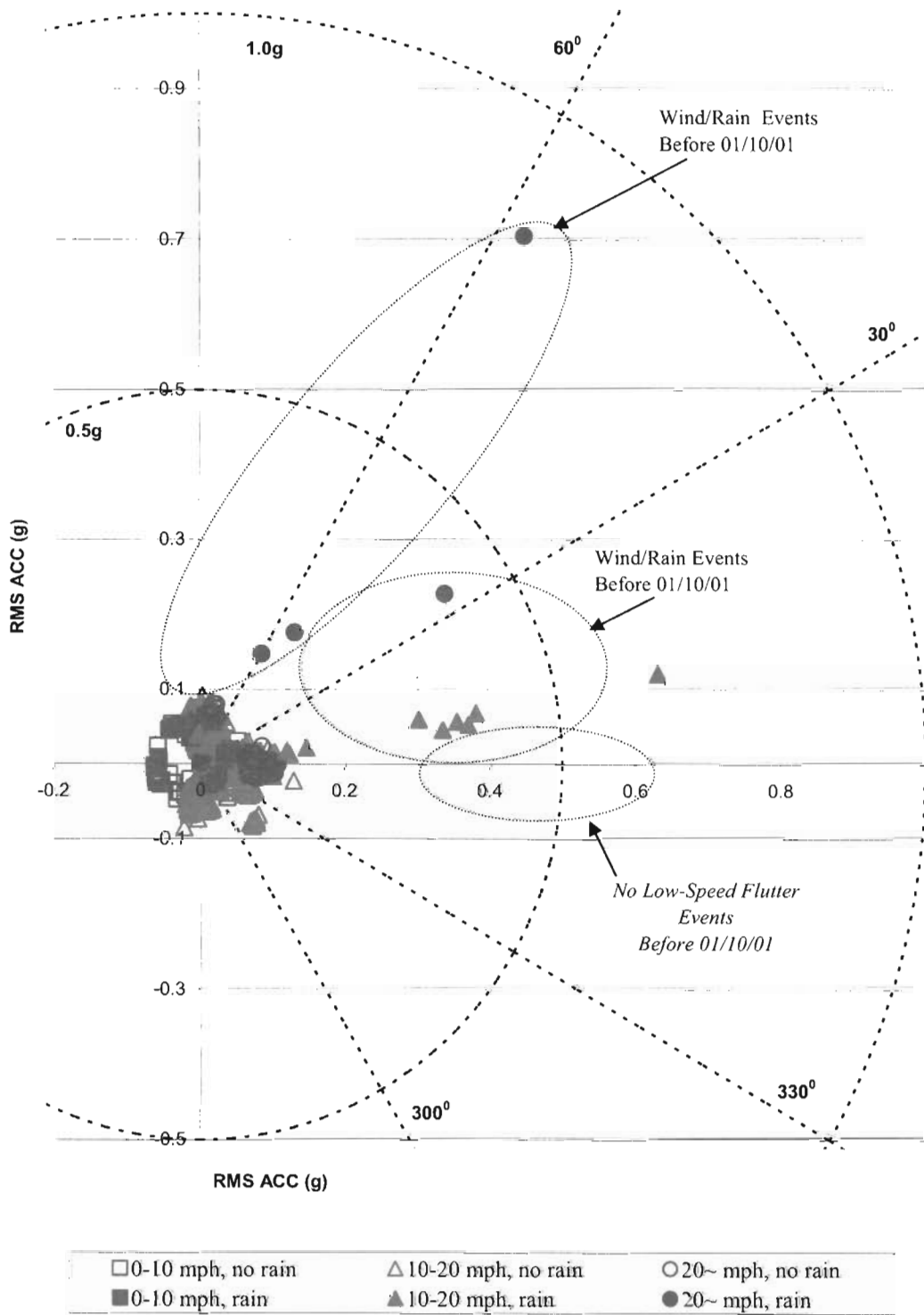


**Figure 5.9.** C14HZ one-minute RMS acceleration distribution with wind speed and direction (Before January 10, 2001–Without Rings)

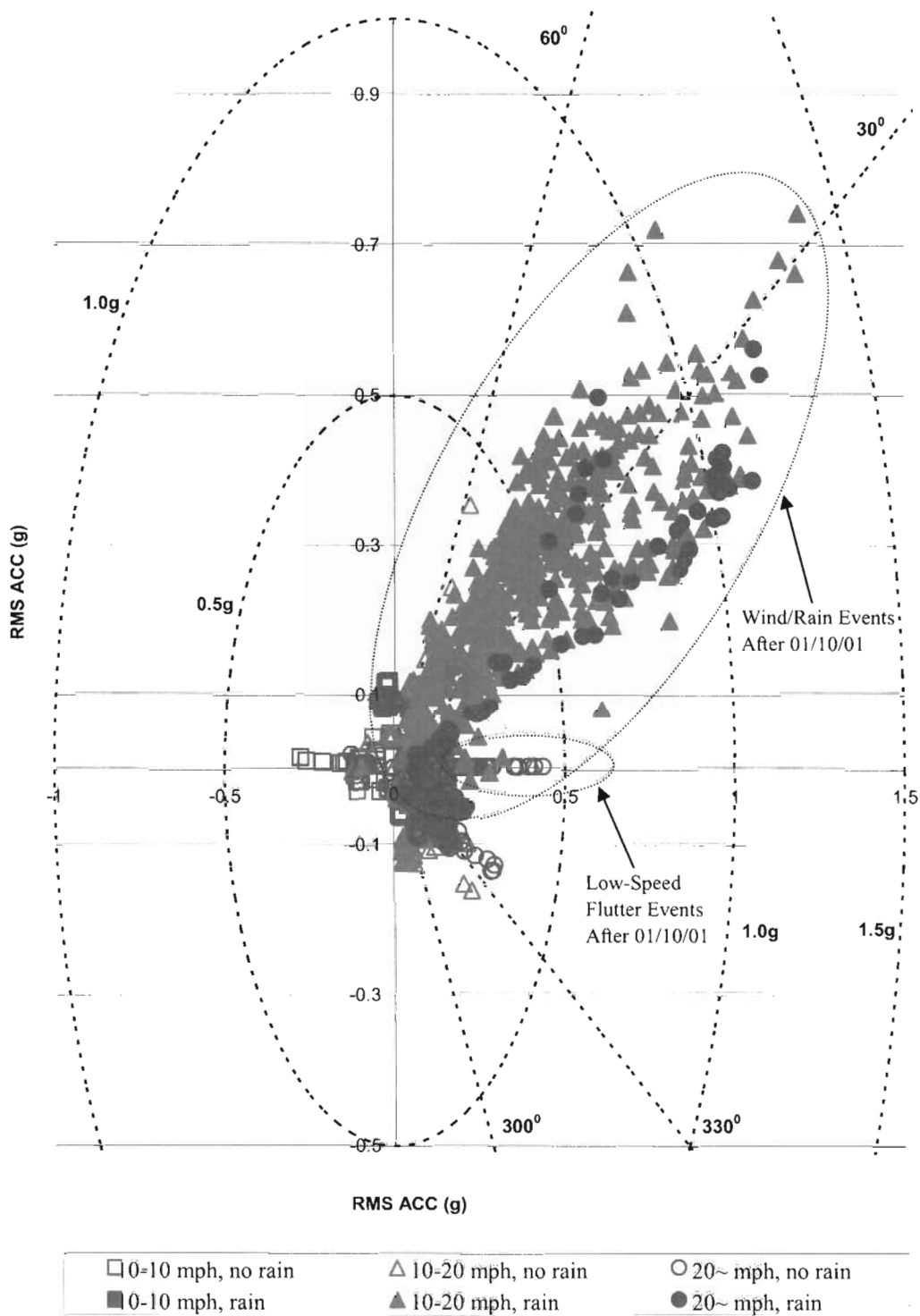


**Figure 5.10.** C14HZ one-minute RMS acceleration distribution with wind speed and direction (After January 10, 2001–Without Rings)

#### 5.4.4. Dominating vibration modes before and after ring installation

Interestingly, aerodynamic rings appear also to have slightly altered the dominating vibration modes of the two “B” cables. Figure 5.11 shows the occurring percentage of each mode as the dominating mode before the rings are installed. Figure 5.12 shows the same relationship after the rings were installed. Before ring installation the three most dominating modes are the 13<sup>th</sup> (39% of all events), 7<sup>th</sup> (18%) and 6<sup>th</sup> (10%). After ring installation, the status changes with the three most frequently occurring modes being the 10<sup>th</sup> (31%), 4<sup>th</sup> (17%) and 7<sup>th</sup> (10%). Also, the 2<sup>nd</sup> mode begins to appear more often after ring installation, while the 3<sup>rd</sup>, 6<sup>th</sup>, 12<sup>th</sup> and 15<sup>th</sup> modes disappear. The dominant modes of vibration after ring installation are lower in general than before ring installation. Due to higher curvatures in the vibration pattern, higher modes could induce higher stresses in the cable, assuming comparable overall cable deflections. Thus, the vibration behavior appears to be somewhat altered after installation of the rings on Cable-Stay B14.

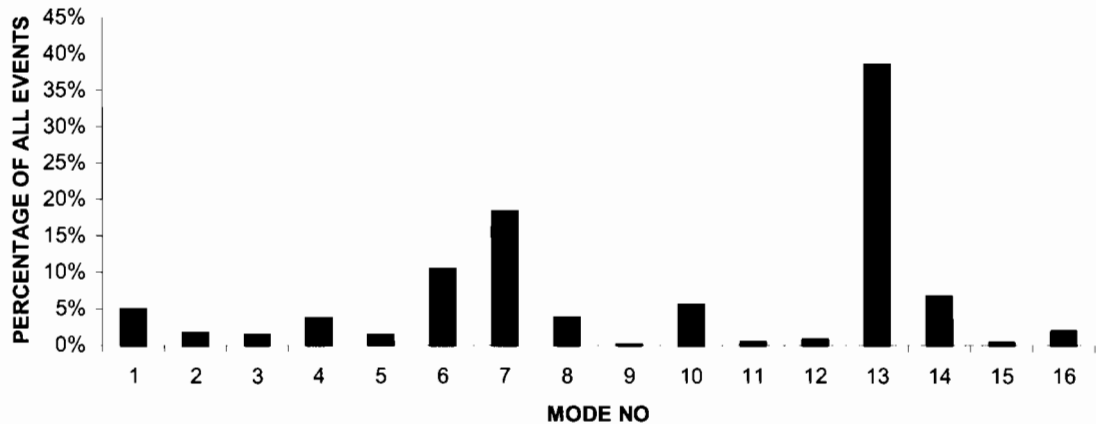


**Figure 5.11** Dominating Mode Distribution of B14HZ  
(Before Ring Installation, i.e. Before January 10, 2001)

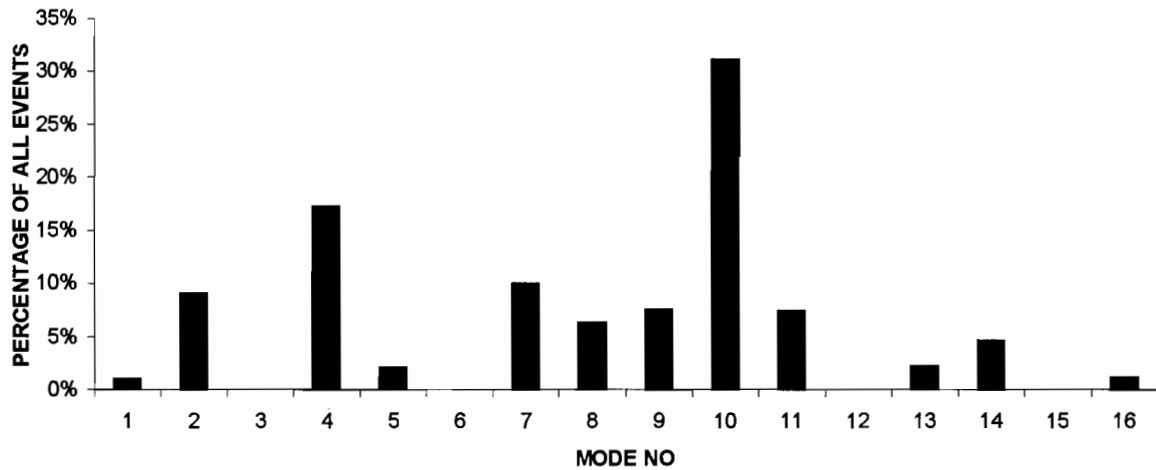


**Figure 5.12** Dominating Mode Distribution of B14HZ  
(After Ring Installation, i.e. After January 10, 2001)

In contrast, for Cable-Stay C14HZ, which is shown in Figures 5.13 and 5.14 and which did not have the rings installed, the dominant modes appear to have remained essentially the same, as expected. The most popular dominating mode is the same, i.e. the 13<sup>th</sup> mode, both before and after January 10, 2001. The second most popular dominating mode changes slightly from the 8<sup>th</sup> before January 10, 2001 to the 7<sup>th</sup> after January 10, 2001. Such a small change could have been caused by slightly varied weather conditions during the time period.

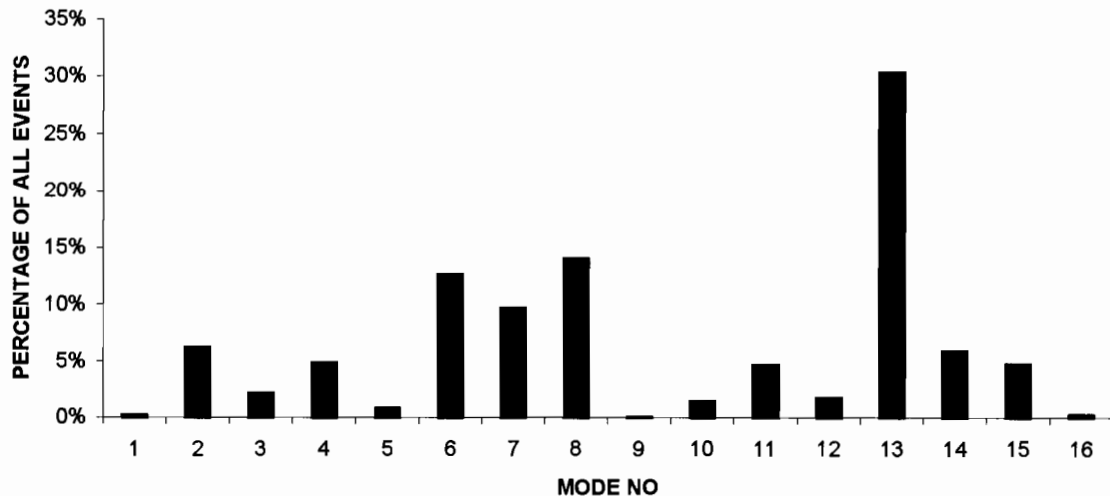


**Figure 5.13** Dominating Mode Distribution of C14HZ  
(Before January 10, 2001, No Rings)

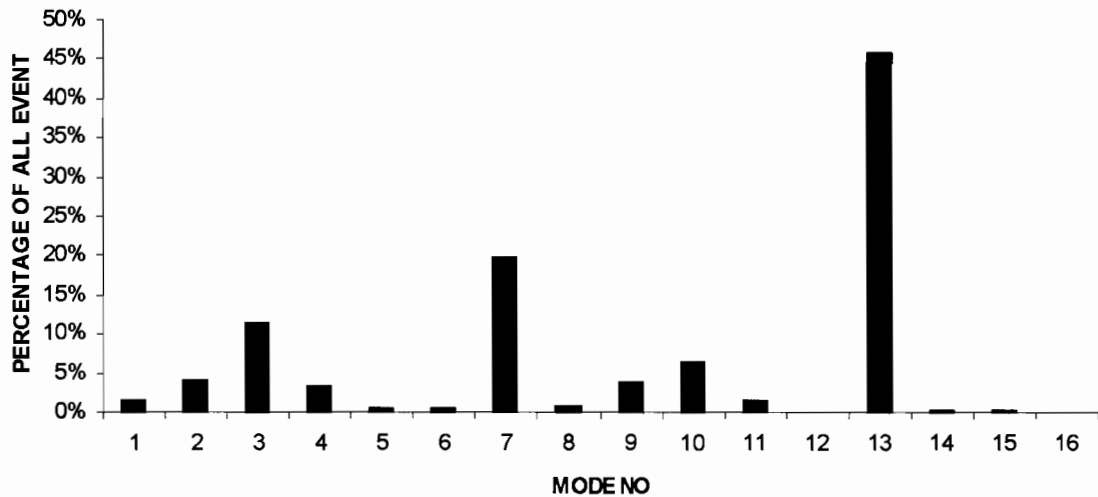


**Figure 5.14** Dominating Mode Distribution of C14HZ  
(After January 10, 2001, No Rings)

## 5.5 Summary

Based on data collected from the Veterans Memorial Bridge, severe wind-rain-induced vibration did not occur on either Cable-Stays B14 or B08 after ring installation, which occurred on January 10, 2001. Wind-rain-induced vibration often occurred on these two cables prior to the ring installation. In contrast, a number of severe wind-rain-induced vibrations occurred on Cable-Stays C14 and C07, where no rings were installed before and after January 10, 2001. Thus, it appears that aerodynamic rings may be suppressing the wind-rain-induced vibrations. However, with the limited number of field data points collected, firm conclusions concerning the effectiveness of the aerodynamic rings cannot be made at this time. Also, as expected, the circular aerodynamic rings do not mitigate cable-stay vibrations due to low-speed flutter (where the wind direction is  $0^\circ$ , or perpendicular to the plane of stays).<sup>14</sup>

Though the number of recorded wind-rain-induced events after the rings were installed was less than desired, TTU researchers have made an extensive effort to evaluate the data collected in the final six months of the research project. Comparisons of the cable-stays before and after the rings were installed are presented in Figures 5.3 – 5.14. Table 5.9 serves as a summary of the findings.

<sup>14</sup> Note that the maximum accelerations are not as critical for this wind case at low speeds compared to wind-rain-induced vibration cases.

**Table 5.9 Cable-Stay Behavior Summary Table**

	<b>B14 Before Rings Before 1/10/01</b>	<b>B14 After Rings After 1/10/01</b>	<b>C14 No Rings Before 1/10/01</b>	<b>C14 No Rings After 1/10/01</b>
<b>WIND VS. RMS ACCEL</b>	Wind-rain (330°)	<u>No</u> wind-rain	Small number of wind-rain (30°)	Large number of wind-rain (30°)
	Low-speed flutter events occurred	Low-speed flutter events occurred	Low-speed flutter did not occur *	Low-speed flutter events occurred
<b>DOMINANT MODES</b>	13 <sup>th</sup>	10 <sup>th</sup>	13 <sup>th</sup>	13 <sup>th</sup>
	Pattern altered after rings installed		Similar before and after 01/10/2001	

\*Note: The lack of low speed flutter events for C14 before 1/10/01 is most likely due to temporary equipment downtimes.

As indicated in Table 5.9, after the rings were installed, no wind-rain-induced vibration events with acceleration >2.5 g were recorded for Cable-Stay B14. In addition, no rain event from an approximate 330° angle was recorded. Also, as indicated in Table 5.9, the dominant vibration modes changed after the rings were installed on Cable-Stay B14. The dominant vibration modes remained the same on Cable-Stay C14, where the rings were not installed. The rings, as expected, did not mitigate low-speed flutter.

Additional possibilities for the improved Cable-Stay B14 behavior include: (1) possible short-term equipment downtimes during unrecorded events<sup>15</sup> and (2) the randomness of particular events occurring at any given time, etc. However, it must be noted that it is also possible that the rings worked—the rings were effective in suppressing vibrations in the wind tunnel. Considering the possibility that the rings were effective, the actual recording of the data to prove this effectiveness is difficult to obtain as the ring effectiveness generally brings the cable-stay accelerations below an acceptable recording threshold.<sup>16</sup> Certainly, the rings have not been proven to not work. Had any wind-rain-induced vibration events been recorded for Cable-Stay B14 after the rings were installed, one could assume the rings did not work.<sup>17</sup>

Unfortunately, the DAQ system was not designed to trigger based on wind direction—only due to wind speed and/or cable acceleration. Thus, evaluation of any “after ring” events was both difficult and time consuming. (A full scale prototype evaluation of the aerodynamic rings was not anticipated at the time the instrumentation and the DAQ system were being developed and installed.) Thus, unfortunately, the overall effectiveness of the

<sup>15</sup> However, it is actually felt by the researchers that the equipment performed remarkably well over the two-year monitoring period, given the relative harsh local environmental conditions at the site and the initially planned six-month testing period.

<sup>16</sup> It must be stressed that wind-rain events were recorded for Cable-Stay B14 before the rings were installed and these same events were noticeably absent after the rings were installed.

<sup>17</sup> Again however, even in this case, it should be noted that a suboptimal ring thickness and/or ring spacing could have been chosen for this prototype evaluation.

aerodynamic rings cannot be stated with complete confidence at this time, though they do appear to work.<sup>18</sup>

## 5.6 Conclusions

1. Wind-rain-induced vibration events occur often for these cable-stays.
2. Wind-rain-induced vibrations appear when a) the wind is combined with rain, b) wind speeds are between 20-30 mph, and c) the wind comes from a direction of either approximately 30° for Cable-Stay C14 or approximately 330° for Cable-Stay B14.
3. Low-speed flutter is often triggered when wind speeds are between 7-11 m/s (15-25 mph) and from either a 0° or 180° wind direction. These are velocity-restricted in response and are not as critical as wind-rain-induced cases.
4. Aerodynamic rings appear to decrease maximum overall cable-stay RMS acceleration values.
5. Aerodynamic rings appear to effectively mitigate wind-rain-induced cable-stay vibration in the field. However, they are unable to suppress low-speed flutter events (i.e. 0° wind), as expected from wind-tunnel tests.
6. Aerodynamic rings appear to somewhat change the dominating vibration mode of the cable-stays, possibly making them favorable for lower stresses.
7. Further study and additional field data collection is needed to conclusively prove the effectiveness of the rings on Cable-Stays B14 and B08.

---

<sup>18</sup> Results of the ratio of the maximum RMS accelerations before and after 1/10/01 shown in Table 4.5 suggest that the rings work.

## CHAPTER 6

### SUMMARY AND CONCLUSIONS

Two highway bridges under the jurisdiction of the Texas Department of Transportation, TxDOT, have experienced a wind-rain-induced cable-stay vibration problem. These two bridges are the Fred Hartman and Veterans Memorial, located in Baytown and Port Arthur, Texas, respectively. This report documents the results of three years of study of the cable stay vibration problem on these two bridges by researchers from Texas Tech University, under contract to TxDOT. The scope of the TTU effort includes background research, wind tunnel tests, and field instrumentation and monitoring. In addition, TTU researchers developed an innovative aerodynamic ring as a mitigation device for the cable-stay vibration problem. Results from a field prototype application of the rings on the Veterans Memorial Bridge are presented. The rings appear to be effective in eliminating the rivulet formation on the cable stay, while at the same time, adding aerodynamic damping to the system. Complimentary research at Johns Hopkins University and at the University of Texas-Austin on cable-stay vibrations and their implications is continuing; the results of these additional research efforts are not included here.

#### 6.1 Wind Tunnel Results

Wind tunnel tests using single degree of freedom (SDOF) and two degrees of freedom (2DOF) cylinders demonstrated vibration characteristics with yawed angles of attack and led to the logical development of an aerodynamic damping device.

A two-dimensional force-damper apparatus was used to study wind-rain-induced cable-stay vibration. The rain rivulet was simulated with a small plastic, smooth circular cord attached longitudinally to the cylinder. Velocity-restricted vibration was observed in a reduced velocity (dimensionless quantity) range of 100 to 175 (see Figure 3.25). This reduced velocity range translates into wind speeds between 7 to 15 m/s (15 to 33 mph) depending on the diameter and natural frequency of vibration of a cable-stay. Circular rings with a cross-sectional dimension of  $D/14$  (where  $D$  is the diameter of cable-stay) placed at a spacing of  $2D$  and  $4D$  suppressed the cable-stay vibrations. These successful wind tunnel results prompted installation of prototype rings on the Veterans Memorial Bridge cable-stays for a field study.

#### 6.2 Field Site Results

##### 6.2.1 Before ring installation on Cable-Stays B08 and B14

TTU researchers instrumented and monitored four of the Veterans Memorial Bridge cable-stays. Several significant events were recorded over a one and one-half year period. In particular, an instantaneous acceleration event of 5g was recorded on October 8, 1999. The plot of this event, shown in Figure 5.2, demonstrates that under favorable conditions, the cable-stay will vibrate and will continue to vibrate until one or more of the parameters causing the favorable conditions ceases. In this case, the vibration began and continued due to a) rain with wind, b) wind speed in the velocity-restricted region, and c) wind from a critical angle for the cable-stay. In this case, the vibration ended once the rainfall ceased. For Cable-Stays B14 and

B08, the critical wind direction angle is approximately  $330^\circ$ . For Cable-Stays C07 and C14, the critical angle is approximately  $30^\circ$ <sup>19</sup>.

### 6.2.2 After ring installation on Cable-Stays B08 and B14

Prototype aerodynamic circular rings, or bands, were manufactured and placed on three Veterans Memorial cable-stays. TTU researchers monitored Cable-Stays B08 and B14 for six months, while an additional cable-stay (A14) with rings was monitored by Johns Hopkins University. Unfortunately, the number of data points collected in the six months after the rings were installed was not large.

Though any conclusions based on this limited data set must be considered with caution, the data appears to suggest that the rings performed as expected in mitigating the wind-rain-induced cable-stay vibrations in “field” (i.e. real world) conditions.<sup>20</sup> That is, it appears the rings were effective in mitigating cable-stay vibrations during wind-rain-induced events, as no wind-rain-induced events occurred on cable-stays with rings during the six-month monitoring period. Nonetheless, as expected, the passive circular rings appear ineffective in mitigating vibrations due to low-speed flutter events (i.e. winds at  $0^\circ$ ).

A distinction is made in this report between “wind-rain-induced” vibrations and “low-speed flutter” response. Low-speed flutter referred to in this report should not be confused with typical flutter, where the response is divergent. Low-speed flutter can have large vibrations, but typically produces less than 2.0 g accelerations. In this document, “low-speed flutter” is used to refer to galloping and is a velocity-restricted response. It generally occurs without rain. In addition, low-speed flutter is not divergent.

In summary, as stated previously, any conclusions stated based on the current field site data are made with reservation, as the number of data points collected to date are few. Nevertheless, though based on limited data, it appears the circular rings work in mitigating wind-rain-induced cable-stay vibrations.

## **6.3 Future Research**

### 6.3.1 Optimized ring geometry, surface and placement

Future work should be directed at determining an optimal cross-sectional size and shape of the circular ring, with aesthetics of the cable-stayed bridge in mind. Several potential changes in the ring and/or cable-stay surface area parameters should be investigated. Smaller rings can be used to decrease drag. The prototype used a ring thickness of  $D/8$ , whereas  $D/10$ ,  $D/12$  or even  $D/20$  may be sufficient. Also, a wider spacing of rings may be adequate. For example, the prototype used a  $3D$  spacing, whereas a  $4D$  or  $5D$  spacing may also be acceptable.

Additionally, for the three prototype cable-stays, the rings were distributed fully from the top of the cable-stay to the lower anchorage. It may be possible that only the lower portion (say  $L/3$ ) of the cable-stay would require being retrofitted with the aerodynamic rings. Finally,

---

<sup>19</sup> See Figure 4.1 for wind direction orientation.

<sup>20</sup> Though the limited data collected is insufficient to confirm the effectiveness of the rings in the field, certainly, the data collected to date does not suggest that the rings do not work. See Section 5.5 for a more complete discussion of field results.

the surface treatment of the cable-stay should be investigated for mitigation effectiveness. If mechanical dampers are to be used in conjunction with an aerodynamic mitigation technique, the optimum magnitude and attachment location of the mechanical damper should be determined. This is also important for use in the development of an analytical model for such a system.

### 6.3.2 Full-scale testing

Full scale testing of the circular rings in natural wind, along with other vibration mitigation devices, should be performed when possible. To accomplish this task, a controlled full-scale test site should be developed. Such a field site must have a large tower with the ability to record actual wind, rain and other meteorological data. One such site is the Wind Engineering Research Field Laboratory in Lubbock. Full-scale testing, using the TTU 200 m (650 foot) tower, would allow confirmation or rejection of numerous, conflicting claims from a variety of mitigation device manufacturers. Knowledge gained from such full-scale tests would allow TxDOT and other government agencies to make better decisions when developing cable-stay vibration mitigation strategies.

### 6.3.3 Flexible cable-stay section model for wind tunnel tests

The results of the testing presented in this report could be used in the development of a flexible aeroelastic wind tunnel model. That is, a flexible scale model of a larger portion of the cable-stay should be subjected to the same yaw, inclination, and rain conditions in the wind tunnel as has been done in the section model studies to date. From these more refined wind tunnel model studies, analytical models can be developed that take into account the fluctuating wind forces on the cylinder caused by rivulet formation and oscillation. If flutter is determined to be a problem, analytical models using a flutter derivative approach with time domain models can be used.

In addition, the following items should be studied to properly determine the mechanism of vibration of the stay-cables:

- Effect of Scruton number, upstream turbulence, intensity of rain and wind combinations and rivulet oscillation.
- Precise flow visualization and flow measurements in the wake.
- Measurement of flutter derivatives.

### 6.3.4 Active control

Mitigation of cable stay vibrations appears to be an excellent candidate for active control technology. Unlike typical building structures designed to resist seismic forces, active control of cable stays should have much less constraints, as massive forces and associated power requirements are not needed.

Two scenarios are possible. An “active only” system would simply sense vibrations in a particular cable stay and energize rings along the cable-stay to damp the oscillations. This active system can be considered “reactive.” An active “smart” system could sense the wind-rain-induced aerodynamic forces on the cables in real time using appropriate sensors, calculate the acceleration magnitude and mode of vibration of the cable-stay, and selectively energize

specific “smart” rings to quickly dissipate the vibration energy. This second type of active system can be considered “proactive.”

Successful implementation of either of the proposed active systems offers the potential for: (a) superior damping, i.e. less fatigue, for the cable stays, (b) a reduction in the number of required aerodynamic rings per cable, (c) elimination of ice buildup on the cable stays, and (d) innovative aesthetic treatments to the overall bridge structure.

## REFERENCES

- Baker, C.J., 1987. Measures to control Vehicle Movement at Exposed Sites During Windy Periods, *Journal of Wind Engineering and Industrial Aerodynamics*, Vol. 25.
- Bosdogianni, A. and Olivari, D., 1996. Wind- and rain-induced oscillations of cables of stayed bridges, *Journal of Wind Engineering and Industrial Aerodynamics*, Vol. 64, pp 171-185.
- Crossbow Technologies, [www.xbow.com/Products/Accelerometers.htm](http://www.xbow.com/Products/Accelerometers.htm), Model CXL04LP3, accessed March 2004.
- Davenport, A.G., 1995. The dynamics of cables in wind, *International Symposium on Cable Dynamics*, Liege, Belgium: A.I.M., 1-12 Insert.
- Flamand, O., 1993. Rain-wind induced vibration of cables, *Proceedings of the First IAWE European & African Regional Conference*, pp 471-479.
- Geurts, C., Vrouwenvelder, T., Staalduinen, P., and Reusink, J., 1998. Numerical modeling of rain-wind-induced vibration: Erasmus Bridge, Rotterdam, *Structural Engineering International*, 2/1998, pp 129-135.
- Hikami, Y. and N. Shiraishi, "Rain-Wind Induced Vibrations of Cables in Cable Stayed Bridges," *Journal of Wind Engineering and Industrial Aerodynamics* 29 (1988): 409-418.
- Matusmoto, M., Shiraishi, N., and Shirato, H., 1992. Rain-wind induced vibration of cables of cable-stayed bridges, *Journal of Wind Engineering and Industrial Aerodynamics*, Vol. 41-44, pp 2011-2022.
- Matsumoto, M., 1998. Observed behavior of prototype cable vibration and its mechanism, *Proceedings of the International Symposium on Advances in Bridge Aerodynamics*, Copenhagen, Denmark, May 10-13.
- Matsumoto, M., Y. Daito, T. Tanamura, Y. Shigemura, S. Sakuma and H. Ishizaki, 1997. Wind-induced Vibration of Cables of Cable-stayed Bridges. The Second East European & African Conference on Wind Engineering, Genova, Italy, 1791-1798.
- Matsumoto, M., J. Aoki, N. Shiraishi, and M. Yamagishi, "Various Mechanism of Inclined Cable Aerodynamics," in *Proceedings of the Ninth International Conference on Wind Engineering*, (New Delhi, India, 1995), 759-770.
- Main, J. and N. Jones, "Full-scale Measurements of Stay-cable Vibration," in *Proceedings of the Tenth International Conference on Wind Engineering*, (Copenhagen, Denmark, 1999).

- Sarkar, P. and T. Gardner (2000). "Model Tests to Study Rain/Wind-Induced Vibration of Stay Cables", Proceedings of ASCE Structures Congress, Philadelphia, PA, May 2000.
- Sarkar, P., K.C. Mehta, T. Gardner, and Z. Zhao (1998). "Aerodynamic Solutions to Cable Vibrations," Proceedings the Texas Section ASCE Fall 1998 Meeting, Dallas, Texas, September 9-11, 1998.
- Sarkar, P. P., 1992. New identification methods applied to the response of flexible bridges to wind, *Ph.D. dissertation* submitted to The Johns Hopkins University, Baltimore, MD.
- Simiu, E., and Scanlan, R.H., Wind Effects on Structures: Fundamentals and Applications to Design, 3<sup>rd</sup> ed., (New York: John Wiley & Sons, 1996), 150-155.
- Verweibe, C., "Exciting Mechanisms of Rain-Wind-Induced Vibrations," Structural Engineering International (1998), 112-117.
- White, F., Fluid Mechanics, 3<sup>rd</sup> ed., (New York: McGraw-Hill, 1994), 411-413.
- Whitlock, Dalrymple, Poston, and Associates, Inc. (1998). Progress Report Number 1, Evaluation and Repair of Stay-Cable Vibrations: Fred Hartman Bridge, Veterans Memorial Bridge. Austin: Texas Department of Transportation.
- Whitlock, Dalrymple, Poston, and Associates, Inc. (1999). Progress Report Number 2, Evaluation and Repair of Stay-Cable Vibrations. Austin: Texas Department of Transportation (Feb 12, 1999).
- Whitlock, Dalrymple, Poston, and Associates, Inc. (2001). Progress Report Number 3 (Final), Evaluation and Repair of Stay-Cable Vibrations. Austin: Texas Department of Transportation.
- Whitlock, Dalrymple, Poston, and Associates, Inc. (2002). Fax submittal from Scott Withoft of WDP and Associates, February 8, 2002.
- Wianecki, J., 1979. Cables wind excited vibrations of cable-stayed bridges, *Proceedings of the 5<sup>th</sup> International Conference on Wind Engineering*, Colorado 1979, pp 1381-1393. Oxford-New York, Pergamon Press.
- Young Instruments, 2004, [www.youngusa.com](http://www.youngusa.com), Model 27005, accessed March 2004.
- Young Instruments, 2004, [www.youngusa.com](http://www.youngusa.com), Model 05305, accessed March 2004.

## Appendix A

**Aerodynamic** Study of fluid flow and resulting forces on a body

**Aerodynamic damping** Friction of air (fluid) opposes vibration of large amplitude

**Divergent** Amplitude continues to increase with each cycle of vibration

**Drag force** Along-wind force

**Flow separation region** Area or region of a body behind the location of separation of flow

**Flutter** One or two-degree-of-freedom aeroelastic instability involving rotational motion

**Force coefficient** Along wind non-dimensional coefficient

**Galloping** Single-degree-of-freedom translational aerolastic instability

**Lift force** Cross-wind force, usually but not necessarily, vertical

**Reduced velocity** Non-dimensional number using the ration of velocity to diameter and system natural frequency

**Reynolds number** Ratio of inertial forces to viscous forces in fluid flow

**Rivulet** A small stream or brook

**Scruton number** A non-dimensional parameter incorporating the ration of structural mass to fluid mass, and structural damping, which is a measure of the propensity of a structure to resonant dynamic response

**Splitter plate** A plate placed along the longitudinal direction of a cylinder (for cable-stays it is axial flow along the cylinder)

**Stagnation point** Point on a body where the approaching flow is brought to rest

**Strouhal number** Non-dimensional vortex-shedding frequency

**Sub-critical range** Low Reynolds number where the drag coefficient for a cylindrical shape is high

**Turbulence** Fluctuations in fluid flow

**Von Karman vortex sheet** Same as vortex shedding but as a sheet rather than eddies

**Vortex shedding** The periodic shedding of eddies formed from the rolling-up of the boundary shed from a bluff body

**Wake** The region of low velocity and turbulent flow in the region downstream of a body

## Appendix B

### Bridge Closure Criteria in High Wind Events

#### Suggested Criteria for Bridge Closure

- (a) In case of a named tropical storm approaching the Houston area, we carefully monitor that storm with the help of the Hurricane Forecast Center. If the strike probability of the storm making landfall in the Houston vicinity is high (say 25%), the bridge should be closed 4-5 hours ahead of the expected time of landfall. Of course a judgment has to be made in conjunction with the local emergency management officials depending on when they issue an order for the evacuation and how long it takes to evacuate Baytown. However, the next criteria should always get precedence.
- (b) When the 3-sec gust recorded at the bridge site on the deck level exceeds 50 mph consecutively three times within a 10 min. period, the TxDOT officials should be informed and immediate action should be taken to close the bridge as soon as possible (it can be rehearsed to time this exercise where TxDOT has been informed of a potentially dangerous wind speed situation on the bridge deck and it takes an action to implement the closure of the bridge).

#### Accident Wind Speeds in Cross Winds

In the U.K., at exposed locations such as embankments or high river bridges, wind-induced high-sided vehicle accidents are a common occurrence. Over 370 wind-induced accidents were reported in the U.K. during one extreme wind event alone in 1990. Accidents are caused either by the vehicle being completely blown over, or by the vehicle deviating significantly from its original path. Mainly three types of accidents can be expected to occur in regular winds that exceeds a certain wind speed: (1) overturning accidents, (2) sideslip accidents, (3) rotation accidents. The critical wind speed for wind-induced accidents depend on (a) the type of accident listed above, (b) the parameters of the vehicle such as type (car, tractor-trailer, van, coaches), mass and mass inertia, road tire friction coefficients, and aerodynamic coefficients, (c) speed of vehicle, (d) wind direction or yaw angle with respect to the vehicle axis. Curves were obtained for different vehicles showing the variation of accident wind speed ( $w$ ) with vehicle speed ( $u$ ) and the angle between the direction of travel and the wind vector ( $\beta$ ). The following conclusions were obtained.

**Standard Car:** Lowest accident wind speed  $w$  is 25 m/s (56 mph) corresponding to  $u = 5$  m/s (11 mph). The vehicle is most at risk for winds normal to the direction of travel. Reducing  $u$  did not increase  $w$ . The conclusion was that speed restrictions in windy periods at exposed sites may well increase the risk of accident.

**Standard Coach:** Lowest accident wind speed  $w$  is 35 m/s (78 mph) corresponding to  $u = 5$  m/s (11 mph). Both overturning and rotation accidents can occur depending on  $\beta$ .

**Standard Large Van:** Only overturning accidents can occur for different combinations of  $u$  and  $\beta$ . Front windward wheel will be the first to lose contact with the ground. Lowest accident wind speed  $w$  is 21 m/s (47 mph) corresponding to  $u = 25$  m/s (56 mph). Accident speed is about 31 m/s (69 mph) if  $u$  is 5 m/s (11 mph). Hence, slowing down does help.

**Articulated Tractor-Trailer Combination:** Only overturning accidents can occur for different combinations of  $u$  and  $\beta$ . Rear windward wheel will be the first to lose contact with the ground (different from the large vans). Lowest accident wind speed  $w$  is 21 m/s (47 mph) corresponding to  $u = 25$  m/s (56 mph). Accident speed is about 28 m/s (63 mph) if  $u$  is 5 m/s (11 mph). Hence, slowing down does help.

Some parameters of the vehicles are:

Vehicle Type→	Car	Coach	Large Van	Tractor/Trailer
<b>Lengths (m) ↓</b>				
CG to Front Axle	1.0	4.0	4.0	3.0
CG to Rear Axle	1.5	2.0	2.0	6.0
Wheelbase	0.75	1.0	1.0	1.0
CG Height	0.5	1.0	1.0	1.5
Frontal Area (sq.m)	2.5	8.0	10.0	10.0
Mass (kg)	1500	7500	6000	10000
Mass Inertia (kg. m <sup>2</sup> )	2000	60000	50000	180000

Based on the above discussion and study by Baker, traffic control on the bridge can be a combination of the following:

- Close the bridge if a named tropical storm or a hurricane is approaching. The time of closure will depend on factors such as estimated time of landfall, evacuation plans, etc.
- Close the bridge if wind gusts on the bridge deck exceeds 50 mph at least three times in a 10 minute period.
- Put a warning sign for high-sided vehicles (trucks, large vans, motor homes) to slow down to 25 mph if wind gusts on the bridge deck exceed 42 mph at least three times in a 10 minute period.